Search for New Physics in the Same Sign Dilepton final state with b Jets and Missing Energy at the LHC

D. Barge, C. Campagnari, D. Kovalskyi, V. Krutelyov

University of California, Santa Barbara

W. Andrews, G. Cerati, D. Evans, F. Golf, I. MacNeill, S. Padhi, Y. Tu, F. Würthwein, A. Yagil, J. Yoo

University of California, San Diego

L. Bauerdick, K. Burkett, I. Fisk, Y. Gao, O. Gutsche, B. Hooberman, S. Jindariani, J. Linacre, V. Martinez Outschoorn

Fermi National Accelerator Laboratory, Batavia, Illinois

Abstract

A search for New Physics in the same sign dilepton final state with at least two b-jets and $\not\!\!E_T$ is performed. This analysis uses a data sample collected with the CMS detector of pp collisions at a centre-of-mass energy of 7 TeV, corresponding to an integrated luminosity of $4.7\ \mathrm{fb}^{-1}$. No excess above the standard model background expectation is observed. Upper limits at 95% confidence level are set on the number of observed events. Information on acceptance and efficiencies are provided so that our results can be used to confront additional models in an approximate way. These limits are also used to constrain a number of new physics models.

1 Introduction

The CMS Collaboration has reported results of searches in the final states with two same-sign isolated leptons, jets and missing energy [1, 2], including a more specific search targeting the same-sign top pair production [3]. The major background in all these analyses is from $t\bar{t}$ production, as shown in Fig. 1.

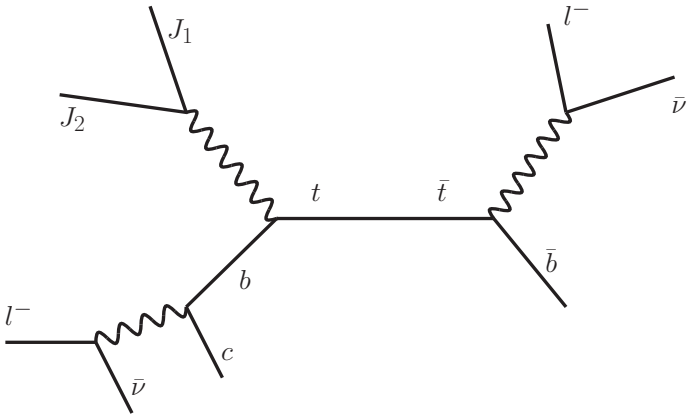

Figure 1: Diagram for $t\bar{t}$ decays giving rise to same-sign dilepton final states

The dominant source of same-sign dileptons in $t\bar{t}$ are events where one of the leptons is from $W \to \ell\nu$ and the other originates from semi-leptonic b-decays. We refer to the first as "real lepton" and the second as "fake lepton". An additional requirement on the number of b-jets ≥ 2, reduces this background significantly, as a b-quark cannot produce an isolated lepton and at the same time provide a b-tag. In other words, the two b-quarks in a top event cannot give three distinct, well separated objects: two tagged jets and one isolated lepton.

Thus, in this note we expand on the results of Reference [2] by requiring that there be ≥ 2 b-tagged jets. For the ee, $\mu\mu$, and $e\mu$ channels, those results were based on three separate analysis notes (References [4, 5, 6]) that differ in the treatment of the fake lepton background. The work described in this note uses the method of Reference [4], and that is where support material can be found. Results consistent with ours have recently been reported by other groups [6, 7].

Same-sign dileptons in association with two or more b-quarks appear naturally in many new physics scenarios. They have been proposed as signatures of supersymmetry (SUSY) where heavy flavor (top or bottom) jets appear naturally [8, 9, 10, 11], in particular in processes with virtual stop contributions [12, 13], those with resonant stop [14], all alternatively described with simplified models (SMS) [15]; color-octet scalar production (either as sgluons in the context of SUSY [16], or non-SUSY in the context of minimal flavor violation [17]); models of maximal flavor violation (MaxFV) [18, 19, 20]; same-sign top quark production from flavor changing neutral currents in the top sector [22]; pair production of $T_{5/3}$ [23]; and top compositeness [24, 25, 26] among others.

As was done in References [1],[2], and [4], we present our results in such a way that they can (reletively) easily be used by phenomenologists to confront many models of new physics that produces same-sign dileptons, b-jets, and missing energy.

In addition, among all potential new physics models we select the following to report the sensitivity of this analysis:

1. the same-sign top pair production via Z' [3, 22];
2. the same-sign top pair production in MaxFV [20];
3. $t\bar{t}t\bar{t}\widetilde{\chi}_1^0\widetilde{\chi}_1^0$ final state via (exclusive) gluino pair production with each gluino decaying a top-stop pair and the stop decaying exclusively to top and LSP, all on-shell;
4. $t\bar{t}t\bar{t}\widetilde{\chi}_1^0\widetilde{\chi}_1^0$ final state via (exclusive) gluino pair production with each gluino decaying to a $t\bar{t}$ and LSP via a virtual stop exchange[21]; this decay mode of the gluino would dominate if all squarks were very massive with the stop being the lightest;
5. $t\bar{t}W^+W^-\chi_1^0\chi_1^0$ final state via (exclusive) sbottom pair production with each sbottom decaying to a top and the lightest chargino, which subsequently decays to a W boson and an LSP;

6. a mix of $t\bar{t}b\bar{b}W^+W^-\widetilde{\chi}_1^0\widetilde{\chi}_1^0$ and $tt\bar{b}\bar{b}W^-W^-\tilde{\chi}_1^0\tilde{\chi}_1^0$ (+c.c.) final states via (exclusive) gluino pair or gluino-sbottom production where each gluino decays to a sbottom and a b-quark and the sbottom subsequently decays as $\widetilde{b} \to t\widetilde{\chi}_1^- \to tW^-\widetilde{\chi}_1^0$, as in the previous case.

The considered models thus have two to four b-jets, and two to four W bosons in the final state with varying kinematics.

All of these new physics scenarios have in common that the isolated same-sign leptons are typically decay products of on-shell W's, thus allowing us to increase the minimum lepton p_T requirements in our search to 20 GeV, which reduces backgrounds even further with respect to the analysis of Ref. [1, 2, 4]. The combination of requiring at least two b-jets and increasing the lepton p_T threshold to 20 GeV reduces the standard model backgrounds by roughly a factor 30 over the more generic search.

For the purpose of this note we restrict ourselves to the ee, $e\mu$, and $\mu\mu$ final states, *i.e.*, we do not consider τ's, except in the case that the τ decays leptonically.

This note is organized as follows. A brief description of the event baseline selections is given in Section 2, followed by the definitions of the signal search regions in Section 3. Estimates of efficiencies for leptons, $\not\!\!E_T$, H_T, and b-tags, components of the event selection, are given in Section 4. This can be used to provide informaton to non-CMS members to better interpret our results (the so-called "outreach" program). Data - Monte Carlo scale factors and their uncertainties are described in Section 4.6; these scale factors are needed to calculate signal acceptances. We then describe methods to predict background contributions in Section 5, including predictions from simulation and from data, detailed in Section 6. Results of background predictions for the defined search regions are compared with observed events in data in Section 7, supported by an exclusive (disjoint) breakdown of contributions in Appendix B. Comparisons of the predicted and observed events, together with inputs relevant to signal selection systematic uncertainties described in Section 8. Supporting information for the outreach program, *e.g.*, a validation of the efficiency model, is given in Section 9. Finally, we interpret our findings as upper limits on production of signal events beyond the background predictions as described in Section 10.

2 Baseline Event Selection

This analysis is based on the same-sign dilepton search documented in AN-2011/468 [4] and corresponds to an integrated luminosity of 4.7 fb^{-1}. In that study we searched for events with two isolated same-sign leptons in association with 2 additional jets and $\not\!\!E_T$. Here we re-use most of the baseline event selection as summarized below. In addition, we require at least 2 b-tagged jets using Simple Secondary Vertex High Efficiency Medium (SSVHEM) working point tagger. This tagger relies on reconstructed secondary vertices with at least two tracks and an IP significance of at least 1.74 and provides a b-jet tagging efficiency of about 60% with a 4% (15%) systematic uncertainty for jet $p_T < 240 (> 240)$ GeV and a tagging rate of light flavor jets in the 2–5% range, increasing with the jet momentum [28].

We thus discuss here only differences and briefly summarize the basic kinematics and triggers. For more details, we refer to [4].

- Events have to pass one of the dilepton triggers without an H_T requirement.
- There should be at least two isolated same-sign leptons (ee, $e\mu$, and $\mu\mu$) with $|\eta| < 2.5$.
- We require both leptons to have $p_T >$ 20 GeV.
- We tighten the relative isolation cut on the leptons from 0.15 to 0.1.
- At least two particle flow jets tagged using the SSVHEM tagger with $p_T > 40$ GeV and $|\eta| < 2.4$ corrected with L1FastL2L3 corrections.
- The selected jets must be separated from the leptons by $\Delta R > 0.4$ (either hypothesis lepton or any additional lepton with $p_T > 20$ GeV passing the ID and isolation selections).
- $\not\!\!E_T > 30$ GeV (we use pfMET).
- We remove dilepton events with invariant mass $M_{ll} < 8$ GeV.
- We veto events if a third lepton is satisfying the following Zveto:

- has $p_T > 10$ GeV;
- (an electron) passes $|\eta| < 2.4$, and a loosened identification, as the WP95 ID-only without any cut on h/e in the endcaps;
- (for a muon) passes all identification requirements of the signal selection except for the calorimeter veto requirements;
- has relative isolation < 0.2;
- makes an opposite-sign same-flavor pair with either of the two "primary" leptons such that the pair has a mass within 15 GeV of the Z mass.

3 Search Regions

As we will demonstrate later in this note, the expected count of events passing the baseline selection is quite small (order 10). Thus, this selection can already be used as a "search region" for new physics. In addition, we define tighter search regions that can be used to increase our sensitivity to various models. We define these search regions by adding the following requirements on top of those of the baseline selection.

- ++ region, including only positively charged lepton pairs. This region is appropriate for final states with same-sign top quarks, *e.g.*, the Z' and MaxFV models. This selection reduces the fake-lepton and charge misidentification backgrounds, while keeping essentially all the same-sign top signal, which is produced primarily from the uu initial state, due to the available PDF luminosities.
- The following tighther H_T and $\not\!\!E_T$ regions are defined to improve sensitivity to SUSY production scenarios. As mentioned in Section 1, all of the SUSY scenarios that we consider explicitely have four b-quarks, up to two hadronically decaying W bosons, and at least two neutrinos and two LSPs to make up for H_T and $\not\!\!E_T$, varying between the model points. When setting limits on a particular model, the search region with the best expected limit is to be used in every particular case.

  1. Low-H_T low-$\not\!\!E_T$region: $H_T > 200$ GeV, $\not\!\!E_T > 50$ GeV.
  2. Low-H_T high-$\not\!\!E_T$region: $H_T > 200$ GeV, $\not\!\!E_T > 120$ GeV.
  3. High-H_T low-$\not\!\!E_T$region: $H_T > 320$ GeV, $\not\!\!E_T > 50$ GeV.
  4. High-H_T high-$\not\!\!E_T$region: $H_T > 320$ GeV, $\not\!\!E_T > 120$ GeV.
  5. Low-H_T low-$\not\!\!E_T$region: $H_T > 200$ GeV, $\not\!\!E_T > 50$ GeV with ≥ 3 btags (all other regions have ≥ 2 btags – The inclusion of a region with ≥ 3 btags was suggested by the Florida group[7]).

  We note that the exact choices of $\not\!\!E_T$ and H_T are somewhat arbitrary. They are similar to those made in the 2011 untagged same-sign analysis [2].

4 Selection Efficiency and Outreach Information

We would like to quote our results as a cross-section, or cross-section limit, that is as model independent as possible. For this we carefully define the acceptance, and provide enough details about the selection efficiency within that acceptance that anybody can use their favorite Monte Carlo generator of new physics, define an acceptance at the hard scatter level (status = 3 in Pythia), and correctly estimate the efficiency for this new physics model to within 50% or so (the so-called "outreach" program). The same steps are done here as in the pre-tagged sample analysis [4] with appropriate modifications considering differences in selections of leptons and an addition of the b-tagged jet requirements.

The event selection efficiency is a combination of

1. the kinematical requirements on leptons and jets
2. the lepton identification and isolation efficiency;
3. the efficiency of the $\not\!\!E_T$ requirement;
4. the efficiency of the H_T requirement;

5. the efficiency of the b-jet tagging requirement.

We derive efficiency functions for components 2 to 5 using a sample of simulated events for the LM6 SUSY model point.[1)] Applicable simulation-to-data corrections (scale factors) are also evaluated based on available comparisons of these effiencies in data and simulation. As described below, the description of the lepton selections does not require an additional scale factor, and the correction for b-tagged jets is small with a scale factor of 0.96.

4.1 Definition of Acceptance

Lepton acceptance is defined for both leptons with $|\eta| < 2.4$ and $p_T > 20$ GeV. The generator-level equivalent of the H_T, $H_T^{\rm gen}$, is comprised of the sum p_T of all colored particles at the hard scatter level that have $p_T > 40$ GeV and $|\eta| < 2.5$. The number of such colored particles defines the number of jets at generator level. A generator-level $\not\!\!E_T$ equivalent, $\not\!\!E_T^{\rm gen}$, is defined as the absolute value of the vector sum of the transverse momentum of all non-interacting particles, e.g. neutrinos and LSP.

4.2 Lepton Efficiencies

The electon and muon selection efficiency dependence as a function of the lepton p_T is shown in Fig. 2. It is derived using LM6 events passing the baseline selections applied to jets and $\not\!\!E_T$. Compared to the pre-tagged sample analysis [4], we obtain a slightly lower efficiency, consistent with the tighter requirement on isolation.

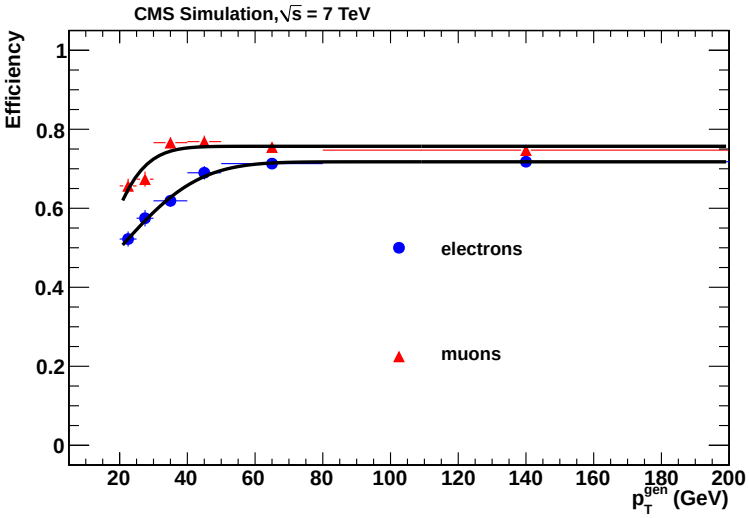

Figure 2: Lepton selection efficiency as a function of p_T, displayed for electrons and muons.

The efficiency dependence can be parameterzied as a function of p_T as

$$\epsilon = \epsilon_\infty \mathrm{erf}\left(\frac{p_T - C}{\sigma}\right) + \epsilon_C \left(1. - \mathrm{erf}\left(\frac{p_T - C}{\sigma}\right)\right), \quad (1)$$

where ϵ_∞ gives the value of the efficiency plateau at high momenta, C is equal to 20 GeV, ϵ_C gives the value of the efficiency at $p_T = C$, and σ describes how fast the transition region is. The results of the fit for electrons and muons are summarized in Table 1.

4.3 Trigger Efficiency

As discussed in Section 2, this analysis uses dilepton triggers; the lepton p_T thresholds are high enough that we do not need the dilepton+H_T triggers. The trigger efficiency, as discussed in Reference [4], is $99 \pm 1\%$ ($96 \pm 3\%$) per electron (muon).

[1)] The LM6 cMSSM model point is defined by the model parameters as $m_0 = 85$ GeV, $m_{1/2} = 400$ GeV, $\tan\beta = 10$, $\mu > 0$, and $A_0 = 0$ GeV.

Table 1: Results of the fit of the dependence in Fig. 2 to the function specified in Eq. 1.

Parameter	Electrons	Muons
ϵ_∞	0.718 ± 0.008	0.757 ± 0.006
ϵ_C	0.498 ± 0.021	0.614 ± 0.026
σ	25.8 ± 4.0	12.9 ± 2.5

4.4 $\not\!\!E_T$ and H_T efficiency turn-on

Our selections on reconstructed jets begin with a requirement of at least two jets with $p_T > 40$ GeV. In the following we proceed with determining H_T and $\not\!\!E_T$ requirements with respect to events that have generator-level requirements on the leptons and colored particles as described in Section 4.1. The efficiency for an event to pass a given reconstructed $\not\!\!E_T$ (H_T) threshold is shown in Fig. 3 as a function of $\not\!\!E_T^{\rm gen}$ ($H_T^{\rm gen}$) in events passing $H_T^{\rm gen} > 200$ GeV ($\not\!\!E_T^{\rm gen} > 30$ GeV). Due to the rather small fraction of events in LM6 simulation having low H_T activity, the H_T curves are made with LM1.[2)] Results of the fits of these curves to $0.5\epsilon_\infty\{\mathrm{erf}[(x - x_{1/2})/\sigma] + 1\}$ are summarized in Table 2. Neither the $\not\!\!E_T$ nor H_T curves show a significant bias in the position of the point with half the plateau efficiency ($x_{1/2}$). The inefficiency at the plateau is essentially negligible. The width of the threshold σ increases with the value of the cut.

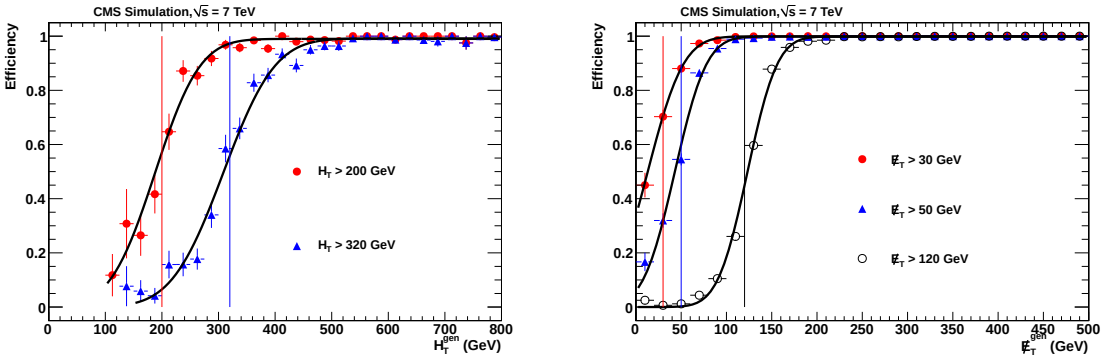

Figure 3: Efficiency for an event to pass a given reconstructed $\not\!\!E_T$ (H_T) threshold as a function of $\not\!\!E_T^{\rm gen}$ ($H_T^{\rm gen}$). The curves are shown for $\not\!\!E_T$ thresholds of 30, 50, and 120 GeV; the thresholds for H_T are 200, 320 GeV.

Table 2: Results of the fit of the dependence in Fig. 3 to $0.5\epsilon_\infty\{\mathrm{erf}[(x - x_{1/2})/\sigma] + 1\}$.

Parameter	H_T		$\not\!\!E_T$		
	> 200 GeV	> 320 GeV	> 30 GeV	> 50 GeV	> 120 GeV
ϵ_∞	0.990 ± 0.002	0.992 ± 0.003	0.999 ± 0.001	0.999 ± 0.001	0.999 ± 0.001
$x_{1/2}$, GeV	187.8 ± 5.5	308.4 ± 3.3	13.1 ± 2.4	43.0 ± 1.1	123.3 ± 0.5
σ, GeV	88.3 ± 9.8	102.0 ± 6.2	44.0 ± 2.8	38.9 ± 1.6	36.6 ± 0.9

4.5 Jet b-tagging efficiency

The b-jet tagging efficiency is defined for b-quarks passing $|\eta| < 2.5$ and matching to a reconstructed jet. A fraction of these b-quark that match to a b-tagged jet is the b-jet tagging efficiency. It shown in Fig. 4 as a function of the b-quark p_T. For b-quarks of $|\eta| < 2.5$, the b-jet tagging efficiency as a function of p_T can be parametrized as

where the parameters p_0, p_1, and p_2 are given in Figure 4 and SF is the data-Monte Carlo scale factor: SF = 0.96 with a 4 (15)% uncertainty for jets with $p_T < 240 (> 240)$ GeV (see Section 4.6.2).

[2)] The LM1 cMSSM model point is defined by the model parameters as $m_0 = 60$ GeV, $m_{1/2} = 250$ GeV, $\tan\beta = 10$, $\mu > 0$, and $A_0 = 0$ GeV.

- $p_T > 90$ GeV $\quad \epsilon = SF \cdot [p_0 \cdot (p_T - 90\ \text{GeV}) + p_1]$
- 90 GeV $< p_T <$ 170 GeV $\quad \epsilon = SF \cdot p_1$
- $p_T > 170$ GeV $\quad \epsilon = SF \cdot [p_2 \cdot (p_T - 170\ \text{GeV}) + p_1]$

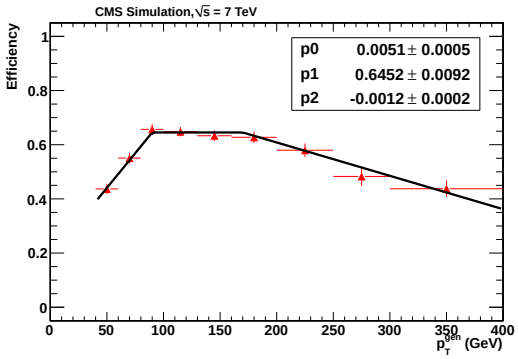

Figure 4: B-jet tagging efficiency as a function of the matching b-quark p_T in LM6 SUSY MC.

4.6 Data - Monte Carlo Scale Factors and their Uncertainties

4.6.1 Data - Monte Carlo Scale Factor for Leptons

The efficiencies of the lepton isolation and identification requirements (including all quality requirements) are measured with the tag&probe method in dilepton Z events using the full 2011 dataset. The efficiency of the identification requirements is a property of the lepton itself and is directly applicable to the leptons in signal events. The efficiency of the isolation requirement, however, is a strong function of all other (mainly hadronic) activity in the event. The following results are based on measurements using the full dataset and compared to simulation that is re-weighted to have a pile-up distribution comparable to that observed in data.

The electron selection efficiencies are measured in events passing the `Ele17...SC8_Mass30` and `Ele17..Ele8_Mass30` triggers, which require one well-identified electron and one super-cluster or GSF electron with $p_T > 8$ GeV forming a pair with a mass above 30 GeV$/c^2$. For higher p_T electrons, the `Ele32...SC_17` triggers are also used, which require one well identified electron and one super-cluster with $p_T > 17$ GeV. In the tag&probe analysis the electron tag is required to match to the well-identified electron from the trigger and also to pass all the electron requirements described in [4]. The probe electron is required to have

- $p_T > 20$ GeV, $|\eta| < 2.4$, excluding the super-clusters with $1.4442 < |\eta| < 1.566$.

The isolation efficiency is measured with the probes passing all electron selections, except for the trigger requirement and the isolation itself. The identification efficiency is measured with probes passing the isolation requirement. Results of the measurement are summarized in Table 3. The contribution from the Z events is based on simple counting in the mass range of 86–96 GeV$/c$. The MC contribution includes W+jets events to match the expected residual backgrounds in this mass window. The following sources of systematic uncertainty are attributed to this measurement: background contribution, selection of dielectron events, factorization of the isolation and ID parts. The size of the background contribution can be estimated using MC alone and also tested in data with the same-sign dielectron events, which should represent the number of backgrounds reasonably well. The effect of backgrounds on the measured efficiency is established to be approximately 2% for the combined identification and isolation selection efficiency. The narrow mass window used to count electron pairs introduces a bias of about 3% to the measured efficiency by rejecting failing probes that happen to have a worse resolution or a shift in the measured momentum. This bias is expected to approximately cancel in data and simulation. We include a half of the 3% as a source of systematics. Based on simulation alone, the combined selection efficiency, measured with respect to the probe electron, differs from the product of the components by approximately 1% or less depending on the momentum range. All of these effects combined give a systematic uncertainty on the total data-to-MC scale factor in the lepton selection efficiencies of 2.5% for $p_T > 20$ GeV.

The muon selection efficiencies are measured using events passing the double-muon trigger. The tag muon is required to pass all of the muon selection requirements described in [4]. The probe muon is required to pass

- $p_T > 20$ GeV$/c$;

		20 - 40 GeV	40 GeV -
ISO	MC	0.9268 ± 0.0004	0.9768 ± 0.0002
	DATA	0.9247 ± 0.0003	0.9737 ± 0.0002
	DATA/MC	0.9977 ± 0.0005	0.9968 ± 0.0003
ID	MC	0.8069 ± 0.0005	0.8500 ± 0.0004
	DATA	0.8005 ± 0.0005	0.8343 ± 0.0004
	DATA/MC	0.9921 ± 0.0008	0.9815 ± 0.0006
ID X ISO	MC	0.7478 ± 0.0005	0.8303 ± 0.0004
	DATA	0.7403 ± 0.0005	0.8124 ± 0.0004
	DATA/MC	0.9899 ± 0.0010	0.9784 ± 0.0007

Table 3: Electron isolation and identification efficiencies measured with the tag&probe method. The uncertainties are statistical only.

- $|\eta| < 2.4$;
- have both the global and the tracker muon types.

Both the isolation and the identification efficiency are measured using probes failing only the requirement in question, assuming the efficiencies factorize. Results of the muon identification and isolation efficiency measurements are presented in Table 4. As expected, the identification efficiency for muons measured in data and in MC agree well, while there is some discrepancy for the isolation efficiency. Similar sources of systematic uncertainty are considered here as those considered for electrons. Most of the reconstructed (probe) muons are real muons and the measurement of the identification efficiency is not affected significantly by backgrounds. With the tighter mass window used here to select events, the backgrounds are estimated to be small. This narrow mass window, however, introduces a bias of about 1.5% to the measured efficiency by rejecting failing probes that happen to have a worse resolution or a shift in the measured momentum. This bias is expected to approximately cancel in data and simulation. We include a half of the 1.5% as a source of systematics. We assign a systematic uncertainty of 1% on the identification and isolation efficiency measurement from a comparison between the simple counting of Z events and fitting the mass shape to a gaussian signal and an exponential background component. Based on studies in MC events, we find that the isolation and the identification efficiencies factorize near-perfectly and do not assign any additional systematic uncertainty. The total systematic uncertainty on the muon efficiency measurement in data, simply covering the full momentum range, is 2%.

		20 - 40 GeV	40 GeV -
ISO	MC	0.9111 ± 0.0003	0.9747 ± 0.0002
	DATA	0.8969 ± 0.0003	0.9668 ± 0.0002
	DATA/MC	0.9844 ± 0.0004	0.9919 ± 0.0002
ID	MC	0.9710 ± 0.0002	0.9612 ± 0.0002
	DATA	0.9666 ± 0.0002	0.9561 ± 0.0002
	DATA/MC	0.9955 ± 0.0003	0.9947 ± 0.0003
ID X ISO	MC	0.8847 ± 0.0003	0.9369 ± 0.0002
	DATA	0.8669 ± 0.0003	0.9244 ± 0.0002
	DATA/MC	0.9799 ± 0.0005	0.9866 ± 0.0003

Table 4: Muon isolation and identification efficiencies measured with the tag&probe method. The uncertainties are statistical only.

The tag&probe results in Tables 3 and 4 show that for leptons with $p_T > 20$ GeV used in this analysis both the ID part and the isolation parts of the lepton selection are reproduced well by simulation, already within the systematic uncertainties quoted above. Application of this measurement based on Z events to the signal events incurs an additional uncertainty due to potential mismodeling of the isolation requirement. In agreement with Ref. [4], we assign a systematic uncertainty of 5% due to modeling of the isolation efficiency for signal events. Considering the small size of the difference between data and simulation reported in Tables 3 and 4, compared to the systematic uncertainty applicable to the analysis, we approximate the scale factor to be 1.0 for both simulated signal and backgrounds and propagate the uncertainty described above to the relevant part of the analysis (signal selections) described in Section 8.

4.6.2 Data - Monte Carlo Scale Factor for b-jets

We apply an average scale factor of 0.96 measured using $t\bar{t}$ events for the SSVHEM tagger [27]. The uncertainty on the scale factor is 4 (15)% for jets with $p_T < 240 (> 240)$ GeV, as recommended by the b-tagging POG [28]. We apply it to the analysis as described in Section 8.

5 Background Contributions

We are following the same strategy in estimating the background contributions as in the pre-tagged sample analysis [4]. Contributions with genuine same-sign isolated lepton pairs are estimated from simulation, while the contributions from leptons arising from jets (fakes) and from genuine opposite-sign pairs with a lepton charge misreconstruction (charge flips) are measured in data using control samples. The data-driven estimates are described in the next section. In addition, as a reference, we are using all relevant available simulated samples to get a feeling of the expected yields from simulation alone. As will be shown later in Section 7, contributions with genuine same-sign isolated dileptons are comparable to those estimated from events with fake leptons, while the predictions from charge flips are relatively low. These findings are in fair agreement with direct estimates from simulation.

We use MC to estimate contributions from the following SM production processes with genuine same-sign isolated dileptons:

- $qqW^{\pm}W^{\pm}, WWW, WWZ, WZZ, ZZZ, WW\gamma, t\bar{t}W, t\bar{t}Z, t\bar{t}\gamma$ and double parton $W^{\pm}W^{\pm}$ with two real leptons in the final state.
- WZ, $W\gamma^{\star}$ (0.25 GeV $< m_{\gamma^{\star}} < 12$ GeV), and ZZ with two real leptons in the final state.
- $W\gamma$ with one real lepton and a photon conversion. This background is a priori not estimated by the fake rate method because the photon is generally isolated.

Details on the samples used and the corresponding cross sections can be found in Ref. [4]. As in the pre-tagged sample analysis, we are assigning a 50% uncertainty to the expected number of events from these samples.

6 Data Driven Background Estimation Methods

We have developed two data-driven methods to estimate the two potentially dominant backgrounds. The first method provides an estimate of the number of events with fake leptons (jets misidentified as leptons). The second method is used to estimate the number of genuine leptons reconstructed with an incorrect charge sign.

6.1 Data Driven prediction for fake lepton backgrounds

To answer some of the questions raised during preapproval, we have added what amounts to a FAQ about the Fake Rate method in Appendix A.

We predict the background from fake leptons using the technique previously implemented in the 2010 data analysis and documented in [29] and currently used in the pre-tagged sample analysis [4]. The idea is to count the number of events for which one lepton passes all final selections and a second lepton fails the nominal requirements but passes a looser set of requirements[3)]. We refer to the former lepton as a "numerator" lepton (n), and the latter a "non-numerator" (denominator and not numerator, or $\bar{n}$). The denominator objects are also referred to as fakeable objects (FO). The ratio of "numerator" to "denominator" objects is called a "fake rate", FR (also known as tight-to-loose ratio, TL). A fake rate function is measured in an independent data sample of multijet events. This fake rate function is measured in bins of lepton p_T and $|\eta|$, separately for electrons and muons.

The numerator selections are detailed in Section 2. The denominator selections are exactly the same as in the inclusive analysis [4]. They are listed below for completeness.

Muon denominator definition is to relax the following muon requirements from Section 2:

[3)] Events must also pass all requirements on number of jets, $\not\!\!E_T$, number of b-tagged jets, and H_T. All jet quantities are calculated after lepton-jet disambiguation, *i.e.*, requiring that the counted jets be separated by $\Delta R > 0.4$ from the leptons.

- χ^2/ndof of global fit < 50 (was < 10);
- transverse impact parameter with respect to the selected vertex is < 2 mm (was < 200 μm);
- the MIP-like requirement on deposits in the ECAL (HCAL) is removed [was ECAL (HCAL) < 4 (6) GeV];
- Iso is set to be $Iso < 0.4$ (was < 0.1).

Electron denominator definition is to relax the following electron requirements from Section 2:

- the impact parameter cut is removed (was < 200 μm);
- Iso is set to be $Iso < 0.6$ (was < 0.10).

We thus use an extrapolation in isolation (and impact parameter) to estimate the fake lepton backgrounds in both electrons and muons. This choice of the denominator is designed to be safe determining contributions from all types of fake lepton candidates arising from jets. It has already been extensively tested in the inclusive (pre-tagged) same-sign dilepton analysis [4], where the fake-isolated leptons are expected to be dominated by heavy flavor jets, in which the lepton candidate is predominantly a real lepton from b/c-quark semileptonic decays. In this analysis, as discussed in detail below, we find that isolated lepton candidates not arising from heavy flavor decays have a much larger fraction (dominant for electrons) of all fake leptons. Closure tests performed on $t\bar{t}$ simulation (still expected to be the dominant source of fakes) confirm this choice of denominator definition works here as well.

Samples of multijet (inclusive QCD) events in data are selected among events with a single lepton trigger present. The same requirements are applied to select the multijet-dominated events as in the inclusive analysis [4].

We repeat all relevant studies performed with 2011 data, as documented in Ref. [4]. These include

- extraction of the fake rates in simulation and data;
- measurement of the fake-rate dependence on the *opposite-side* jet p_T, as a measure of the dependence on the progenitor parton momentum in data;
- closure tests on $t\bar{t}$ after the baseline and search region selections.

Results of other tests performed in Refs. [4, 29] apply here in part, with the main caveat that they are the most relevant for fakes not from the heavy flavor as well:

- closure tests in W+jets and double-fake in QCD MC samples (even though none of these are expected to contribute significantly even at the baseline selection level);
- estimates of the residual W+jet and Z contamination in the sample;
- comparison with the fake rate measured in events with enhanced heavy flavor contribution using b-tagging (the variation observed here is up to about 20% for electrons and muons in both simulation and data and are fractionally much less important here).

We arrive to essentially the same conclusions on the performance of the fake rate method as we did in the past. In particular, we find that the method works reasonably well, still with a systematic uncertainty of about 50%. In the following we summarize the measurement of the fake rate and provide several highlights of the studies with the current dataset.

The nominal fake rates are measured requiring an "opposite side" jet with $p_T > 40$ GeV, separated by $\Delta R > 1.0$ from the FO. The electron fake rates are measured separately for triggers with an isolation requirement and for triggers without any isolation requirement on the electron. Results of the measurement are summarized in Table 5 for triggers with calorimeter isolation (as used for $e\mu$ events), and in Table 6 for triggers with both the calorimeter and tracker isolation requirements (as used for ee events). Results for electron triggers without an isolation requirement are provided in Table 7 as a reference. The muon fake rates are measured using all single-muon triggers described in Ref. [4]. The measurement is summarized in Table 8.

$\lvert\eta\rvert$ \ p_T	10.000 – 15.000	15.000 – 20.000	20.000 – 25.000	25.000 – 35.000	35.000 – 55.000
0.000 – 1.000	0.1905 ± 0.0064	0.1110 ± 0.0059	0.1082 ± 0.0065	0.1202 ± 0.0071	0.1909 ± 0.0133
1.000 – 1.479	0.1953 ± 0.0108	0.1304 ± 0.0108	0.1168 ± 0.0093	0.1248 ± 0.0098	0.2030 ± 0.0173
1.479 – 2.000	0.1454 ± 0.0125	0.1199 ± 0.0115	0.1076 ± 0.0078	0.1098 ± 0.0076	0.1431 ± 0.0111
2.000 – 2.500	0.1832 ± 0.0125	0.1814 ± 0.0137	0.1370 ± 0.0096	0.1607 ± 0.0097	0.2106 ± 0.0134

Table 5: Electron fake rate measured in bins of the electron candidate p_T and η for electrons collected using triggers with a calorimeter isolation requirement.

$\lvert\eta\rvert$ \ p_T	10.000 – 15.000	15.000 – 20.000	20.000 – 25.000	25.000 – 35.000	35.000 – 55.000
0.000 – 1.000	0.2656 ± 0.0198	0.1917 ± 0.0241	0.1527 ± 0.0252	0.1755 ± 0.0277	0.2738 ± 0.0487
1.000 – 1.479	0.2389 ± 0.0318	0.2553 ± 0.0450	0.1000 ± 0.0286	0.1294 ± 0.0364	0.2833 ± 0.0582
1.479 – 2.000	0.1318 ± 0.0298	0.0690 ± 0.0235	0.1310 ± 0.0280	0.1356 ± 0.0257	0.1622 ± 0.0350
2.000 – 2.500	0.1786 ± 0.0324	0.1981 ± 0.0387	0.1260 ± 0.0294	0.1449 ± 0.0300	0.2430 ± 0.0415

Table 6: Electron fake rate measured in bins of the electron candidate p_T and η for electrons collected using triggers with calorimeter and tracker isolation requirements.

Figures 5 and 6 show the projection on p_T and $|\eta|$ of these fake rates for electrons and muons, respectively. Electron fake rates measured for triggers with an isolation requirement are slightly higher than those for triggers without an isolation requirement, as expected. The difference, even though it's not very large, is significant enough and we treat fake rates for these triggers separately. The dependence of the fake rates on the away-jet momentum is also shown on these figures.

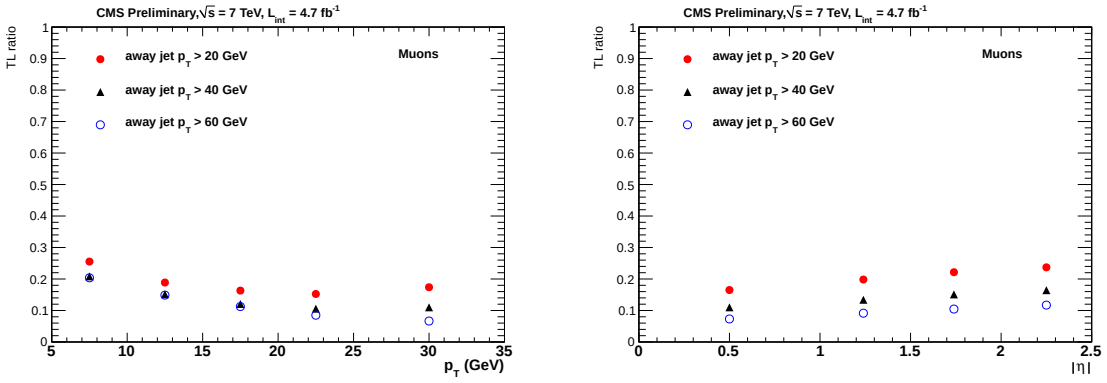

Figure 5: Muon fake rate projected on p_T (left) and $|\eta|$ (right). The fake rates are shown separately for measurements with a requirement for an away jet p_T to be above 20 GeV (red circles), 40 GeV (black circles), and 60 GeV (blue circles).

p_T / $\lvert\eta\rvert$	10.000 – 15.000	15.000 – 20.000	20.000 – 25.000	25.000 – 35.000	35.000 – 55.000
0.000 – 1.000	0.1432 ± 0.0124	0.1079 ± 0.0152	0.0732 ± 0.0166	0.1152 ± 0.0217	0.1319 ± 0.0355
1.000 – 1.479	0.1341 ± 0.0217	0.1333 ± 0.0278	0.0732 ± 0.0235	0.1300 ± 0.0336	0.2105 ± 0.0540
1.479 – 2.000	0.1203 ± 0.0282	0.0714 ± 0.0243	0.1235 ± 0.0258	0.0952 ± 0.0226	0.1635 ± 0.0363
2.000 – 2.500	0.1258 ± 0.0270	0.2243 ± 0.0403	0.1094 ± 0.0276	0.1493 ± 0.0308	0.2128 ± 0.0422

Table 7: Electron fake rate measured in bins of the electron candidate p_T and η for electrons collected using triggers without isolation requirements.

p_T / $\lvert\eta\rvert$	5.000 – 10.000	10.000 – 15.000	15.000 – 20.000	20.000 – 25.000	25.000 – 35.000
0.000 – 1.000	0.1823 ± 0.0024	0.1293 ± 0.0019	0.1051 ± 0.0025	0.0907 ± 0.0034	0.0948 ± 0.0008
1.000 – 1.479	0.2169 ± 0.0037	0.1621 ± 0.0031	0.1290 ± 0.0040	0.1036 ± 0.0053	0.1139 ± 0.0013
1.479 – 2.000	0.2392 ± 0.0038	0.1741 ± 0.0032	0.1347 ± 0.0041	0.1339 ± 0.0059	0.1300 ± 0.0014
2.000 – 2.500	0.2391 ± 0.0055	0.1813 ± 0.0047	0.1418 ± 0.0060	0.1208 ± 0.0088	0.1459 ± 0.0023

Table 8: Muon fake rate measured in bins of the muon candidate p_T and η. The uncertainties are statistical only.

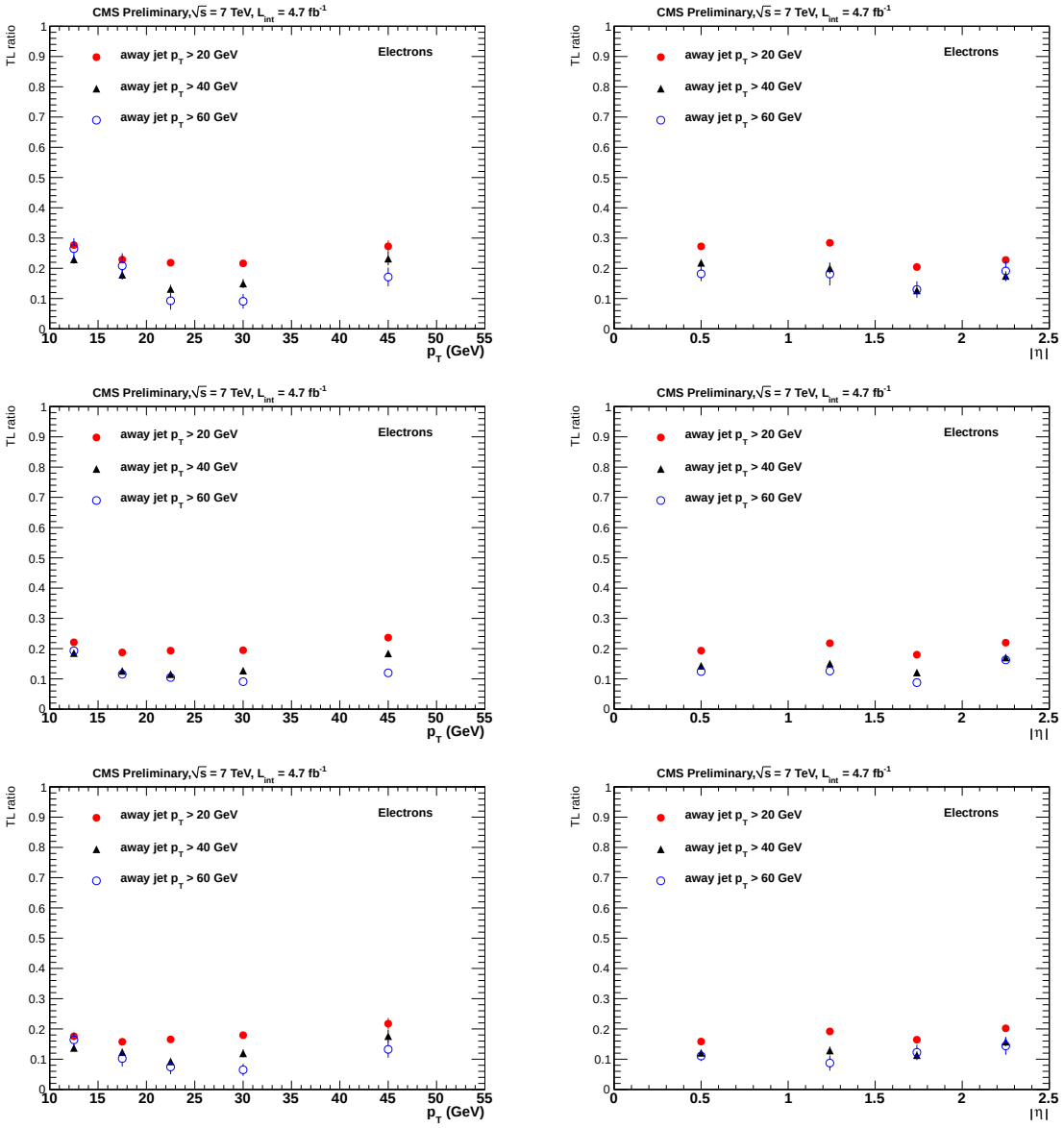

Figure 6: Electron fake rate projected on p_T (left) and $|\eta|$ (right) for electrons collected by the triggers with calorimeter and tracker isolation requirements (top), with a calorimeter isolation requirement (middle) and without an isolation requirement (bottom). The fake rates are shown separately for measurements with a requirement for an away jet p_T to be above 20 GeV (red filled circles), 40 GeV (black up triangles), and 60 GeV (blue open circles).

The application of the fake rate method to predict this background is exactly the same as in the inclusive analysis [4]. As in the inclusive same-sign analysis, the measured fake rates are restricted to $p_T < 55(35)$ GeV for electrons (muons), where we find negligible contamination from electroweak sources (W/Z production) to the sample used to extarct the fake rates. The values for the highest measured p_T range apply for all leptons with larger momenta. Measurements for lepton $p_T < 20$ GeV are given for completeness, they are not used in the analysis.

We test that the fake rates measured in QCD are applicable to the dilepton samples by performing closure tests on the simulated $t\bar{t}$ sample.[4)] Other dilepton processes with fakes, W+jets with one fake and QCD with two fakes, are expected to contribute negligibly to the events selected in this analysis; available samples for these processes do not have events passing the baseline selections. The following selections are applied to events entering the closure tests:

1. select events passing the baseline selections;
2. require that one lepton is matched to a leptonic W decay and the other (fake) lepton is not matched to a leptonic W decay;
3. scale the number of fake leptons failing the full lepton selections and passing the FO selections by $FR/(1-FR)$ as a function of the fake lepton p_T and $|\eta|$ — this is the prediction of the number of fakes passing full lepton selections;
4. compare the predicted and observed number of fake leptons.

Selection	result	ElectronFR		Muon FR	
		ee	$e\mu$	$\mu\mu$	$e\mu$
Baseline	observed	37	31	11	4
	predicted	52 ± 4	65 ± 4	17 ± 4	15 ± 3
	δ	0.29 ± 0.13	0.52 ± 0.09	0.35 ± 0.25	0.73 ± 0.14
	$\langle\delta\rangle$	0.42 ± 0.08		0.53 ± 0.14	
	$\langle\delta\rangle$	0.44 ± 0.07			

Table 9: Fake rate closure test on $t\bar{t}$ MC events. The difference δ is defined as $(p-o)/p$, where p and o are the predicted and observed counts, respectively. The number of events are as counted in the $t\bar{t}$ MC sample.

Table 9 shows the result of the closure test. Just as in the untagged analysis [4], there is a background overprediction in the $t\bar{t}$ MC. The systematic uncertainty of $\pm 50\%$ per fake lepton is estimated for the fake rate method. This value is dominated by the results of the closure tests. Our understanding of these results is that the main underlying cause is the dependence of the fake rate on parent parton momentum. The momentum spectrum of partons from ISR/FSR differs from that of the b-jets or light-flavor-quark jets ($W \to q\bar{q}'$) arising from the $t \to Wb$ decays. The mix of the spectra varies, but the range of the fake rate variation can be tested in data QCD events used to measure the fake rate by applying varying thresholds to the away jet, as illustrated in Figs. 5 and 6.

We compute the contributions from double-fake and single-fake events separately and assign a 50% systematic uncertainty on the combined estimate.

We have neglected any "signal contamination". Signal contamination enters when there is a significant source of two isolated leptons, with one or both failing the numerator cuts, but passing the denominator cuts comprising a significant fraction of the total number of $N_{n\bar{n}}$ or $N_{\overline{nn}}$ samples. Without an additional correction that can be easily applied, a contribution from events with two real same-sign dileptons failing the numerator selections will overestimate the background contribution by approximately 3% of the count of the real same-sign dileptons passing the numerator selections. Considering the size of the uncertainty on the background, this effect can be safely ignored in the estimates of the fake leptons until the rate of same-sign dileptons passing the full selections is at least an order of magnitude higher than that expected from fakes alone.

6.2 Data Driven prediction for charge mis-reconstruction backgrounds

Following our original studies [1] of the electron charge misreconstruction, we apply the requirement for electrons that all three charge measurements for a GSF electron agree. This dramatically reduces the rate of charge mis-

[4)] A large `/TTJets_TuneZ2_7TeV-madgraph-tauola/Fall11-PU_S6_START42_V14B-v2` sample with an equivalent luminosity of about 0.4 ab^{-1} is used for the closure test.

measurement for electrons to the point that this background is only $\approx 10\%$ of the total. Note that, while small, this is a much larger fraction than in the pre-tagged analysis sample, were "fake" lepton backgrounds are dominant [1, **?**, 4]. Even though this background is small, it is not necessarily well-reproduced in simulation. We apply the data-driven method used in the previous analysis[1, 2, 4] here as well.

The following steps are done:

1. Measure the probability for an electron to have its charge misreconstructed in bins of $|\eta|$ and p_T using single electron gun Monte Carlo. This is the same probability as measured in the pre-tagged same-sign sample analysis [4].

2. Calibrate this probability using Z events in data. This step should be repeated here because of the tighter isolation requirement applied to electrons.

   (a) Use a Z sample in data to control this probability. The sample is selected from dielectron events with 76 GeV $< m_{ll} <$ 106 GeV, $\not\!\!E_T$ $<$ 20 GeV, and transverse mass $<$ 25 GeV. Here transverse mass is calculated based on whichever lepton has higher p_T.

   (b) Apply this probability to the opposite sign events in this control sample to obtain a predicted number of same-sign Z candidates. Compare this with the actual yield of double-charged Z candidates to establish validity of the approach.

   (c) If the expected and observed yields agree reasonably well in the previous step, continue using the probability measured in the first step and include the discrepancy as a systematic uncertainty.

3. Apply this (calibrated) probability to all the electrons in opposite-sign dilepton events that pass the selection. This produces the data-driven charge flip prediction shown in the tables in Section 7.

4. The p_T distribution of leptons from top is slightly harder than that for leptons from Z. The calibration step above thus does not fully sample the lepton spectrum for our background sample. We assign an additional systematics of 20% to account for this effect.

In the calibration step we find 390 events with same-sign electron pairs in data in the Z control region. This needs to be compared with the sum of the expected same-sign events as estimated from opposite-sign dielectrons, 360 ± 4, plus a contribution from fakes, 11 ± 6. These comparisons are consistent within statistics and no additional data-driven correction is necessary for the simulated charge misidentification probabilities. The number of events expected directly from simulation is 393 ± 12, also in a good agreement with the numbers above. The same-sign dielectron mass distribution observed in data is compared to the expectation from simulation in Fig. 7. The total systematic uncertainty on the charge flip prediction is 20%, accounting for both the potential residual miscalibration (less than 5%) and the difference in the lepton spectra in Drell-Yan events and in the background $t\bar{t}$ events.

7 Event Yields and Background Estimation

In the following Tables 10 to 16 we summarize the background estimates and compare them to the observed counts of events in data for the baseline and search region selections defined in Sections 2 and 3. In each table the expectations from the simulation alone are given in the upper part. These are used to get a feeling of the expected contributions. Among these MC expectations, only those with actual final state isolated same-sign leptons are used for the final result as described in Section 5. The lower part of each table is the main result of the analysis used for comparisons with data and setting constraints on various models. These include the predictions for the fake-lepton and charge misidentification backgrounds derived as described in Section 6.

To reiterate and make it absolutely clear. The total background prediction in a given signal region is the sum of three distinct components:

1. The data-driven charge misidentification prediction (row "Charge Flips" in Tables 10 to 15).

2. The data-driven sum of single fakes (SF) and double fakes (DF) predictions (row "SF+DF" in Tables 10 to 15).

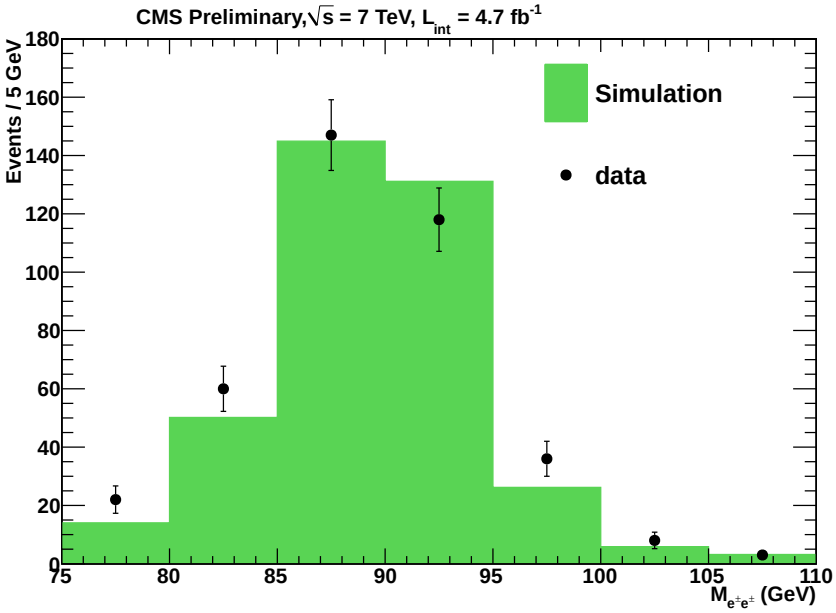

Figure 7: Same-sign ee invariant mass distribution compared with $Z \to ee$ Monte Carlo expectations. Cuts on $\not\!\!E_T < 20$ GeV and transverse mass < 25 GeV have been applied to reduce backgrounds from $W+$ jets. The highest p_T lepton has been used in the calculation of the transverse mass.

3. The total MC prediction for processes that naturally give isolated same-sign dileptons, see Section 5 (row "MC Pred" in Tables 10 to 15; this is the sum of the rows starting from "$V\gamma$" down to and including the tribosons – although in practice only ttW and ttZ matter). Note that for the dominant physics backgrounds we normalized the MC to $\sigma(pp \to ttW) = 0.1633 \pm 0.082$ pb and $\sigma(pp \to ttZ) = 0.139 \pm 0.070$ pb.

Details on the systematics of the background predictions are given in the corresponding sections. The final estimates on these uncertainties are rather simple:

1. The charge flip contribution has a 20% systematic.
2. The predicted number of fakes has a 50% systematic in all modes.
3. The MC prediction for "real" same-sign isolated dileptons has an uncertainty of 50%.

Source	ee	$\mu\mu$	eμ	all
$t\bar{t} \to \ell\ell X$	0.604 ± 0.102	0.000 ± 0.013	0.653 ± 0.105	1.256 ± 0.147
$t\bar{t}$ other	0.000 ± 0.013	0.000 ± 0.013	0.000 ± 0.013	0.000 ± 0.013
$t\bar{t} \to \ell(b \to \ell)X$	0.069 ± 0.035	0.140 ± 0.049	0.094 ± 0.043	0.303 ± 0.074
$t\bar{t} \to \ell(\not{b} \to \ell)X$	0.546 ± 0.095	0.020 ± 0.017	0.628 ± 0.108	1.195 ± 0.145
t, s-channel	0.000 ± 0.057	0.000 ± 0.057	0.000 ± 0.057	0.000 ± 0.057
t, t-channel	0.077 ± 0.077	0.000 ± 0.055	0.000 ± 0.055	0.077 ± 0.077
tW	0.000 ± 0.045	0.000 ± 0.045	0.016 ± 0.045	0.016 ± 0.045
$Z \to ee$	0.000 ± 0.429	0.000 ± 0.429	0.000 ± 0.429	0.000 ± 0.429
$Z \to \mu\mu$	0.000 ± 0.429	0.000 ± 0.429	0.000 ± 0.429	0.000 ± 0.429
$Z \to \tau\tau$	0.000 ± 0.429	0.000 ± 0.429	0.000 ± 0.429	0.000 ± 0.429
W+jets	0.000 ± 1.808	0.000 ± 1.808	0.000 ± 1.808	0.000 ± 1.808
WW	0.000 ± 0.019	0.000 ± 0.019	0.000 ± 0.019	0.000 ± 0.019
Vγ	0.000 ± 0.248	0.000 ± 0.248	0.000 ± 0.248	0.000 ± 0.248
$W\gamma^* \to \ell\nu ee$	0.000 ± 0.097	0.000 ± 0.097	0.000 ± 0.097	0.000 ± 0.097
$W\gamma^* \to \ell\nu\mu\mu$	0.000 ± 0.075	0.000 ± 0.075	0.000 ± 0.075	0.000 ± 0.075
$W\gamma^* \to \ell\nu\tau\tau$	0.000 ± 0.028	0.000 ± 0.028	0.000 ± 0.028	0.000 ± 0.028
WZ	0.034 ± 0.012	0.017 ± 0.008	0.031 ± 0.012	0.082 ± 0.019
ZZ	0.000 ± 0.000	0.001 ± 0.001	0.002 ± 0.001	0.003 ± 0.001
dp$W^{\pm}W^{\pm}$	0.000 ± 0.004	0.000 ± 0.004	0.000 ± 0.004	0.000 ± 0.004
spW^-W^-	0.000 ± 0.001	0.000 ± 0.001	0.003 ± 0.002	0.003 ± 0.002
spW^+W^+	0.000 ± 0.006	0.000 ± 0.006	0.000 ± 0.006	0.000 ± 0.006
$t\bar{t}\gamma$	0.000 ± 0.059	0.000 ± 0.059	0.000 ± 0.059	0.000 ± 0.059
$t\bar{t}W$	0.572 ± 0.025	0.733 ± 0.028	1.284 ± 0.038	2.590 ± 0.053
$t\bar{t}Z$	0.120 ± 0.009	0.159 ± 0.010	0.271 ± 0.013	0.549 ± 0.019
$WW\gamma$	0.000 ± 0.015	0.000 ± 0.015	0.000 ± 0.015	0.000 ± 0.015
WWW	0.001 ± 0.000	0.001 ± 0.000	0.001 ± 0.001	0.003 ± 0.001
WWZ	0.000 ± 0.000	0.000 ± 0.000	0.001 ± 0.001	0.001 ± 0.001
WZZ	0.000 ± 0.000	0.001 ± 0.000	0.001 ± 0.000	0.002 ± 0.001
ZZZ	0.000 ± 0.000	0.000 ± 0.000	0.000 ± 0.000	0.000 ± 0.000
Total MC	2.023 ± 0.166	1.072 ± 0.060	2.984 ± 0.163	6.079 ± 0.240
LM6	0.000 ± 0.000	0.186 ± 0.186	0.383 ± 0.275	0.569 ± 0.332
SF	1.13 ± 0.67	0.30 ± 0.20	1.92 ± 0.74	3.36 ± 1.02
DF	0.04 ± 0.12	0.02 ± 0.02	0.02 ± 0.09	0.08 ± 0.16
SF + DF	$1.17 \pm 0.63 \pm 0.58$	$0.32 \pm 0.20 \pm 0.16$	$1.95 \pm 0.72 \pm 0.97$	$3.43 \pm 0.98 \pm 1.72$
Charge Flips	$0.509 \pm 0.036 \pm 0.102$	- $\pm$ -	$0.544 \pm 0.032 \pm 0.109$	$1.053 \pm 0.048 \pm 0.211$
MC Pred	$0.727 \pm 0.029 \pm 0.364$	$0.913 \pm 0.031 \pm 0.456$	$1.596 \pm 0.042 \pm 0.798$	$3.235 \pm 0.059 \pm 1.618$
Total Pred	$2.403 \pm 0.633 \pm 0.695$	$1.234 \pm 0.199 \pm 0.484$	$4.087 \pm 0.725 \pm 1.263$	$7.724 \pm 0.983 \pm 2.369$
data	2	2	3	7

Table 10: Observed event yields in baseline ($\not\!\!E_T >$ 30 GeV, at least 2 jets with p_T $>$ 40 GeV, and at least two of these jets b-tagged using SSVHEM) high-p_T (p_T $>$ 20/20) dileptons compared to expectations from simulation alone, and from the data-driven methods. The upper part of the table is based on simulation only and is used only as a reference. The lower part is the main result of the analysis. The SF (DF) contributions are for events with one (two) fake leptons. The *MC Pred* contribution includes contributions from genuine same-sign lepton pairs (a sum of the rows from $V\gamma$ down to ZZZ). Entries with zero contributing events are reported with an uncertainty corresponding to one event. This uncertainty is not added to the total MC contribution. Systematic uncertainties (the second uncertainty if present) are displayed only for the final combined type of background, no systematic uncertainty is added for estimates with zero entries. Systematic uncertainties are 100% correlated among the channels.

Source	ee	$\mu\mu$	eμ	all
$t\bar{t} \to \ell\ell X$	0.380 ± 0.083	0.000 ± 0.013	0.414 ± 0.085	0.794 ± 0.119
$t\bar{t}$ other	0.000 ± 0.013	0.000 ± 0.013	0.000 ± 0.013	0.000 ± 0.013
$t\bar{t} \to \ell(b \to \ell)X$	0.038 ± 0.028	0.094 ± 0.041	0.025 ± 0.025	0.157 ± 0.055
$t\bar{t} \to \ell(\not{b} \to \ell)X$	0.343 ± 0.077	0.004 ± 0.013	0.321 ± 0.075	0.669 ± 0.108
t, s-channel	0.000 ± 0.057	0.000 ± 0.057	0.000 ± 0.057	0.000 ± 0.057
t, t-channel	0.000 ± 0.055	0.000 ± 0.055	0.000 ± 0.055	0.000 ± 0.055
tW	0.000 ± 0.045	0.000 ± 0.045	0.000 ± 0.045	0.000 ± 0.045
$Z \to ee$	0.000 ± 0.429	0.000 ± 0.429	0.000 ± 0.429	0.000 ± 0.429
$Z \to \mu\mu$	0.000 ± 0.429	0.000 ± 0.429	0.000 ± 0.429	0.000 ± 0.429
$Z \to \tau\tau$	0.000 ± 0.429	0.000 ± 0.429	0.000 ± 0.429	0.000 ± 0.429
W+jets	0.000 ± 1.808	0.000 ± 1.808	0.000 ± 1.808	0.000 ± 1.808
WW	0.000 ± 0.019	0.000 ± 0.019	0.000 ± 0.019	0.000 ± 0.019
Vγ	0.000 ± 0.248	0.000 ± 0.248	0.000 ± 0.248	0.000 ± 0.248
$W\gamma^* \to \ell\nu ee$	0.000 ± 0.097	0.000 ± 0.097	0.000 ± 0.097	0.000 ± 0.097
$W\gamma^* \to \ell\nu\mu\mu$	0.000 ± 0.075	0.000 ± 0.075	0.000 ± 0.075	0.000 ± 0.075
$W\gamma^* \to \ell\nu\tau\tau$	0.000 ± 0.028	0.000 ± 0.028	0.000 ± 0.028	0.000 ± 0.028
WZ	0.011 ± 0.006	0.005 ± 0.004	0.015 ± 0.007	0.031 ± 0.011
ZZ	0.000 ± 0.000	0.000 ± 0.000	0.001 ± 0.001	0.001 ± 0.001
dp$W^{\pm}W^{\pm}$	0.000 ± 0.004	0.000 ± 0.004	0.000 ± 0.004	0.000 ± 0.004
spW^-W^-	0.000 ± 0.001	0.000 ± 0.001	0.000 ± 0.001	0.000 ± 0.001
spW^+W^+	0.000 ± 0.006	0.000 ± 0.006	0.000 ± 0.006	0.000 ± 0.006
$t\bar{t}\gamma$	0.000 ± 0.059	0.000 ± 0.059	0.000 ± 0.059	0.000 ± 0.059
$t\bar{t}W$	0.422 ± 0.021	0.503 ± 0.023	0.898 ± 0.031	1.823 ± 0.044
$t\bar{t}Z$	0.058 ± 0.006	0.075 ± 0.007	0.134 ± 0.009	0.267 ± 0.013
$WW\gamma$	0.000 ± 0.015	0.000 ± 0.015	0.000 ± 0.015	0.000 ± 0.015
WWW	0.000 ± 0.000	0.001 ± 0.000	0.001 ± 0.000	0.002 ± 0.001
WWZ	0.000 ± 0.000	0.000 ± 0.000	0.000 ± 0.000	0.000 ± 0.000
WZZ	0.000 ± 0.000	0.001 ± 0.000	0.000 ± 0.000	0.001 ± 0.001
ZZZ	0.000 ± 0.000	0.000 ± 0.000	0.000 ± 0.000	0.000 ± 0.000
Total MC	1.254 ± 0.119	0.683 ± 0.048	1.809 ± 0.120	3.746 ± 0.176
LM6	0.000 ± 0.000	0.186 ± 0.186	0.224 ± 0.224	0.410 ± 0.291
SF	0.06 ± 0.50	0.30 ± 0.20	1.32 ± 0.66	1.69 ± 0.85
DF	0.04 ± 0.12	0.02 ± 0.02	0.02 ± 0.09	0.08 ± 0.16
SF + DF	$0.10 \pm 0.45 \pm 0.05$	$0.32 \pm 0.20 \pm 0.16$	$1.34 \pm 0.64 \pm 0.67$	$1.76 \pm 0.80 \pm 0.88$
Charge Flips	$0.255 \pm 0.018 \pm 0.051$	- $\pm$ -	$0.272 \pm 0.016 \pm 0.054$	$0.527 \pm 0.024 \pm 0.105$
MC Pred	$0.492 \pm 0.023 \pm 0.246$	$0.585 \pm 0.024 \pm 0.293$	$1.049 \pm 0.034 \pm 0.525$	$2.127 \pm 0.047 \pm 1.064$
Total Pred	$0.848 \pm 0.450 \pm 0.256$	$0.906 \pm 0.198 \pm 0.334$	$2.663 \pm 0.637 \pm 0.853$	$4.417 \pm 0.804 \pm 1.385$
data	2	1	2	5

Table 11: Observed event yields in the "++" search region (baseline selection with both leptons positively charged) compared to expectations from simulation alone, and from the data-driven methods. The upper part of the table is based on simulation only and is used only as a reference. The lower part is the main result of the analysis. The SF (DF) contributions are for events with one (two) fake leptons. The *MC Pred* contribution includes contributions from genuine same-sign lepton pairs (a sum of the rows from $V\gamma$ down to ZZZ). Entries with zero contributing events are reported with an uncertainty corresponding to one event. This uncertainty is not added to the total MC contribution. Systematic uncertainties (the second uncertainty if present) are displayed only for the final combined type of background, no systematic uncertainty is added for estimates with zero entries. Systematic uncertainties are 100% correlated among the channels.

Source	ee	$\mu\mu$	eμ	all
$t\bar{t} \to \ell\ell X$	0.017 ± 0.013	0.000 ± 0.013	0.017 ± 0.017	0.034 ± 0.021
$t\bar{t}$ other	0.000 ± 0.013	0.000 ± 0.013	0.000 ± 0.013	0.000 ± 0.013
$t\bar{t} \to \ell(b \to \ell)X$	0.000 ± 0.013	0.020 ± 0.020	0.000 ± 0.013	0.020 ± 0.020
$t\bar{t} \to \ell(\not{b} \to \ell)X$	0.059 ± 0.030	0.000 ± 0.013	0.099 ± 0.040	0.157 ± 0.050
t, s-channel	0.000 ± 0.057	0.000 ± 0.057	0.000 ± 0.057	0.000 ± 0.057
t, t-channel	0.000 ± 0.055	0.000 ± 0.055	0.000 ± 0.055	0.000 ± 0.055
tW	0.000 ± 0.045	0.000 ± 0.045	0.000 ± 0.045	0.000 ± 0.045
$Z \to ee$	0.000 ± 0.429	0.000 ± 0.429	0.000 ± 0.429	0.000 ± 0.429
$Z \to \mu\mu$	0.000 ± 0.429	0.000 ± 0.429	0.000 ± 0.429	0.000 ± 0.429
$Z \to \tau\tau$	0.000 ± 0.429	0.000 ± 0.429	0.000 ± 0.429	0.000 ± 0.429
W+jets	0.000 ± 1.808	0.000 ± 1.808	0.000 ± 1.808	0.000 ± 1.808
WW	0.000 ± 0.019	0.000 ± 0.019	0.000 ± 0.019	0.000 ± 0.019
Vγ	0.000 ± 0.248	0.000 ± 0.248	0.000 ± 0.248	0.000 ± 0.248
$W\gamma^* \to \ell\nu ee$	0.000 ± 0.097	0.000 ± 0.097	0.000 ± 0.097	0.000 ± 0.097
$W\gamma^* \to \ell\nu\mu\mu$	0.000 ± 0.075	0.000 ± 0.075	0.000 ± 0.075	0.000 ± 0.075
$W\gamma^* \to \ell\nu\tau\tau$	0.000 ± 0.028	0.000 ± 0.028	0.000 ± 0.028	0.000 ± 0.028
WZ	0.010 ± 0.007	0.001 ± 0.003	0.000 ± 0.003	0.011 ± 0.007
ZZ	0.000 ± 0.000	0.000 ± 0.000	0.001 ± 0.001	0.001 ± 0.001
dp$W^{\pm}W^{\pm}$	0.000 ± 0.004	0.000 ± 0.004	0.000 ± 0.004	0.000 ± 0.004
sp$W^{-}W^{-}$	0.000 ± 0.001	0.000 ± 0.001	0.001 ± 0.001	0.001 ± 0.001
sp$W^{+}W^{+}$	0.000 ± 0.006	0.000 ± 0.006	0.000 ± 0.006	0.000 ± 0.006
$t\bar{t}\gamma$	0.000 ± 0.059	0.000 ± 0.059	0.000 ± 0.059	0.000 ± 0.059
$t\bar{t}W$	0.098 ± 0.010	0.121 ± 0.011	0.244 ± 0.016	0.463 ± 0.022
$t\bar{t}Z$	0.016 ± 0.003	0.023 ± 0.004	0.041 ± 0.005	0.080 ± 0.007
$WW\gamma$	0.000 ± 0.015	0.000 ± 0.015	0.000 ± 0.015	0.000 ± 0.015
WWW	0.000 ± 0.000	0.000 ± 0.000	0.000 ± 0.000	0.001 ± 0.000
WWZ	0.000 ± 0.000	0.000 ± 0.000	0.000 ± 0.000	0.000 ± 0.000
WZZ	0.000 ± 0.000	0.000 ± 0.000	0.000 ± 0.000	0.000 ± 0.000
ZZZ	0.000 ± 0.000	0.000 ± 0.000	0.000 ± 0.000	0.000 ± 0.000
Total MC	0.199 ± 0.035	0.165 ± 0.023	0.404 ± 0.047	0.768 ± 0.063
LM6	0.000 ± 0.000	0.186 ± 0.186	0.383 ± 0.275	0.569 ± 0.332
SF	0.00 ± 0.58	0.00 ± 0.37	0.32 ± 0.57	0.32 ± 0.57
DF	0.00 ± 0.14	0.00 ± 0.10	0.00 ± 0.16	0.00 ± 0.16
SF + DF	$0.00 \pm 0.50 \pm 0.00$	$0.00 \pm 0.31 \pm 0.00$	$0.32 \pm 0.47 \pm 0.16$	$0.32 \pm 0.47 \pm 0.16$
Charge Flips	$0.023 \pm 0.007 \pm 0.005$	- $\pm$ -	$0.022 \pm 0.006 \pm 0.004$	$0.045 \pm 0.009 \pm 0.009$
MC Pred	$0.123 \pm 0.013 \pm 0.062$	$0.145 \pm 0.012 \pm 0.073$	$0.288 \pm 0.017 \pm 0.144$	$0.557 \pm 0.024 \pm 0.278$
Total Pred	$0.146 \pm 0.501 \pm 0.062$	$0.145 \pm 0.315 \pm 0.073$	$0.635 \pm 0.474 \pm 0.217$	$0.926 \pm 0.474 \pm 0.322$
data	1	0	1	2

Table 12: Observed event yields in the low-H_T high-$\not{E}_T$ region ($H_T > 200$ GeV, $\not{E}_T >$ 120 GeV) compared to expectations from simulation alone, and from the data-driven methods. The upper part of the table is based on simulation only and is used only as a reference. The lower part is the main result of the analysis. The SF (DF) contributions are for events with one (two) fake leptons. The *MC Pred* contribution includes contributions from genuine same-sign lepton pairs (a sum of the rows from $V\gamma$ down to ZZZ). Entries with zero contributing events are reported with an uncertainty corresponding to one event. This uncertainty is not added to the total MC contribution. Systematic uncertainties (the second uncertainty if present) are displayed only for the final combined type of background, no systematic uncertainty is added for estimates with zero entries. Systematic uncertainties are 100% correlated among the channels.

Source	ee	$\mu\mu$	eμ	all
$t\bar{t} \to \ell\ell X$	0.235 ± 0.065	0.000 ± 0.013	0.159 ± 0.054	0.394 ± 0.084
$t\bar{t}$ other	0.000 ± 0.013	0.000 ± 0.013	0.000 ± 0.013	0.000 ± 0.013
$t\bar{t} \to \ell(b \to \ell)X$	0.042 ± 0.030	0.054 ± 0.029	0.044 ± 0.031	0.140 ± 0.052
$t\bar{t} \to \ell(\not{b} \to \ell)X$	0.270 ± 0.067	0.016 ± 0.016	0.386 ± 0.086	0.672 ± 0.110
t, s-channel	0.000 ± 0.057	0.000 ± 0.057	0.000 ± 0.057	0.000 ± 0.057
t, t-channel	0.000 ± 0.055	0.000 ± 0.055	0.000 ± 0.055	0.000 ± 0.055
tW	0.000 ± 0.045	0.000 ± 0.045	0.016 ± 0.045	0.016 ± 0.045
$Z \to ee$	0.000 ± 0.429	0.000 ± 0.429	0.000 ± 0.429	0.000 ± 0.429
$Z \to \mu\mu$	0.000 ± 0.429	0.000 ± 0.429	0.000 ± 0.429	0.000 ± 0.429
$Z \to \tau\tau$	0.000 ± 0.429	0.000 ± 0.429	0.000 ± 0.429	0.000 ± 0.429
W+jets	0.000 ± 1.808	0.000 ± 1.808	0.000 ± 1.808	0.000 ± 1.808
WW	0.000 ± 0.019	0.000 ± 0.019	0.000 ± 0.019	0.000 ± 0.019
Vγ	0.000 ± 0.248	0.000 ± 0.248	0.000 ± 0.248	0.000 ± 0.248
$W\gamma^* \to \ell\nu ee$	0.000 ± 0.097	0.000 ± 0.097	0.000 ± 0.097	0.000 ± 0.097
$W\gamma^* \to \ell\nu\mu\mu$	0.000 ± 0.075	0.000 ± 0.075	0.000 ± 0.075	0.000 ± 0.075
$W\gamma^* \to \ell\nu\tau\tau$	0.000 ± 0.028	0.000 ± 0.028	0.000 ± 0.028	0.000 ± 0.028
WZ	0.019 ± 0.009	0.013 ± 0.007	0.010 ± 0.006	0.042 ± 0.013
ZZ	0.000 ± 0.000	0.000 ± 0.000	0.001 ± 0.001	0.001 ± 0.001
dp$W^{\pm}W^{\pm}$	0.000 ± 0.004	0.000 ± 0.004	0.000 ± 0.004	0.000 ± 0.004
spW^-W^-	0.000 ± 0.001	0.000 ± 0.001	0.003 ± 0.002	0.003 ± 0.002
spW^+W^+	0.000 ± 0.006	0.000 ± 0.006	0.000 ± 0.006	0.000 ± 0.006
$t\bar{t}\gamma$	0.000 ± 0.059	0.000 ± 0.059	0.000 ± 0.059	0.000 ± 0.059
$t\bar{t}W$	0.376 ± 0.020	0.430 ± 0.021	0.768 ± 0.029	1.574 ± 0.041
$t\bar{t}Z$	0.066 ± 0.007	0.099 ± 0.008	0.162 ± 0.010	0.327 ± 0.015
$WW\gamma$	0.000 ± 0.015	0.000 ± 0.015	0.000 ± 0.015	0.000 ± 0.015
WWW	0.000 ± 0.000	0.000 ± 0.000	0.001 ± 0.001	0.002 ± 0.001
WWZ	0.000 ± 0.000	0.000 ± 0.000	0.001 ± 0.001	0.001 ± 0.001
WZZ	0.000 ± 0.000	0.000 ± 0.000	0.000 ± 0.000	0.001 ± 0.000
ZZZ	0.000 ± 0.000	0.000 ± 0.000	0.000 ± 0.000	0.000 ± 0.000
Total MC	1.008 ± 0.100	0.612 ± 0.041	1.552 ± 0.112	3.172 ± 0.156
LM6	0.000 ± 0.000	0.186 ± 0.186	0.383 ± 0.275	0.569 ± 0.332
SF	0.51 ± 0.59	0.00 ± 0.37	0.98 ± 0.67	1.49 ± 0.85
DF	0.00 ± 0.14	0.00 ± 0.10	0.00 ± 0.16	0.00 ± 0.16
SF + DF	$0.51 \pm 0.51 \pm 0.25$	$0.00 \pm 0.31 \pm 0.00$	$0.98 \pm 0.60 \pm 0.49$	$1.49 \pm 0.79 \pm 0.75$
Charge Flips	$0.122 \pm 0.017 \pm 0.024$	- $\pm$ -	$0.158 \pm 0.017 \pm 0.032$	$0.281 \pm 0.024 \pm 0.056$
MC Pred	$0.462 \pm 0.024 \pm 0.231$	$0.542 \pm 0.024 \pm 0.271$	$0.948 \pm 0.031 \pm 0.474$	$1.952 \pm 0.046 \pm 0.976$
Total Pred	$1.093 \pm 0.512 \pm 0.345$	$0.542 \pm 0.315 \pm 0.271$	$2.087 \pm 0.597 \pm 0.683$	$3.723 \pm 0.787 \pm 1.229$
data	2	1	2	5

Table 13: Observed event yields in the low-H_T low-$\not{E}_T$ region ($H_T > 200$ GeV, $\not{E}_T >$ 50 GeV) compared to expectations from simulation alone, and from the data-driven methods. The upper part of the table is based on simulation only and is used only as a reference. The lower part is the main result of the analysis. The SF (DF) contributions are for events with one (two) fake leptons. The *MC Pred* contribution includes contributions from genuine same-sign lepton pairs (a sum of the rows from $V\gamma$ down to ZZZ). Entries with zero contributing events are reported with an uncertainty corresponding to one event. This uncertainty is not added to the total MC contribution. Systematic uncertainties (the second uncertainty if present) are displayed only for the final combined type of background, no systematic uncertainty is added for estimates with zero entries. Systematic uncertainties are 100% correlated among the channels.

Source	ee	$\mu\mu$	eμ	all
$t\bar{t} \to \ell\ell X$	0.067 ± 0.031	0.000 ± 0.013	0.078 ± 0.040	0.146 ± 0.050
$t\bar{t}$ other	0.000 ± 0.013	0.000 ± 0.013	0.000 ± 0.013	0.000 ± 0.013
$t\bar{t} \to \ell(b \to \ell)X$	0.025 ± 0.025	0.040 ± 0.026	0.019 ± 0.019	0.085 ± 0.041
$t\bar{t} \to \ell(\not{b} \to \ell)X$	0.109 ± 0.043	0.016 ± 0.016	0.188 ± 0.060	0.313 ± 0.076
t, s-channel	0.000 ± 0.057	0.000 ± 0.057	0.000 ± 0.057	0.000 ± 0.057
t, t-channel	0.000 ± 0.055	0.000 ± 0.055	0.000 ± 0.055	0.000 ± 0.055
tW	0.000 ± 0.045	0.000 ± 0.045	0.000 ± 0.045	0.000 ± 0.045
$Z \to ee$	0.000 ± 0.429	0.000 ± 0.429	0.000 ± 0.429	0.000 ± 0.429
$Z \to \mu\mu$	0.000 ± 0.429	0.000 ± 0.429	0.000 ± 0.429	0.000 ± 0.429
$Z \to \tau\tau$	0.000 ± 0.429	0.000 ± 0.429	0.000 ± 0.429	0.000 ± 0.429
W+jets	0.000 ± 1.808	0.000 ± 1.808	0.000 ± 1.808	0.000 ± 1.808
WW	0.000 ± 0.019	0.000 ± 0.019	0.000 ± 0.019	0.000 ± 0.019
Vγ	0.000 ± 0.248	0.000 ± 0.248	0.000 ± 0.248	0.000 ± 0.248
$W\gamma^* \to \ell\nu ee$	0.000 ± 0.097	0.000 ± 0.097	0.000 ± 0.097	0.000 ± 0.097
$W\gamma^* \to \ell\nu\mu\mu$	0.000 ± 0.075	0.000 ± 0.075	0.000 ± 0.075	0.000 ± 0.075
$W\gamma^* \to \ell\nu\tau\tau$	0.000 ± 0.028	0.000 ± 0.028	0.000 ± 0.028	0.000 ± 0.028
WZ	0.009 ± 0.006	0.001 ± 0.003	0.006 ± 0.004	0.016 ± 0.008
ZZ	0.000 ± 0.000	0.000 ± 0.000	0.000 ± 0.000	0.000 ± 0.000
dp$W^{\pm}W^{\pm}$	0.000 ± 0.004	0.000 ± 0.004	0.000 ± 0.004	0.000 ± 0.004
sp$W^{-}W^{-}$	0.000 ± 0.001	0.000 ± 0.001	0.001 ± 0.001	0.001 ± 0.001
sp$W^{+}W^{+}$	0.000 ± 0.006	0.000 ± 0.006	0.000 ± 0.006	0.000 ± 0.006
$t\bar{t}\gamma$	0.000 ± 0.059	0.000 ± 0.059	0.000 ± 0.059	0.000 ± 0.059
$t\bar{t}W$	0.201 ± 0.015	0.214 ± 0.015	0.414 ± 0.021	0.829 ± 0.030
$t\bar{t}Z$	0.037 ± 0.005	0.055 ± 0.006	0.094 ± 0.008	0.187 ± 0.011
$WW\gamma$	0.000 ± 0.015	0.000 ± 0.015	0.000 ± 0.015	0.000 ± 0.015
WWW	0.000 ± 0.000	0.000 ± 0.000	0.001 ± 0.001	0.002 ± 0.001
WWZ	0.000 ± 0.000	0.000 ± 0.000	0.000 ± 0.000	0.000 ± 0.000
WZZ	0.000 ± 0.000	0.000 ± 0.000	0.000 ± 0.000	0.000 ± 0.000
ZZZ	0.000 ± 0.000	0.000 ± 0.000	0.000 ± 0.000	0.000 ± 0.000
Total MC	0.449 ± 0.061	0.327 ± 0.034	0.803 ± 0.078	1.579 ± 0.105
LM6	0.000 ± 0.000	0.186 ± 0.186	0.383 ± 0.275	0.569 ± 0.332
SF	0.27 ± 0.54	0.00 ± 0.37	0.54 ± 0.59	0.81 ± 0.74
DF	0.00 ± 0.14	0.00 ± 0.10	0.00 ± 0.16	0.00 ± 0.16
SF + DF	$0.27 \pm 0.45 \pm 0.14$	$0.00 \pm 0.31 \pm 0.00$	$0.54 \pm 0.50 \pm 0.27$	$0.81 \pm 0.67 \pm 0.40$
Charge Flips	$0.049 \pm 0.011 \pm 0.010$	- $\pm$ -	$0.069 \pm 0.012 \pm 0.014$	$0.118 \pm 0.016 \pm 0.024$
MC Pred	$0.247 \pm 0.017 \pm 0.124$	$0.271 \pm 0.016 \pm 0.136$	$0.518 \pm 0.023 \pm 0.259$	$1.036 \pm 0.033 \pm 0.518$
Total Pred	$0.569 \pm 0.453 \pm 0.185$	$0.271 \pm 0.315 \pm 0.136$	$1.122 \pm 0.496 \pm 0.373$	$1.962 \pm 0.672 \pm 0.658$
data	1	1	0	2

Table 14: Observed event yields in the high-H_T low-$\not{E}_T$ region ($H_T > 320$ GeV, $\not{E}_T > 50$ GeV) compared to expectations from simulation alone, and from the data-driven methods. The upper part of the table is based on simulation only and is used only as a reference. The lower part is the main result of the analysis. The SF (DF) contributions are for events with one (two) fake leptons. The *MC Pred* contribution includes contributions from genuine same-sign lepton pairs (a sum of the rows from $V\gamma$ down to ZZZ). Entries with zero contributing events are reported with an uncertainty corresponding to one event. This uncertainty is not added to the total MC contribution. Systematic uncertainties (the second uncertainty if present) are displayed only for the final combined type of background, no systematic uncertainty is added for estimates with zero entries. Systematic uncertainties are 100% correlated among the channels.

Source	ee	$\mu\mu$	eμ	all
$t\bar{t} \to \ell\ell X$	0.000 ± 0.013	0.000 ± 0.013	0.017 ± 0.017	0.017 ± 0.017
$t\bar{t}$ other	0.000 ± 0.013	0.000 ± 0.013	0.000 ± 0.013	0.000 ± 0.013
$t\bar{t} \to \ell(b \to \ell)X$	0.000 ± 0.013	0.020 ± 0.020	0.000 ± 0.013	0.020 ± 0.020
$t\bar{t} \to \ell(\not{b} \to \ell)X$	0.033 ± 0.023	0.000 ± 0.013	0.050 ± 0.029	0.082 ± 0.037
t, s-channel	0.000 ± 0.057	0.000 ± 0.057	0.000 ± 0.057	0.000 ± 0.057
t, t-channel	0.000 ± 0.055	0.000 ± 0.055	0.000 ± 0.055	0.000 ± 0.055
tW	0.000 ± 0.045	0.000 ± 0.045	0.000 ± 0.045	0.000 ± 0.045
$Z \to ee$	0.000 ± 0.429	0.000 ± 0.429	0.000 ± 0.429	0.000 ± 0.429
$Z \to \mu\mu$	0.000 ± 0.429	0.000 ± 0.429	0.000 ± 0.429	0.000 ± 0.429
$Z \to \tau\tau$	0.000 ± 0.429	0.000 ± 0.429	0.000 ± 0.429	0.000 ± 0.429
W+jets	0.000 ± 1.808	0.000 ± 1.808	0.000 ± 1.808	0.000 ± 1.808
WW	0.000 ± 0.019	0.000 ± 0.019	0.000 ± 0.019	0.000 ± 0.019
Vγ	0.000 ± 0.248	0.000 ± 0.248	0.000 ± 0.248	0.000 ± 0.248
$W\gamma^* \to \ell\nu ee$	0.000 ± 0.097	0.000 ± 0.097	0.000 ± 0.097	0.000 ± 0.097
$W\gamma^* \to \ell\nu\mu\mu$	0.000 ± 0.075	0.000 ± 0.075	0.000 ± 0.075	0.000 ± 0.075
$W\gamma^* \to \ell\nu\tau\tau$	0.000 ± 0.028	0.000 ± 0.028	0.000 ± 0.028	0.000 ± 0.028
WZ	0.004 ± 0.004	0.001 ± 0.003	0.000 ± 0.003	0.006 ± 0.005
ZZ	0.000 ± 0.000	0.000 ± 0.000	0.000 ± 0.000	0.000 ± 0.000
dp$W^{\pm}W^{\pm}$	0.000 ± 0.004	0.000 ± 0.004	0.000 ± 0.004	0.000 ± 0.004
sp$W^{-}W^{-}$	0.000 ± 0.001	0.000 ± 0.001	0.001 ± 0.001	0.001 ± 0.001
sp$W^{+}W^{+}$	0.000 ± 0.006	0.000 ± 0.006	0.000 ± 0.006	0.000 ± 0.006
$t\bar{t}\gamma$	0.000 ± 0.059	0.000 ± 0.059	0.000 ± 0.059	0.000 ± 0.059
$t\bar{t}W$	0.070 ± 0.009	0.080 ± 0.009	0.168 ± 0.013	0.317 ± 0.018
$t\bar{t}Z$	0.013 ± 0.003	0.015 ± 0.003	0.032 ± 0.005	0.060 ± 0.006
$WW\gamma$	0.000 ± 0.015	0.000 ± 0.015	0.000 ± 0.015	0.000 ± 0.015
WWW	0.000 ± 0.000	0.000 ± 0.000	0.000 ± 0.000	0.001 ± 0.000
WWZ	0.000 ± 0.000	0.000 ± 0.000	0.000 ± 0.000	0.000 ± 0.000
WZZ	0.000 ± 0.000	0.000 ± 0.000	0.000 ± 0.000	0.000 ± 0.000
ZZZ	0.000 ± 0.000	0.000 ± 0.000	0.000 ± 0.000	0.000 ± 0.000
Total MC	0.120 ± 0.025	0.116 ± 0.022	0.269 ± 0.036	0.504 ± 0.049
LM6	0.000 ± 0.000	0.186 ± 0.186	0.383 ± 0.275	0.569 ± 0.332
SF	0.00 ± 0.58	0.00 ± 0.37	0.15 ± 0.54	0.15 ± 0.54
DF	0.00 ± 0.14	0.00 ± 0.10	0.00 ± 0.16	0.00 ± 0.16
SF + DF	$0.00 \pm 0.50 \pm 0.00$	$0.00 \pm 0.31 \pm 0.00$	$0.15 \pm 0.44 \pm 0.07$	$0.15 \pm 0.44 \pm 0.07$
Charge Flips	$0.014 \pm 0.006 \pm 0.003$	- $\pm$ -	$0.011 \pm 0.005 \pm 0.002$	$0.026 \pm 0.008 \pm 0.005$
MC Pred	$0.087 \pm 0.010 \pm 0.044$	$0.096 \pm 0.010 \pm 0.048$	$0.202 \pm 0.014 \pm 0.101$	$0.385 \pm 0.020 \pm 0.193$
Total Pred	$0.101 \pm 0.501 \pm 0.044$	$0.096 \pm 0.315 \pm 0.048$	$0.363 \pm 0.438 \pm 0.126$	$0.560 \pm 0.438 \pm 0.207$
data	0	0	0	0

Table 15: Observed event yields in the high-H_T high-$\not{E}_T$ region ($H_T > 320$ GeV, $\not{E}_T > 120$ GeV) compared to expectations from simulation alone, and from the data-driven methods. The upper part of the table is based on simulation only and is used only as a reference. The lower part is the main result of the analysis. The SF (DF) contributions are for events with one (two) fake leptons. The *MC Pred* contribution includes contributions from genuine same-sign lepton pairs (a sum of the rows from $V\gamma$ down to ZZZ). Entries with zero contributing events are reported with an uncertainty corresponding to one event. This uncertainty is not added to the total MC contribution. Systematic uncertainties (the second uncertainty if present) are displayed only for the final combined type of background, no systematic uncertainty is added for estimates with zero entries. Systematic uncertainties are 100% correlated among the channels.

Source	ee	$\mu\mu$	eμ	all
$t\bar{t} \to \ell\ell X$	0.000 ± 0.013	0.000 ± 0.013	0.000 ± 0.013	0.000 ± 0.013
$t\bar{t}$ other	0.000 ± 0.013	0.000 ± 0.013	0.000 ± 0.013	0.000 ± 0.013
$t\bar{t} \to \ell(b \to \ell)X$	0.000 ± 0.013	0.020 ± 0.020	0.000 ± 0.013	0.020 ± 0.020
$t\bar{t} \to \ell(\not{b} \to \ell)X$	0.000 ± 0.013	0.000 ± 0.013	0.019 ± 0.019	0.019 ± 0.019
t, s-channel	0.000 ± 0.057	0.000 ± 0.057	0.000 ± 0.057	0.000 ± 0.057
t, t-channel	0.000 ± 0.055	0.000 ± 0.055	0.000 ± 0.055	0.000 ± 0.055
tW	0.000 ± 0.045	0.000 ± 0.045	0.000 ± 0.045	0.000 ± 0.045
$Z \to ee$	0.000 ± 0.429	0.000 ± 0.429	0.000 ± 0.429	0.000 ± 0.429
$Z \to \mu\mu$	0.000 ± 0.429	0.000 ± 0.429	0.000 ± 0.429	0.000 ± 0.429
$Z \to \tau\tau$	0.000 ± 0.429	0.000 ± 0.429	0.000 ± 0.429	0.000 ± 0.429
W+jets	0.000 ± 1.808	0.000 ± 1.808	0.000 ± 1.808	0.000 ± 1.808
WW	0.000 ± 0.019	0.000 ± 0.019	0.000 ± 0.019	0.000 ± 0.019
Vγ	0.000 ± 0.248	0.000 ± 0.248	0.000 ± 0.248	0.000 ± 0.248
$W\gamma^* \to \ell\nu ee$	0.000 ± 0.097	0.000 ± 0.097	0.000 ± 0.097	0.000 ± 0.097
$W\gamma^* \to \ell\nu\mu\mu$	0.000 ± 0.075	0.000 ± 0.075	0.000 ± 0.075	0.000 ± 0.075
$W\gamma^* \to \ell\nu\tau\tau$	0.000 ± 0.028	0.000 ± 0.028	0.000 ± 0.028	0.000 ± 0.028
WZ	0.005 ± 0.005	0.000 ± 0.003	0.000 ± 0.003	0.005 ± 0.005
ZZ	0.000 ± 0.000	0.000 ± 0.000	0.000 ± 0.000	0.000 ± 0.000
dp$W^{\pm}W^{\pm}$	0.000 ± 0.004	0.000 ± 0.004	0.000 ± 0.004	0.000 ± 0.004
spW^-W^-	0.000 ± 0.001	0.000 ± 0.001	0.000 ± 0.001	0.000 ± 0.001
spW^+W^+	0.000 ± 0.006	0.000 ± 0.006	0.000 ± 0.006	0.000 ± 0.006
$t\bar{t}\gamma$	0.000 ± 0.059	0.000 ± 0.059	0.000 ± 0.059	0.000 ± 0.059
$t\bar{t}W$	0.014 ± 0.003	0.029 ± 0.006	0.043 ± 0.007	0.086 ± 0.010
$t\bar{t}Z$	0.003 ± 0.001	0.006 ± 0.002	0.014 ± 0.003	0.023 ± 0.004
$WW\gamma$	0.000 ± 0.015	0.000 ± 0.015	0.000 ± 0.015	0.000 ± 0.015
WWW	0.000 ± 0.000	0.000 ± 0.000	0.000 ± 0.000	0.000 ± 0.000
WWZ	0.000 ± 0.000	0.000 ± 0.000	0.000 ± 0.000	0.000 ± 0.000
WZZ	0.000 ± 0.000	0.000 ± 0.000	0.000 ± 0.000	0.000 ± 0.000
ZZZ	0.000 ± 0.000	0.000 ± 0.000	0.000 ± 0.000	0.000 ± 0.000
Total MC	0.021 ± 0.006	0.055 ± 0.021	0.076 ± 0.021	0.152 ± 0.030
LM6	0.000 ± 0.000	0.000 ± 0.000	0.000 ± 0.000	0.000 ± 0.000
SF	0.00 ± 0.58	0.00 ± 0.37	0.15 ± 0.54	0.15 ± 0.54
DF	0.00 ± 0.14	0.00 ± 0.10	0.00 ± 0.16	0.00 ± 0.16
SF + DF	$0.00 \pm 0.50 \pm 0.00$	$0.00 \pm 0.31 \pm 0.00$	$0.15 \pm 0.44 \pm 0.07$	$0.15 \pm 0.44 \pm 0.07$
Charge Flips	$0.003 \pm 0.002 \pm 0.001$	- $\pm$ -	$0.005 \pm 0.002 \pm 0.001$	$0.008 \pm 0.003 \pm 0.002$
MC Pred	$0.021 \pm 0.006 \pm 0.011$	$0.036 \pm 0.006 \pm 0.018$	$0.057 \pm 0.007 \pm 0.028$	$0.113 \pm 0.011 \pm 0.057$
Total Pred	$0.024 \pm 0.501 \pm 0.011$	$0.036 \pm 0.315 \pm 0.018$	$0.211 \pm 0.438 \pm 0.080$	$0.270 \pm 0.438 \pm 0.094$
data	0	0	0	0

Table 16: Observed event yields in the low-H_T low-$\not{E}_T$ region ($H_T > 200$ GeV, $\not{E}_T >$ 50 GeV) requiring at least three b-tagged jets compared to expectations from simulation alone, and from the data-driven methods. The upper part of the table is based on simulation only and is used only as a reference. The lower part is the main result of the analysis. The SF (DF) contributions are for events with one (two) fake leptons. The *MC Pred* contribution includes contributions from genuine same-sign lepton pairs (a sum of the rows from $V\gamma$ down to ZZZ). Entries with zero contributing events are reported with an uncertainty corresponding to one event. This uncertainty is not added to the total MC contribution. Systematic uncertainties (the second uncertainty if present) are displayed only for the final combined type of background, no systematic uncertainty is added for estimates with zero entries. Systematic uncertainties are 100% correlated among the channels.

The background estimations in all signal regions are in a good agreement with the observation. We see no evidence of a contribution beyond Standard Model expectations. We also note that the background with respect to the inclusive same-sign dilepton search is suppressed by about an order of magnitude due to the b-tag requirements. As seen in the yield tables above, the contribution from fake leptons from b-quark decays in $t\bar{t}$, which is the dominant in the pre-tagged sample analysis [4], is now suppressed and is no longer a dominant one. This confirms our initial expectation from requiring two b-tagged jets. The H_T and $\not\!\!E_T$ distributions of the 7 events in the baseline region, together with the background expectations, are shown in Figure 8 and 9.

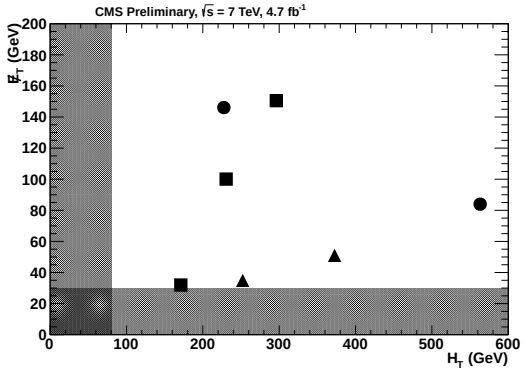

Figure 8: Distribution of $\not\!\!E_T$ vs. H_T for the 7 events in the baseline region $\not\!\!E_T >$ 30 GeV and $H_T > 80$ GeV; ee events: circles; $e\mu$ events: squares; $\mu\mu$ events: triangles.

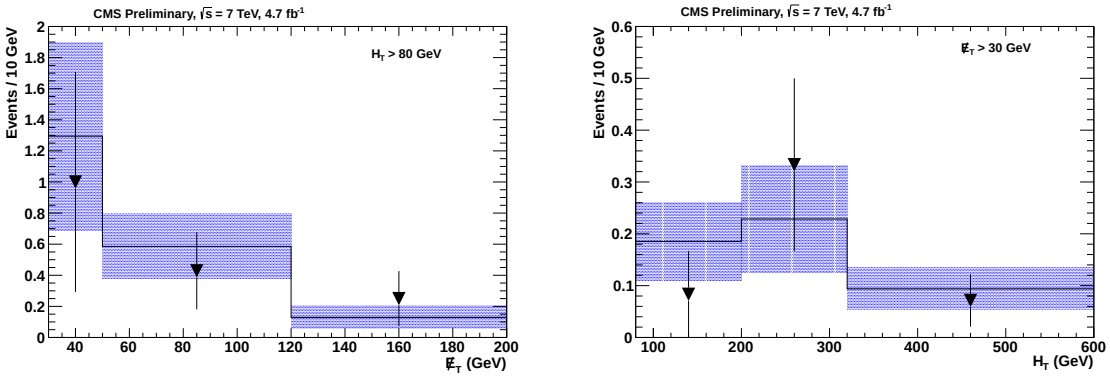

Figure 9: $\not\!\!E_T$ and H_T distribution for the events in the baseline region (points). Also shown as a histogram is the result of the background prediction. The shading around the histogram represents the uncertainty in the background prediction.

8 Acceptance Systematics

Systematic uncertainties on signal event selections arise from uncertainties on event selections expected in simulation compared to the actual performance of the detector. The uncertainties associated with the data - Monte Carlo scale factors are discussed in Section 4.6. As this search is in many ways similar to the inclusive same-sign dilepton search [4], our treatment of efficiency systematics parallels the one in that analysis. In this section, we briefly summarize those results, and describe the uncertanties due to the b-tagging requirement.

The only new source of systematics in this analysis is from the uncertainty on the b-jet tagging efficiency. As already mentioned in Section 4.6.2, this uncertainty is 4 (15)% for jets with $p_T < 240 (> 240)$ GeV. As an illustration of the b-jet momentum distribution, we compare them in Fig. 10 for $t\bar{t}$ events (before the same-sign requirement) and for the LM9 cMSSM SUSY benchmark point.[5] While most of the b-jets from $t\bar{t}$ are below

[5] The LM9 point is defined by the common scalar mass (m0) $= 1.45$ TeV, the common gaugino mass (m1/2) = 175 GeV, the ratio of the Higgs expectation values (tanβ) $= 10$, tri-linear coupling (A0) = 0 and the sign of the Higgsino mass parameter (μ) > 0.

240 GeV, those from LM9 have a large contribution from higher momenta. Our target searches include final states with two or more b-quark jets. This means the efficiency to select two b-jets, as well as its uncertainty varies among the signal final states considered

- same-sign top pair production, as from Z' exchange, is similar in topology to that of the opposite-sign $t\bar{t}$ production and has only two b-jets in the final state with most of them with $p_T < 240$ GeV. The b-tagging uncertainty is then approximately 8% and the corresponding per-event scale factor is 0.922 ± 0.073.
- direct sbottom pair production has two b-jets in the final state with a large fraction of b-jets with $p_T > 240$ GeV. The b-tagging efficiency scale factor is still 0.922, but its uncertainty varies among the signal model points from as low as 8% to as high as 29%. This uncertainty is evaluated event-by-event and then point-by-point in the limit setting procedure.
- gluino pair production with stops in the final states considered here all have four b-jets in the final state. Now the efficiency scale factor changes as well depending on the number of b-jets in the acceptance. This is evaluated event-by-event and point-by point in the limit setting procedure.

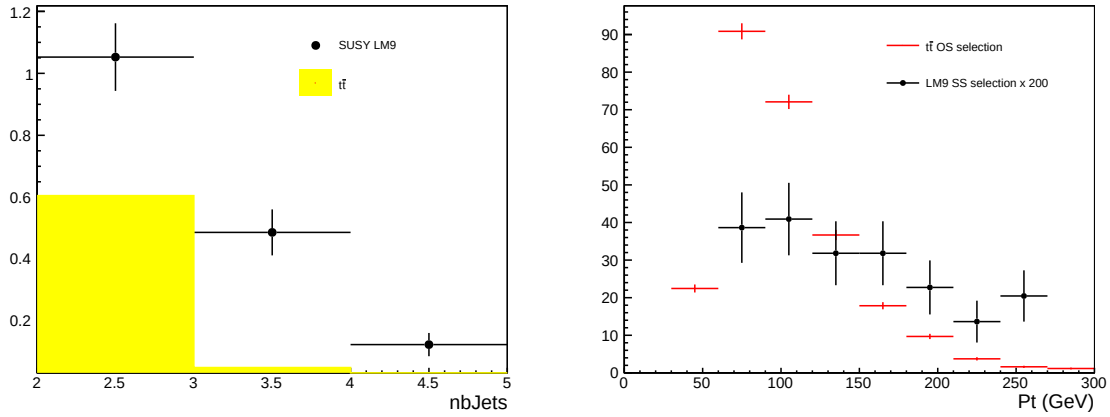

Figure 10: Differential distributions of leading b-tag jet p_T for the LM9 benchmark point and $t\bar{t}$ simulations. The normalization is arbitraty.

A summary of systematic uncertainties is given in Table 17. Here the b-tagging systematics is applicable only to the same-sign top production signature.

Table 17: Summary of systematic uncertainties on the signal selection and expectation. Reported values are fractional, relative to the total cross section. The energy scale, b-tagging, and PDF uncertainties are calculated separately in every model point. These uncertainties quoted here are relevant to the Z' model.

Source	ee	$\mu\mu$	$e\mu$	all
Lepton selection	12%	12%	11%	11%
Energy scale	8%	8%	8%	8%
ISR/FSR and PDF	2%	2%	2%	2%
b-tag selection	8%	8%	8%	8%
Total without luminosity	17%	17%	17%	17%
Integrated luminosity	4.5%	4.5%	4.5%	4.5%
Total	17%	17%	17%	17%

8.1 Event-by-event b-tagging scale factor and associated systematic uncertainty for signal regions wih ≥ 2 btags

We evaluate an event-by-event b-tagging scale factor (SF_{event}) as follows:

- for each MC event passing the event selection we start from the scale factors SF_i associated with the two or more tagged jets. Note that SF_i can in principle be a function of jet η, p_T, etc. Following the btag group recommendations it is taken as a constant: $SF = 0.96$[27, 28]

- For events with two b-tagged jets: $SF_{\rm event} = SF^2$.
- For events with three b-tagged jets: $SF_{\rm event} = SF^3 + 3SF^2(1-SF)$.
- For events with four b-tagged jets: $SF_{\rm event} = SF^4 + 4SF^3(1-SF) + 6SF^2(1-SF)^2$.

Note that the procedure above would not work if $SF > 1$, but this is not an issue since $SF = 0.96$. It also implicitly assumes that all b-tags are from b-quarks. For the models under consideration, we have verified that the MC contribution to the acceptance from events that need at least one tag from $udsgc$ in order to pass the ≥ 2 tags requirement is small. For example, in the Z' model, this contribution is only $\approx 4\%$. Note that the bias in $SF_{\rm event}$ due to the improper treatment of these events is 4% times some quantity proportional to the difference in scale factors between b-jets and $usdgc$ jets. Therefore, it is $<<$ 4% and we think it can be ignored.

In order to calculate the uncertainty (δSF) on the event-by-event $SF_{\rm event}$, we also need the single jet b-tagging efficiency (ϵ). We do not need a very precise value for ϵ, since the uncertainty δSF is only weakly dependent on it. We take $\epsilon = 0.643$, independent of p_T and η for jets of $|\eta| < 2.5$. The uncertainty on ϵ is the same as that on the scale factors, $\delta\epsilon = 4\%(15\%)$ (relative) for $p_T < 240$ GeV (> 240 GeV). The procedure is the following:

- For each event passing the requirements at RECO level, we look at the status=3 information and we calculate the total probability (p) of tagging two or more jets, and its uncertainty (δp).
- The calculation of p and δp is based on the number of status=3 b-quarks of $p_T > 40$ GeV and $|\eta| < 2.5$.
- An event with two reconstructed b-tags can have < 2 such status=3 b-quarks. This is rare and happens for example when a 39 GeV b-quark is reconstructed as a 41 GeV b-jet. In these cases we calculate p and δp assuming that there are two 40 GeV b-quarks at status=3.
- The uncertainty associated with the event is then $(\frac{|\delta p|}{p})SF_{\rm event}$.

The probabilities p are calculated as follows (N here is the number of status=3 b-quarks and we write the equations without the assumption that ϵ is constant):

- $N = 2$: $\quad p = \epsilon_1\epsilon_2$.
- $N = 3$: $\quad p = \epsilon_1\epsilon_2 + \epsilon_1\epsilon_3 + \epsilon_2\epsilon_3 - 2\epsilon_1\epsilon_2\epsilon_3$.
- $N = 4$:

$$p = \prod \epsilon_i \quad + \quad \sum_j (1-\epsilon_j) \prod_{i\neq j} \epsilon_i \quad + \quad \sum_{j<k} (1-\epsilon_j)(1-\epsilon_k) \prod_{i\neq j,k} \epsilon_i$$

The uncertainties δp are calculated from the equations above assuming full correlation between jets, *e.g.*, for $N = 2$ we have $\delta p = \delta\epsilon_1 \cdot \epsilon_2 + \delta\epsilon_2 \cdot \epsilon_1$, etc.

8.2 Event-by-event b-tagging scale factor and associated systematic uncertainty for signal regions with ≥ 3 b-tags

The treatment of Section 8.1 for ≥ 2 b-tags is extended here to the case of ≥ 3 b-tags. The event-by-event b-tagging scale factor ($SF_{\rm event}$) is evaluated as follows:

- For events with 3 b-tagged jets $SF_{\rm event} = SF^3$.
- For events with 4 b-tagged jets $SF_{\rm event} = SF^4 + 4SF^3(1-SF)$.

The uncertainty is calculated starting from the probability p of having ≥ 3 b-tagged jets in events with at least $N = 3$ b-quarks at status=3. This probability is

- $N = 3$: $\quad p = \epsilon_1\epsilon_2\epsilon_3$.
- $N = 4$:

$$p = \prod \epsilon_i \quad + \quad \sum_j (1-\epsilon_j) \prod_{i\neq j} \epsilon_i$$

where ϵ_i is the probability of tagging the i-th b-quark. The uncertainties δp are calculated from the equations above assuming full correlation between jets, *e.g.*, for $N = 3$ we have $\delta p = \sum_i \delta\epsilon_i \prod_{i\neq j} \epsilon_j$, etc.

	Region 1	Region 2	Region 3	Region 4	Region 5	Region 6	Region 7
No. of jets	≥ 2	≥ 2	≥ 2	≥ 2	≥ 2	≥ 2	≥ 3
No. of btags	≥ 2	≥ 2	≥ 2	≥ 2	≥ 2	≥ 2	≥ 3
Lepton charges	$++/--$	$++$	$++/--$	$++/--$	$++/--$	$++/--$	$++/--$
$\not\!\!E_T$	≥ 30 GeV	≥ 30 GeV	≥ 120 GeV	≥ 50 GeV	≥ 50 GeV	≥ 120 GeV	≥ 50 GeV
H_T	≥ 80 GeV	≥ 80 GeV	≥ 200 GeV	≥ 200 GeV	≥ 320 GeV	≥ 320 GeV	≥ 200 GeV
BG from charge flips	1.1 ± 0.2	0.5 ± 0.1	0.05 ± 0.01	0.3 ± 0.1	0.12 ± 0.03	0.026 ± 0.009	0.008 ± 0.004
BG from fakes	3.4 ± 2.0	1.8 ± 1.2	0.32 ± 0.50	1.5 ± 1.1	0.81 ± 0.78	0.15 ± 0.45	0.15 ± 0.45
BG from rare SM	3.2 ± 1.6	2.1 ± 1.1	0.56 ± 0.28	2.0 ± 1.0	1.04 ± 0.52	0.39 ± 0.20	0.11 ± 0.06
Total expected BG	7.7 ± 2.6	4.4 ± 1.6	0.9 ± 0.6	3.7 ± 1.5	2.0 ± 0.9	0.6 ± 0.5	0.3 ± 0.5
No. data events	7	5	2	5	2	0	0
N_{UL} (12% uncert.)	7.4	6.9	5.2	7.3	4.7	2.8	2.8
N_{UL} (20% uncert.)	7.7	7.2	5.4	7.6	4.8	2.8	2.8
N_{UL} (30% uncert.)	8.1	7.6	5.8	8.2	5.1	2.8	2.8
N_{UL} (20% uncert.) fakes down by factor 2	8.5	7.7	5.4	8.0	5.0	2.8	2.8

Table 18: A summary of the results of this search. For each signal region, we show its most important kinematical requirements, the prediction for the three background (BG) components as well as the total, the event yield, and the 95% CL upper limit on the number of non-SM events in each region calculated under three different assumptions for the event efficiency uncertainty (see text for more details). In the last line we show the effect of reducing the fake backgrounds by a factor of 2, as was suggested at the preapproval presentation based on the closure results in $t\bar{t}$ MC. This large change in the fake background prediction has only a small impact on the upper limits.

9 Further outreach information

As mentioned in Section 4, we want to provide enough information so that anybody can use their favorite Monte Carlo generator of new physics, define an acceptance at the hard scatter level (status = 3 in Pythia), and correctly estimate the efficiency for this new physics model to within 50% or so.

The relevant information on selection efficiencies is given in Section 4. In this Section we give the second missing ingredients for this program, namely the 95% upper limits on the number of events for the various signal regions. We also show how well our efficiency model works in a few cases.

9.1 Limits on number of events

In Table 18 we summarize the results of the counting experiments in the various signal regions that are given in more details in Tables 10 to 16; in addition, for each signal region we give the 95% CL upper limit on the number of non-SM events (N_{UL}) calculated using the CL_s method.

The value of N_{UL} is a key ingredient to allow phenomenologists to interpret our data: basically any model that predicts an event yield $> N_{UL}$ is excluded at 95% CL. Uncertainties in the efficiency need to be included in N_{UL}. This is tricky because the components of the efficiency uncertainty associated with the JES and the btagging differ model-by-model. Fortunately, this is not a big effect. In order to show that it is not, in Table 18 we give N_{UL} with uncertainties of 12%, 20%, and 30%. The first value (12%) corresponds to the "minimum uncertainty", *i.e.* the uncertainty due to lepton efficiency and luminosity only; the other two values (20% and 30%) are "typical" uncertainty values when including JES and btagging.

9.2 Testing the efficiency model

The efficiency model is evaluated by applying it to a few scenarios considered in Section 10. For each model considered here, points near the exclusion curve are selected and the yield obtained by applying the full analysis selection is compared to that estimated by applying the efficiencies detailed in Section 4 to generator level objects. Figure 11 shows the performance of the efficiency model applied to the scenario of same sign top production due to t-channel exchange of a new massive Z' boson. The comparison was performed using the same signal region considered in Section 10.1. The estimated and actual yields agree to within 20%. When the mass of the Z' is large compared to the mass to the top, the mass of the boson only weakly influences the kinematics of the final state so that the performance of the efficiency model is expected to be relatively constant, as observed.

Several models involving stop or sbottom production were also considered in Section 10. As a worst case scenario,

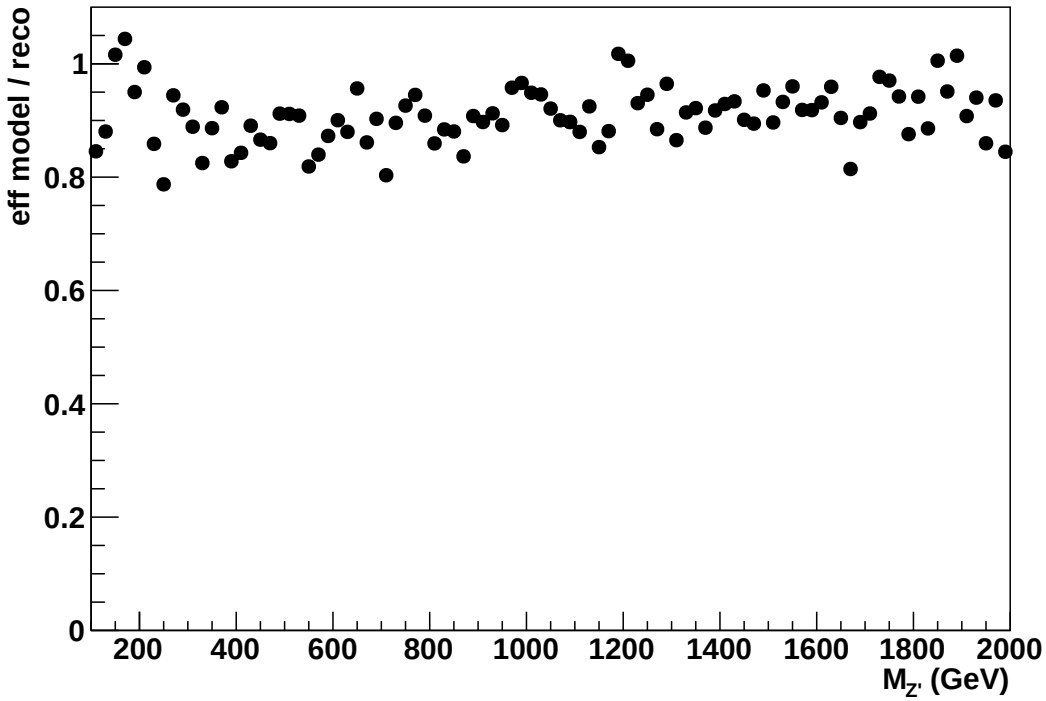

Figure 11: Test of the efficiency model applied to same sign top production due to a Z'. The figure shows the ratio of the yield estimated by applying the efficiency model to generator level objects to the yield obtained by applying the full analysis selection to reconstructed objects. Estimated and actual yields agree to within 20%.

$m(\widetilde{g}), m(\widetilde{t})$ (GeV)	Actual Yield	Estimated Yield	Estimated / Actual
800, 280	133	181	1.36
800, 430	125	184	1.47
650, 380	99	146	1.48

Table 19: Test of the efficiency model applied to the $\widetilde{g}$ to $t\widetilde{t}$ model. The table shows the ratio of the yield estimated by applying the efficiency model to generator level objects to the yield obtained by applying the full analysis selection to reconstructed objects. Estimated and actual yields agree to within 50%

the efficiency model was tested for a few relevant points in the parameter phase space for the $\widetilde{g}$ to $t\widetilde{t}$ model. The results of these tests are recorded in Table 19 . The comparison was performed using the $H_T > 320$ GeV, $\not\!\!E_T > 120$ GeV signal region. Estimated yields are found to agree with those obtained using the full analysis selection to within 50%.

10 Searches for Specific Models

Our signature, two isolated same-sign leptons, at least two b-tagged jets, and $\not\!\!E_T$, is common to many different new physics scenarios. Here we refine our analysis to define dedicated signal regions for a few of these scenarios, and provide 95% C.L. upper limits on their respective model parameter space.

10.1 Same sign top production due to a Z'

This is an extension of the 2010 CMS published CMS analysis[3]. The main difference is that here in order to improve the signal-to-noise we require two b-tagged jets. This would not have made sense in 2010, since at the time the integrated luminosity was low enough that the analysis was almost background free without requiring b-tags.

10.1.1 Theoretical Discussion, Z' model

Recent measurements of the inclusive forward-backward $t\bar{t}$ production asymmetry (A_{FB}) from the Tevatron experiments show deviations from the standard model (SM) expectations [30, 31, 32]. Several attempts have been made to explain this asymmetry [22, 33, 34, 35]. One of the most natural ways to induce such an asymmetry would be through Flavor Changing Neutral Currents (FCNC) in the top quark sector. The forward-backward asymmetry in $u\bar{u} \to t\bar{t}$ would then be generated by t-channel exchange of a new massive Z' boson that couples chirally to u and t at the same vertex, as shown in Fig. 12 [22]. The same type of interaction would also give rise to same-sign top pair production, as illustrated in Fig. 13 and Fig. 14. In this case, the initial state involves two u-quarks and thus the cross section at the LHC is enhanced due to the large valence quark parton density of the proton.

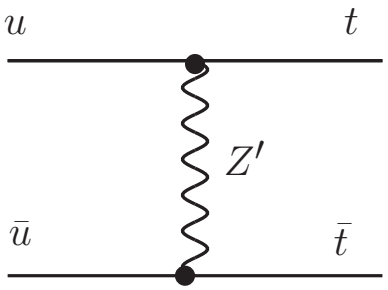

Figure 12: Diagram for $t\bar{t}$ production induced by Z' exchange which can generate a forward-backward asymmetry.

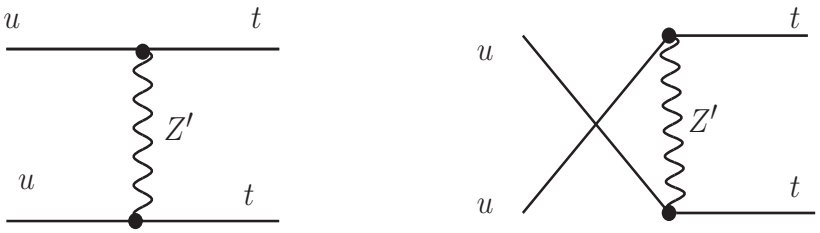

Figure 13: Diagrams for tt pair production induced by Z' exchange in the t-channel.

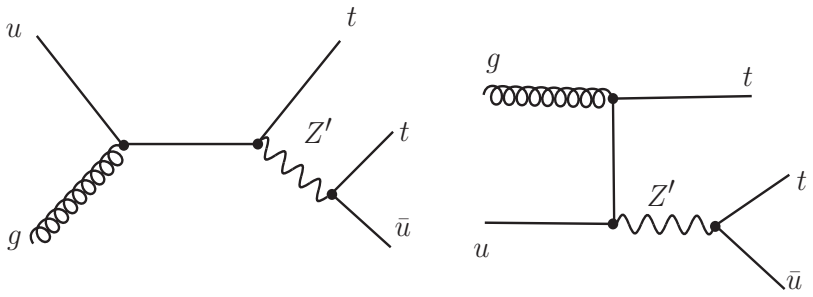

Figure 14: Diagrams for $tt\bar{u}$ production induced by Z' exchange in the s-channel

We consider the model of Reference [22]. The relevant $u - t - Z'$ interaction term in the Lagrangian is:

$$\mathcal{L} = g_W \bar{u}\gamma^\mu (f_L P_L + f_R P_R) t Z'_\mu + h.c \tag{2}$$

where g_W is the weak coupling strength. The left-handed coupling is set to $f_L = 0$, due to the $B_d - \bar{B}_d$ mixing constraint [36]. The right-handed coupling f_R and the Z' mass are free parameters in the model. Within this model there is a narrow range of parameter space consistent with the Tevatron measurements of $\sigma(p\bar{p} \to t\bar{t})$ and A_{FB}, which is not excluded by direct searches for same-sign tops. This region is illustrated in Fig. 15.

Monte Carlo events for this model were generated using Madgraph in the same way as for the 2010 analysis (see

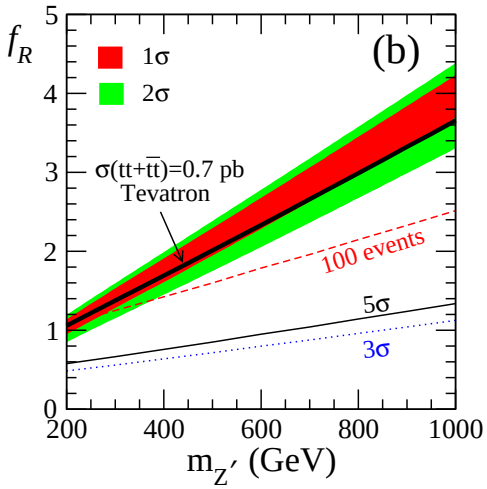

Figure 15: From Reference [22]; the shaded area covers the parameter space consistent with the A_{FB} and $\sigma(t\bar{t})$ from the Tevatron; The line indicated by the arrow shows the Tevatron limit inferred by the authors from same sign top searches at the Tevatron; the remaining lines represent the expectations of Reference [22]. for LHC searches in 1 fb^{-1}.

Reference [37]).

10.1.2 Signal region definition for same sign top from Z'

In this study we search for same-sign dileptons originating from tt or ttj pair production as described above. At the LHC $uu \to tt$ dominates over $\bar{u}\bar{u} \to \bar{t}\bar{t}$, thus we concentrate on same-sign positive leptons. The $\not\!\!E_T$ and H_T cuts are typical of a dilepton top analysis: two or more jets of $p_T > 40$ GeV, $\not\!\!E_T > 30$ GeV and $H_T > 80$ GeV. This corresponds to Table 11: 5 events observed and $4.42 \pm 0.80 \pm 1.39$ expected from background.

10.1.3 Limits on the Z' model

Using the results from Section 10.1.2, we set a limit at 95% CL of 7.2 events using the CL_S method. The expected limit is 6.4 events. In the MC we find $Acc \times Eff \times BR = 0.00233$, independent of Z' mass. This results in an upper limit on the cross-section of 0.67 pb. The limit includes uncertainty on JES (12%), b-tagging (10%), lepton efficiencies (11%), luminosity (4.5%), and PDF (3%). Our limit is a factor of 25 more stringent than our 2010 result[3] and also a factor of 5.5 better than that of Atlas[38].

The cross-section limit is turned into an exclusion limit in the $m(Z')$ vs f_R plane using the LO calculation of the $pp \to tt$ cross-section in this model. This is shown in Figure 16, together with the corresponding plot from the 2010 analysis. The region of parameter space consistent with the Tevatron measurements of A_{FB} is excluded.

For $M_{Z'} >> M_{\rm top}$ the Lagrangian of equation 1 is equivalent to $\mathcal{L} = -\frac{1}{2}\frac{C_{RR}}{\Lambda^2}[\bar{u}\gamma^\mu t][\bar{u}\gamma_\mu t] + h.c.$ [39], with $\frac{C_{RR}}{\Lambda^2} = \frac{2g_W^2 f_R^2}{M_{Z'}^2}$. Our limit on f_R, calculated for $M_{Z'} = 2$ TeV, would then correspond to $\frac{C_{RR}}{\Lambda^2} < 0.6$ TeV^{-2} at 95% confidence. This is more stringent than the limit recently reported by CDF: $\frac{C_{RR}}{\Lambda^2} < 3.7$ TeV^{-2} [40].

10.2 Maximally Flavor Violation Model (MXFV)

10.2.1 Theoretical discussion of MXFV

This is a model [18, 19, 20] with a new scalar SU(2) doublet field $\Phi_{FV} = (\eta^0, \eta^+)$ that couples the first and third generation quarks (q_1, q_3) via a Lagrangian term $\mathcal{L}_{FV} = \xi_{13}\Phi_{FV}q_1q_3$. Remarkably, it appears that this model is largely consistent with constraints from flavor physics.

The model results in same sign top pairs in the final state as follows

- Single η^0 production: $ug \to t\eta^0 \to tt\bar{u}, t\bar{t}u$
- η^0 pair production: $u\bar{u} \to \eta^0\eta^0 \to tt\bar{u}\bar{u}, uu\bar{t}\bar{t}, t\bar{t}u\bar{u}$

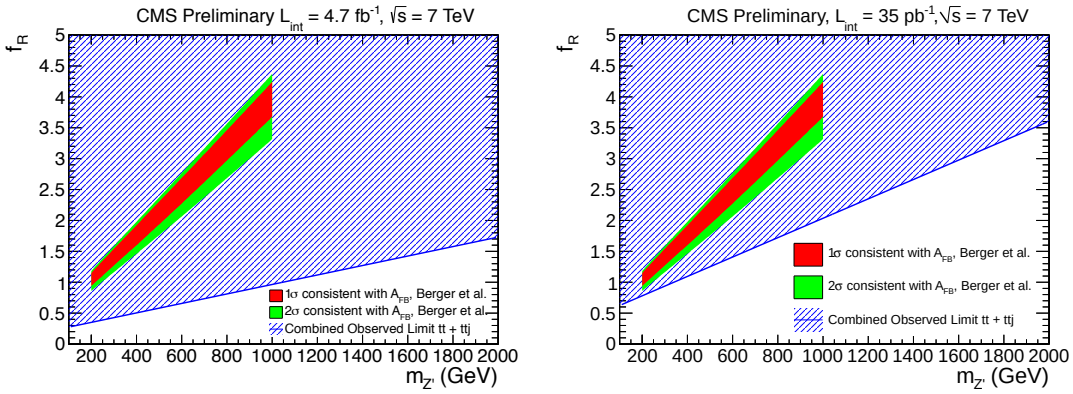

Figure 16: Exclusion regions from the 2011 analysis (left) and the 2010 analysis (right). The exclusions are obtained using the LO cross-section for tt production. Note that the cross-section is proportional to f_R^4.

- η^0 t-channel exchange: $uu \to tt$, $\bar{u}\bar{u} \to \overline{tt}$

Monte Carlo events were generated using LHE files[41] interfaced with Madgraph. Madgraph was used to decay the top quarks in order to preserve spin-correlations. The cross-sections at LO for same sign tt pairs for the three processes in the MXFV model is shown in Figure 17. The t-channel process is the dominant for $\xi = 1$. At smaller values of ξ, $ug \to \eta^0 \to tt\bar{u}$ becomes more important, since its cross-section varies as ξ^2, while in the t-channel case it goes as ξ^4.

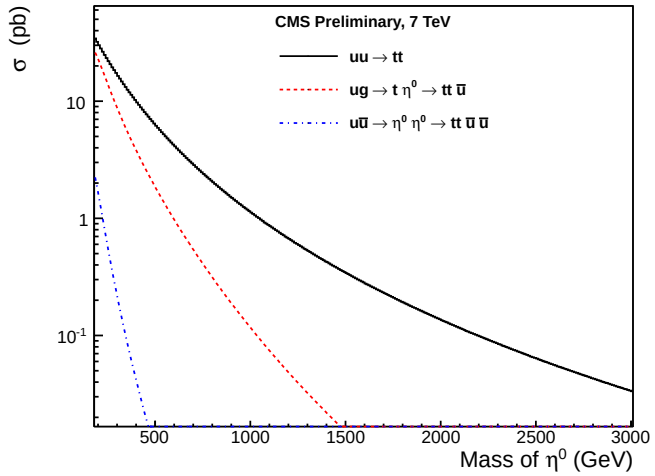

Figure 17: Cross section at LO for the tt final state in the three MXFV modes as a function of η^0 mass for $\xi = 1$.

10.2.2 Signal region definition for the MXFV model

The properties of the final state in this model are basically the same as in the Z' model. Thus, we use the same signal region definition (see Section 10.1.2).

10.2.3 Limits for the MXFV model

Our limits in the ξ-M(η^0) plane are shown in Figure 18. They are calculated using the LO cross-section for this model. Our limits are better than those of CDF[20].

10.3 $\widetilde{g} \to t\widetilde{t}$ Model

10.3.1 Theoretical discussion of the $\widetilde{g} \to t\widetilde{t}$ Model

This is an interesting model for stop pair production through gluino decays[42][43][15][11]. It is a "realistic" and well-motivated model in the sense that it applies to the situation where all the squarks except the stop are

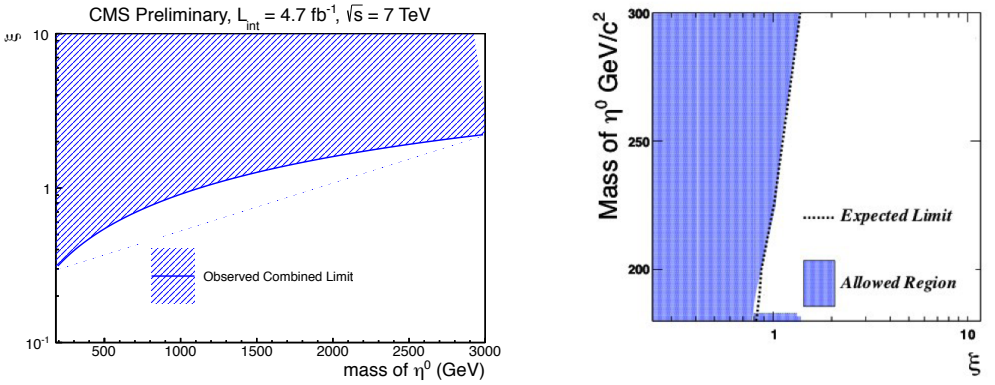

Figure 18: Limits in the ξ-Mass(χ^0) plane. Left: CMS. Right: CDF

very heavy. A "light" stop is of course generally favored in SUSY, and LHC results are pointing to "heavy" superpartners. Then if the stop is light enough the gluino would decay with 100% BR as $\widetilde{g} \to t\widetilde{t}$ and then the stop would decay as $\widetilde{t} \to t\chi_1^0$, if kinematically accessible. The parameters of the model are $M(\widetilde{g})$, $M(\widetilde{t})$, $M(\chi_1^0)$.

The final state after gluino pair production is then $tt\overline{t}\overline{t}\chi_1^0\chi_1^0$. It is the same final state as the `T1tttt` simplified model[21], except that it proceeds through an intermediate on-shell stop. This final state is rich in leptons, and has four b-quarks. The same sign dilepton + b-tags + $\not\!\!E_T$ signature is a particularly good way to go after it.

10.3.2 Signal region definition for the $\widetilde{g} \to t\widetilde{t}$ Model

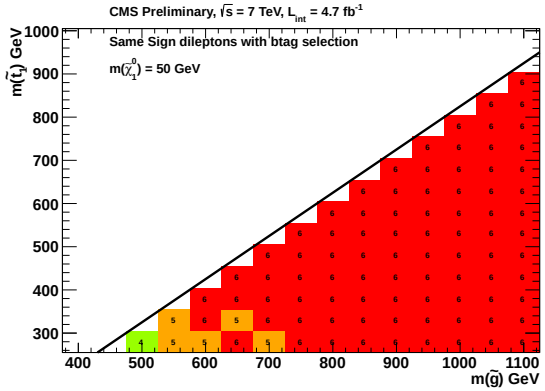

Figure 19: The signal region with the best expected limit as a function of $m(\widetilde{g})$ vs. $m(\widetilde{t})$ plane for $m(\chi_1^0)$=50 GeV.

For each point in parameter space we use the signal region that gives the best expected limit. Limits are calculated using all experimental uncertainties; the JES and b-tag uncertainties are calculated point-by-point. An example of this optimization is shown in Figure 19, where we show the choice of signal region that gives the best expected limit in the $m(\widetilde{g})$ vs. $m(\widetilde{t})$ plane for the choice $m(\chi_1^0)$ = 50 GeV.

10.3.3 Limits for the $\widetilde{g} \to t\widetilde{t}$ Model

The limits on the production cross-section in this model in the gluino mass vs. stop mass plane for two choices of the LSP mass are shown in Figure 20. Using the NLO+NLL cross-section for gluino pair production, we also place a limit on the mass parameters of this model. We basicaly can exclude $m(\widetilde{g})$ up to about 800 GeV for all kinematically allowed values of the stop mass: $m(t) + m(\chi_1^0) < m(\widetilde{t}) < m(\widetilde{g}) - m(t)$.

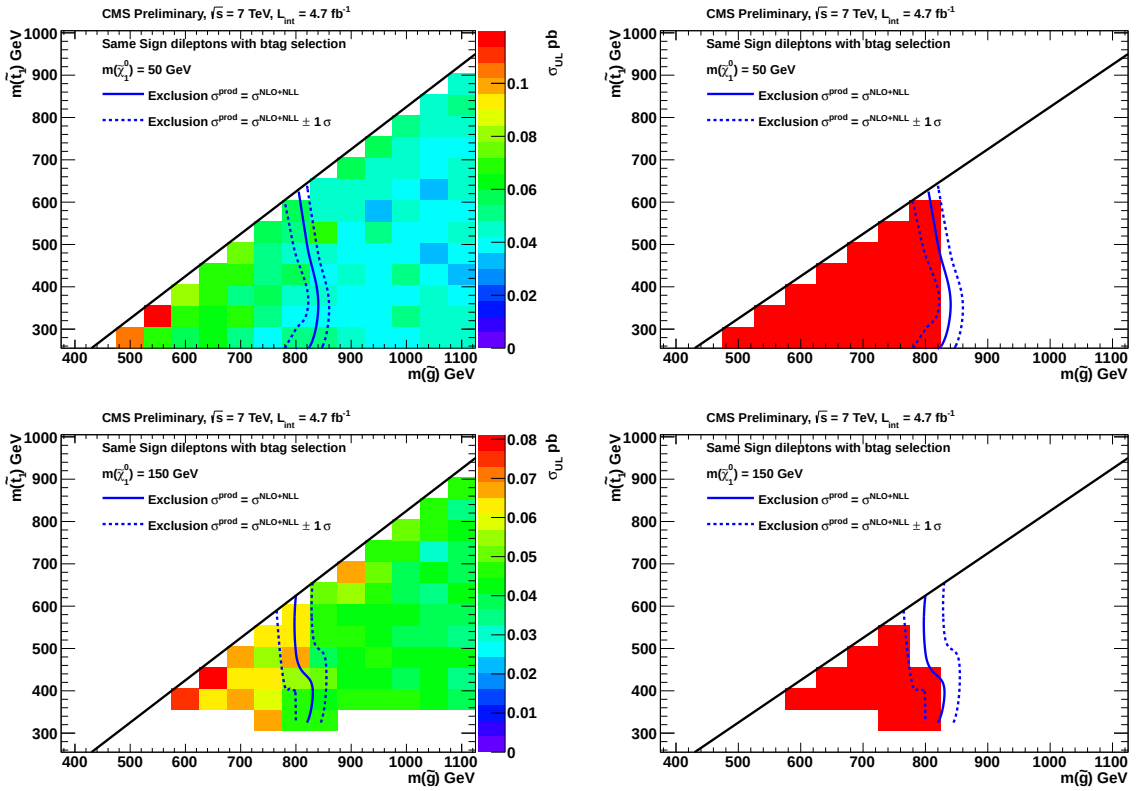

Figure 20: Left top plot: Cross section limits in the $m(\widetilde{g})$ vs. $m(\widetilde{t})$ plane for $m(\chi_1^0)$ = 50 GeV (left). Right top plot: Map of excluded MC points for $m(\chi_1^0)$ = 50 GeV. Bottom left plot: Same as left top plot but for $m(\chi_1^0)$ = 150 GeV. Bottom right plot: Same as right top plot but for $m(\chi_1^0)$ = 150 GeV. The limit curves have been smoothed.

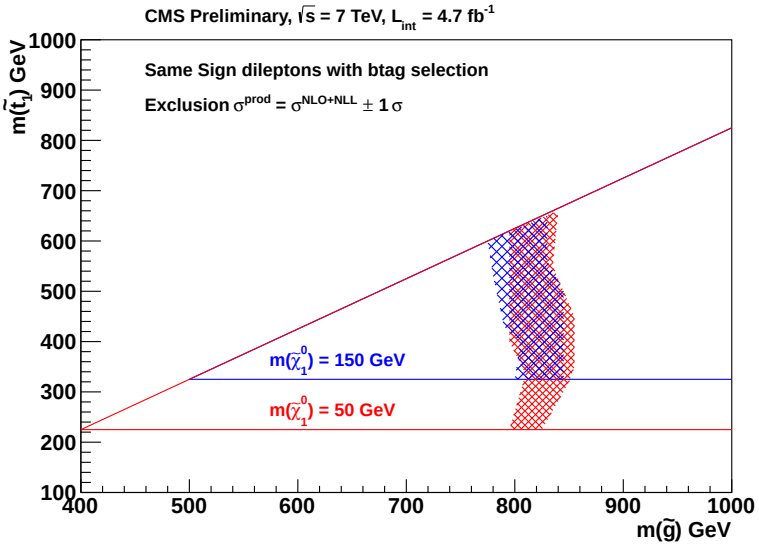

Figure 21: Exclusion lines in the $m(\widetilde{g})$ vs. $m(\widetilde{t})$ plane for $m(\chi_1^0)$ = 50 GeV and $m(\chi^{\pm})$ = 150 GeV. The width of the lines reflects the cross-section uncertainty. The kinematical boundaries of this model are also shown. The limit curves have been smoothed, and the thickness of the bands represent the uncertainty on the gluino pair production cross-section.

10.4 T1tttt Model

10.4.1 Theoretical discussion of the T1tttt Model

The T1tttt simplified model[21] is very similar to the model of Section 10.3. In this model it is assumed that all squarks are very heavy, but the stop is somewhat lighter than the other squarks[12][13]. Then the gluino would decay as $\widetilde{g} \rightarrow t\bar{t}\chi_1^0$ through virtual stops. Other gluino decay modes would be suppressed because the stop is the lightest squark. The final state after gluino pair production is $tt\bar{t}\bar{t}\chi_1^0\chi_1^0$, just as in Section 10.3. The model parameters are $M(\widetilde{g})$ and $M(\chi_1^0)$.

10.4.2 Signal region definition for the T1tttt Model

For each point in parameter space we use the signal region that gives the best expected limit, see Figure 22. The limits include all experimental uncertainties. The JES and b-tag uncertainties are calculated point-by-point.

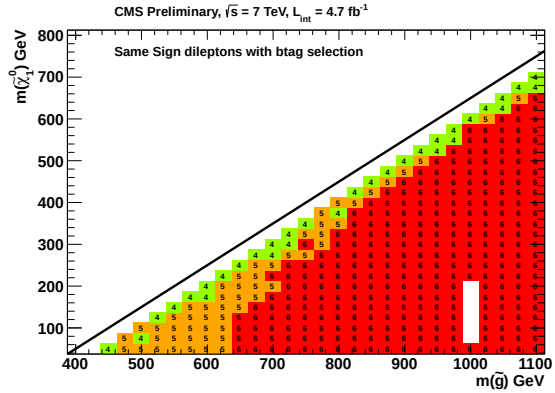

Figure 22: The signal region with the best expected limit as a function of $m(\widetilde{g})$ vs. $m(\widetilde{t})$ plane for $m(\chi_1^0)$=50 GeV.

10.4.3 Limits for the T1tttt Model

The limit on the production cross-section in this model in the gluino mass vs. LSP mass plane shown in Figure 23. Using the NLO+NLL cross-section for gluino pair production, we place a limit on the mass parameters as shown in Figure 23. Basically we exclude $m(\widetilde{g})$ up to about 820 GeV with a small dependence on $m(\chi_1^0)$.

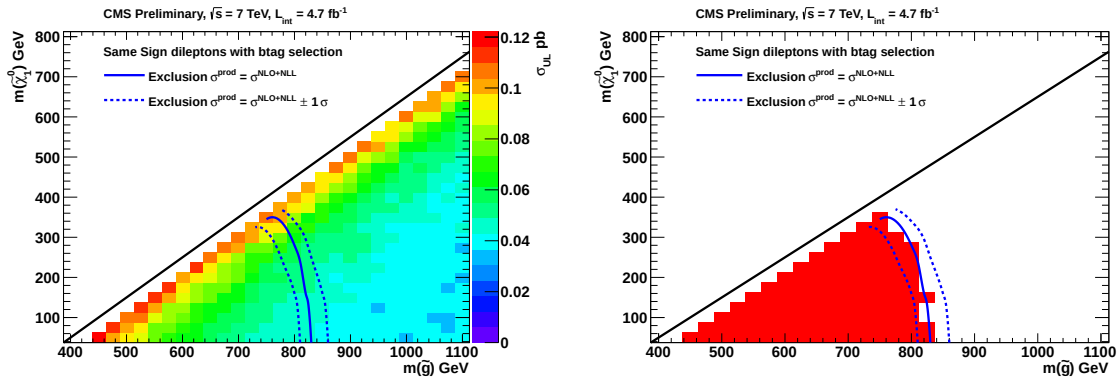

Figure 23: Left plot: Cross section limits in pb for the $m(\widetilde{g})$ vs. $m(\chi_1^0)$ plane for the T1tttt model. Right plot: a map of the MC points excluded by this analysis, using the central value for the production cross-section. The limit curves have been smoothed. A version of this Figure with smoothed limit lines suitable for publication is repeated as Figure 31.

10.5 Sbottom pair production model

In this model we have $pp \to \tilde{b}\tilde{b}$. The sbottom decays as $\tilde{b} \to t\chi^-$ followed by $\chi^- \to W^-\chi_1^0$. The final state is $t\bar{t}W^+W^-\chi_1^0\chi_1^0$. The model parameters are $M(\widetilde{b})$, $M(\chi_1^0)$, and $M(\chi^\pm)$. For simplicity, we only consider mass parameters such that the χ^- is on-shell.

10.5.1 Signal region definition for the sbottom pair production model

For each point in parameter space we use the signal region that gives the best expected limit, see Figure 24. The limits include all experimental uncertainties. The JES and b-tag uncertainties are calculated point-by-point.

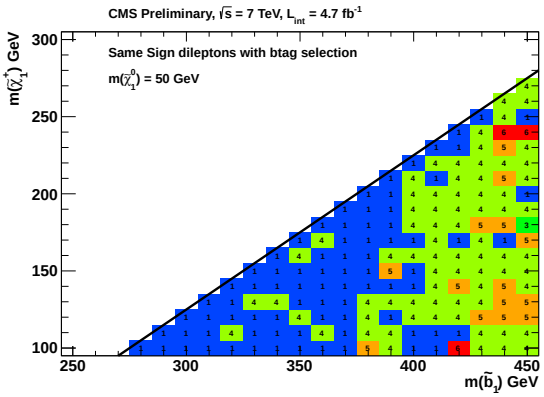

Figure 24: The signal region with the best expected limit as a function of $m(\chi^\pm))$ vs. $m(\widetilde{b})$ plane for $m(\chi_1^0)$=50 GeV.

10.5.2 Limits for the sbottom pair production model

The limit on the production cross-section in this model in the sbottom mass vs. $\chi^\pm$ mass plane is shown in Figure 25 for $m(\chi_1^0)$=50 GeV. We exclude sbottoms of mass below $\approx$ 370 GeV. Note that the bulk of the exclusion comes from SR1 (see Figure 24), which has a very modest $\not\!\!E_T >$ 30 GeV requirement. Thus, we do not expect this limit to depend strongly on the LSP mass.

The region near $m(\widetilde{b}) = 370$ GeV is approximately where the best SR changes from SR1 to SR4, see Figure 24. This unfortunately enhances statistical fluctuations around the limit curve in Figure 25. This is why we smoothed the limit line into a vertical line. Finally, in Figure 26 we show the limit on the sbottom pair production cross-section as a function of the sbottom mass. As argued above, the limit is insentive to the LSP mass; a detailed examination of Figure 25 shows that it is also insensitive to the chargino mass (as long as the mass parameters are within the kinematically allowed ranges).

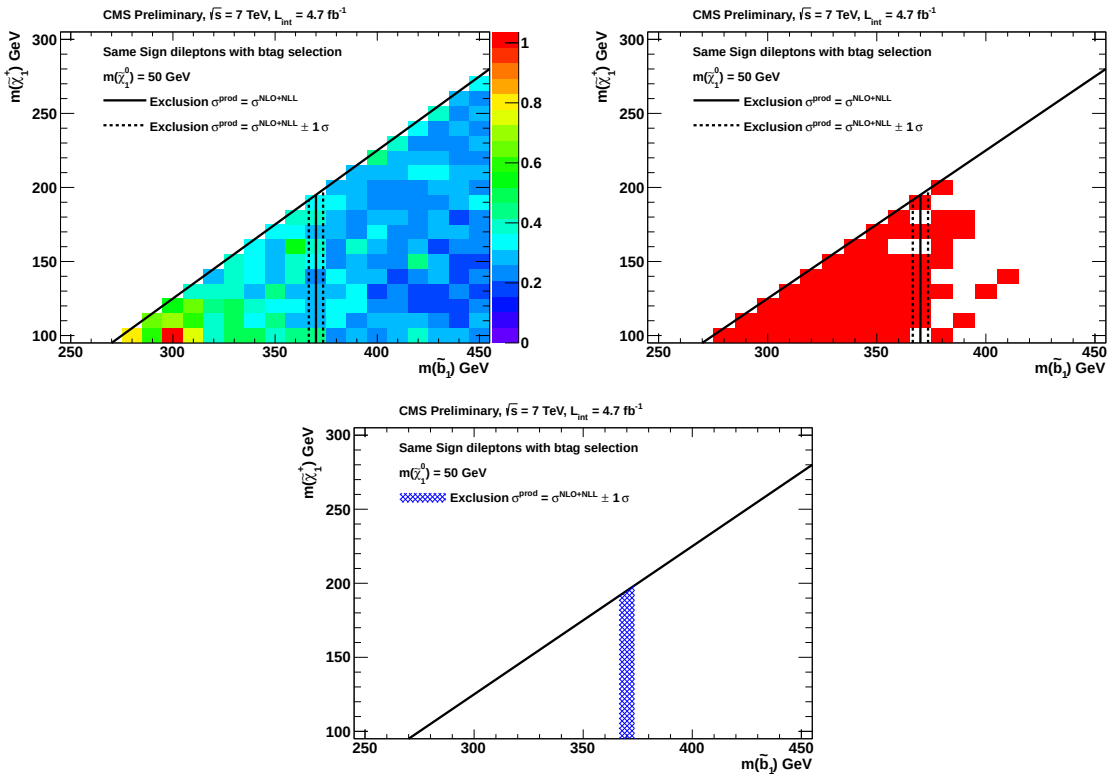

Figure 25: Top Left plot: Cross section limits in the $m(\widetilde{b})$ vs. $m(\chi^{\pm})$ plane for the sbottom pair production model with $m(\chi_1^0)$=50 GeV. Top Right plot: a map of the MC points excluded by this analysis, using the central value for the production cross-section. Bottom plot: Same as top left but on a white background. The thickness of the band represents the uncertainty on the sbottom pair production cross-section. The limit curve has been smoothed.

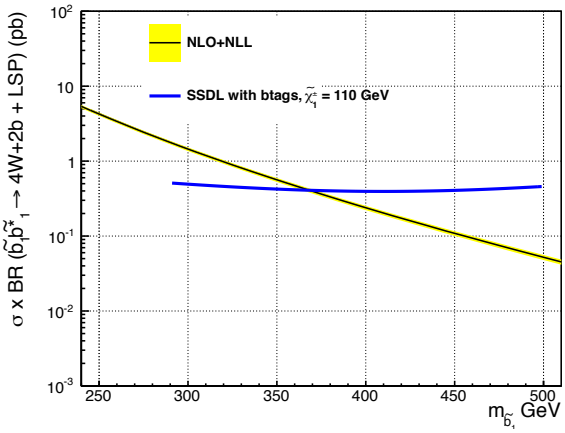

Figure 26: Cross section limits as a function of sbottom mass in the sbottom pair production model, compared with the sbottom pair-production coss-section.

10.6 $\widetilde{g} \to \widetilde{b}b$ Model

This model is mostly gluino pair production followed by $\widetilde{g} \to \widetilde{b}b$, $\widetilde{b} \to t\chi^-$ and $\chi^- \to W^-\chi_1^0$. The final state is $t\bar{t}b\bar{b}W^+W^-\chi_1^0\chi_1^0$ or $ttb\bar{b}W^+W^-\chi_1^0\chi_1^0$ $(+c.c.)$. The model also includes the $bg \to \widetilde{b}\widetilde{g}$ process, in which case the final state is $tb\bar{b}W^+W^-\chi_1^0\chi_1^0$ $(+c.c.)$. The model parameters are $M(\widetilde{g})$, $M(\widetilde{b})$, $M(\chi_1^0)$, and $M(\chi^\pm)$. For simplicity we only consider mass parameters such that the χ^- is on shell.

10.6.1 Signal region definition for the $\widetilde{g} \to \widetilde{b}\bar{b}$ Model

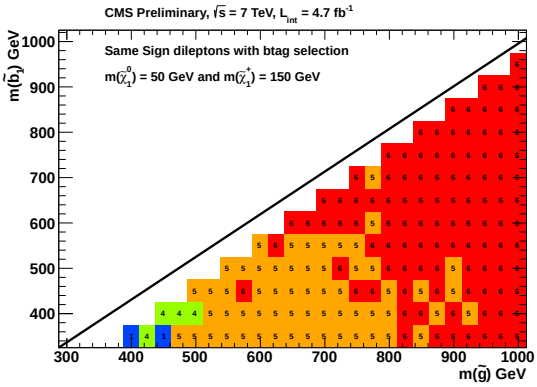

Figure 27: The signal region with the best expected limit as a function of $m(\widetilde{g})$ vs. $m(\widetilde{b})$ for $m(\chi_1^0)$=50 GeV and $m(\chi^\pm)$=150 GeV, in the gluino to sbottom decay model.

For each point in parameter space we use the signal region that gives the best expected limit. Limits are calculated using all experimental uncertainties; the JES and b-tag uncertainties are calculated point-by-point. An example of this optimization is shown in Figure 27, where we show the choice of signal region that gives the best expected limit in the $m(\widetilde{g})$ vs. $m(\widetilde{b})$ plane for the choice $m(\chi_1^0)$=50 GeV and $m(\chi^\pm)$=150 GeV.

10.6.2 Limits for the $\widetilde{g} \to \widetilde{b}\bar{b}$ Model

We choose to present the limits as a function of gluino mass and sbottom mass. This is because the gluino mass is the parameter that drives the production cross-section, and the sbottom mass is a particularly interesting parameter.

Figure 28 shows the limits in the $m(\widetilde{g})$ vs. $m(\widetilde{b})$ plane for $m(\chi_1^0)$ = 50 GeV and $m(\chi^\pm)$ = 150 GeV.

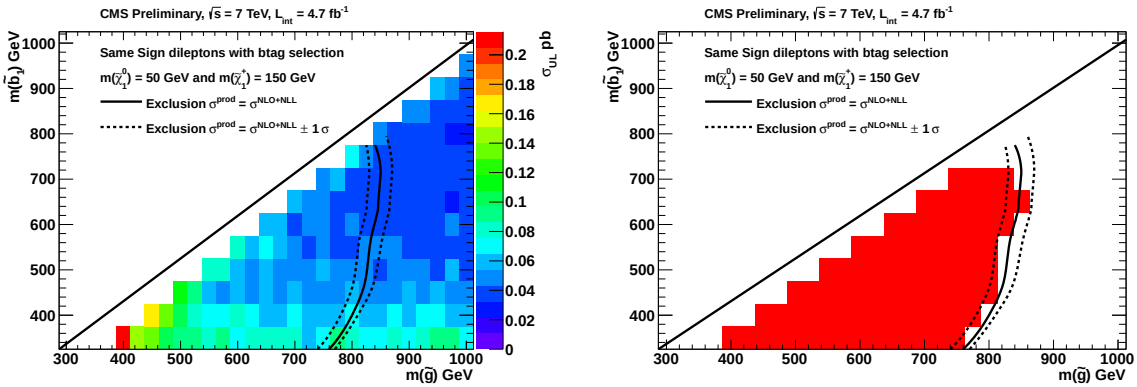

Figure 28: Left plot: Cross section limits in pb in the $m(\widetilde{g})$ vs. $m(\widetilde{b})$ plane for $m(\chi_1^0)$ = 50 GeV and $m(\chi^\pm)$ = 150 GeV. Right: a map of the MC points excluded by this analysis. The limit curves have been smoothed.

To test the sensitivity of the limits to the chargino mass, we perform a more limited scan in the neighborhood of $m(\widetilde{g})$ = 800 GeV for $m(\chi^\pm)$ = 200 and 300 GeV. The results are shown in Figure 29. Finally, in Figure 30 we show exclusion regions for the extreme values of $m(\chi^\pm)$ = 150 and 300 GeV on the same plot, after having smoothed the limit curves.

In summary, in this model we exclude gluino masses below about 800 GeV and sbottom masses up to their kinematical limit, with little sensitivity on the chargino mass.

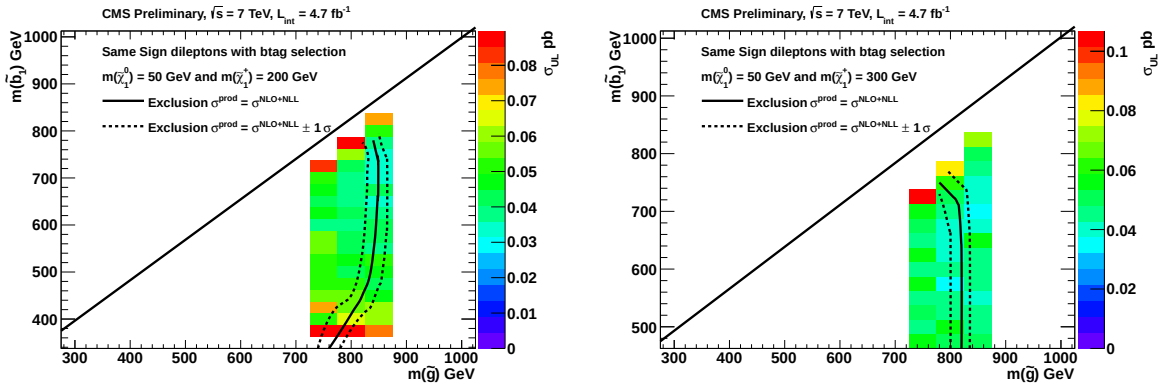

Figure 29: Cross section limits in pb in the $m(\widetilde{g})$ vs. $m(\widetilde{b})$ plane for $m(\chi_1^0)$ = 50 GeV and $m(\chi^{\pm})$ = 200 and 300 GeV. The limit curves have been smoothed.

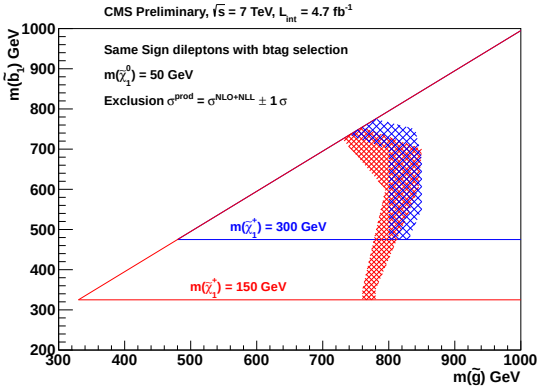

Figure 30: Exclusion lines in the $m(\widetilde{g})$ vs. $m(\widetilde{b})$ plane for $m(\chi_1^0)$ = 50 GeV and $m(\chi^{\pm})$ = 150 and 300 GeV. The width of the lines reflects the cross-section uncertainty. The kinematical boundaries of this model are also shown. The limit curves have been smoothed, and the thickness of the bands represent the uncertainty on the gluino pair production cross-section.

10.7 Additional SUSY plots

In this Section we collect a few additional SUSY plots. These are candidate plots for the public `twiki` page and/or the journal publication.

Figure31 is shows the smoothed limit curve for the `T1tttt` on a white background.

Figure 32 shows the acceptance map for the various models.

Figure 33 shows the gluino mass limits in the models with gluino-pair production considered here. Not surprisingly, we find that the gluino mass limit is fairly insensitive to the details of the decay chain, since the limit is driven by the gluino cross-section.

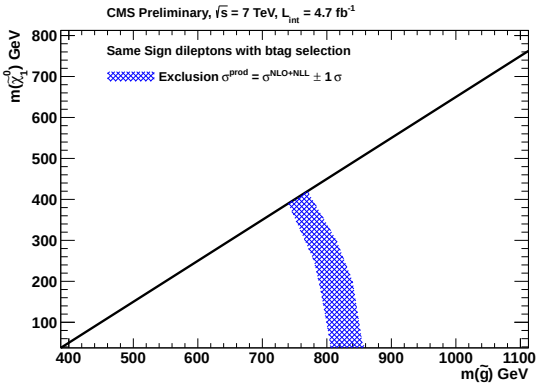

Figure 31: Exclusion curve for the `T1tttt` model. The band shows the uncertainty on the gluino production cross-section. This is basically the same information as shown in Figure 23, after smoothing the limit curves.

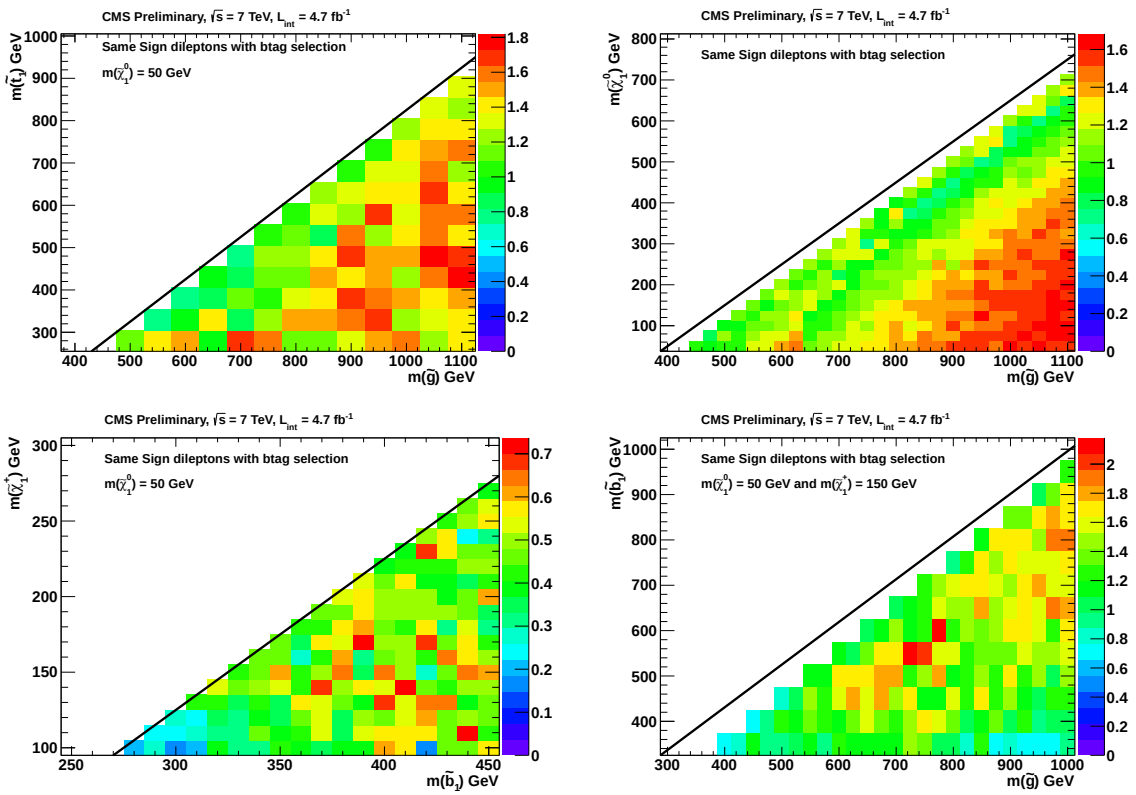

Figure 32: Acceptances for SUSY models considered here.

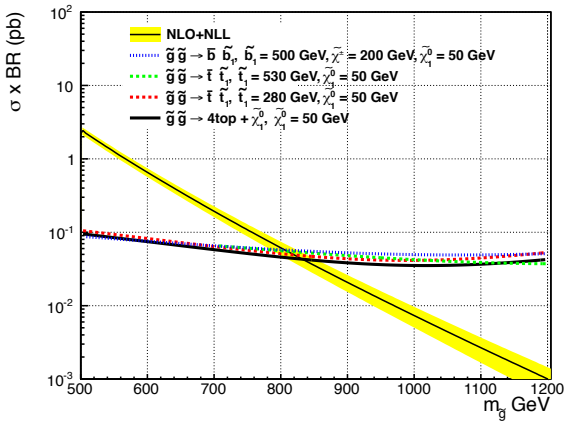

Figure 33: Gluino pair-production cross-section as a function of gluino mass compared with limits on the cross-section from the models considered here.

11 Conclusion

In conclusion, the first search using same-sign dileptons with b-jets and $\not\!\!E_T$ has been presented. In the proton-proton collision data sample corresponding to an integrated luminosity of 4.7 fb^{-1} at $\sqrt{s}$ = 7 TeV, no significant deviations from the Standard Model expectations are observed. We use this data to set 95% CL. on the number of observed events for a number of plausible signal regions defined in terms of requirements in $\not\!\!E_T$and H_T, the number of b-tagged jets (2 or 3), and also the sign of the leptons (only positive dileptons or both positive and negative dileptons). We also provide enough information so that interested phenomenologists could interpret our limits in their favorite new physics models.

In addition, we set limits on the parameter space of six new physics models:

1. A model with a Z' vector boson with flavor violating couplings to $u-$ and t-quarks.
2. A model with a neutral scalar with flavor violating couplings to $u-$ and t-quarks.
3. A SUSY model of stop production from two body gluino decays: $pp \to \widetilde{g}\widetilde{g}$ followed by $\widetilde{g} \to t\widetilde{t}$ and $\widetilde{t} \to t\chi_1^0$.
4. A SUSY model of stop pair production from three body gluino decays: $pp \to \widetilde{g}\widetilde{g}$ followed by $\widetilde{g} \to t\widetilde{t}\chi_1^0$.
5. A SUSY model of sbottom pair production: $pp \to \tilde{b}\tilde{b}$ followed by $\tilde{b} \to t\chi^-$ and $\chi^- \to W^-\chi_1^0$.
6. A SUSY model of sbottom production from gluino decays: $pp \to \widetilde{g}\widetilde{g}$ followed by $\widetilde{g} \to \widetilde{b}b$, $\widetilde{b} \to t\chi^-$, and $\chi^- \to W^-\chi_1^0$.

And that's all for now.

References

[1] S. Chatrchyan *et al.* [CMS Collaboration], *"Search for new physics with same-sign isolated dilepton events with jets and missing transverse energy at the LHC,"* JHEP **1106**, 077 (2011) [arXiv:1104.3168 [hep-ex]].

[2] CMS Collaboration, *"Search for new physics with same-sign isolated dilepton events with jets and missing energy"*, CMS PAS SUS-11-010/SUS-11-025, in preparation.

[3] S. Chatrchyan *et al.* [CMS Collaboration], *"Search for Same-Sign Top-Quark Pair Production at $\sqrt{s}$ = 7 TeV and Limits on Flavour Changing Neutral Currents in the Top Sector,"* JHEP **1108**, 005 (2011) [arXiv:1106.2142 [hep-ex]].

[4] *"Search for New Physics with Same-Sign dileptons using the 2011 dataset of CMS"*, CMS AN-2011/468.

[5] *"Search for new physics with same-sign di-leptons, jets, and missing transverse energy with 4.7 fb^{-1} of data"*, CMS AN-2011/437.

[6] *Search for New Physics in the Same-Sign Di-Lepton Channel Using 4.7 fb^{-1} of 7 TeV pp Collisions"*, CMS AN-2011/466.

[7] *Search for stop and sbottom production with same-sign di-leptons, b-tagged jets and MET* CMS AN-2012/001.

[8] A. G. Cohen, D. B. Kaplan and A. E. Nelson, *"The More minimal supersymmetric standard model,"* Phys. Lett. B **388**, 588 (1996) [hep-ph/9607394].

[9] S. Dimopoulos and G. F. Giudice, *"Naturalness constraints in supersymmetric theories with nonuniversal soft terms,"* Phys. Lett. B **357**, 573 (1995) [hep-ph/9507282].

[10] R. Barbieri, G. R. Dvali and L. J. Hall, *"Predictions from a U(2) flavor symmetry in supersymmetric theories,"* Phys. Lett. B **377**, 76 (1996) [hep-ph/9512388].

[11] M. Papucci, J. T. Ruderman and A. Weiler, *"Natural SUSY Endures,"* arXiv:1110.6926 [hep-ph].

[12] B. S. Acharya, P. Grajek, G. L. Kane, E. Kuflik, K. Suruliz and L. -T. Wang, *"Identifying Multi-Top Events from Gluino Decay at the LHC,"* arXiv:0901.3367 [hep-ph].

[13] G. L. Kane, E. Kuflik, R. Lu and L. -T. Wang, *"Top Channel for Early SUSY Discovery at the LHC,"* Phys. Rev. D **84**, 095004 (2011) [arXiv:1101.1963 [hep-ph]].

[14] S. Kraml and A. R. Raklev, *"Same-sign top quarks as signature of light stops at the LHC,"* Phys. Rev. D **73**, 075002 (2006) [hep-ph/0512284].

[15] R. Essig, E. Izaguirre, J. Kaplan and J. G. Wacker, *"Heavy Flavor Simplified Models at the LHC,"* arXiv:1110.6443 [hep-ph].

[16] T. Plehn and T. M. P. Tait, *"Seeking Sgluons,"* J. Phys. G G **36**, 075001 (2009) [arXiv:0810.3919 [hep-ph]].

[17] M. Gerbush, T. J. Khoo, D. J. Phalen, A. Pierce and D. Tucker-Smith, *"Color-octet scalars at the CERN LHC,"* Phys. Rev. D **77**, 095003 (2008) [arXiv:0710.3133 [hep-ph]].

[18] S. Bar-Shalom and A. Rajaraman, *"Models and phenomenology of maximal flavor violation,"* Phys. Rev. D **77**, 095011 (2008) [arXiv:0711.3193 [hep-ph]].

[19] S. Bar-Shalom, A. Rajaraman, D. Whiteson and F. Yu, *"Collider Signals of Maximal Flavor Violation: Same-Sign Leptons from Same-Sign Tops at the Tevatron,"* Phys. Rev. D **78**, 033003 (2008) [arXiv:0803.3795 [hep-ph]].

[20] T. Aaltonen *et al.* [CDF Collaboration], *"Search for Maximal Flavor Violating Scalars in Same-Charge Lepton Pairs in $p\bar{p}$ Collisions at $\sqrt{s}$ = 1.96-TeV,"* Phys. Rev. Lett. **102**, 041801 (2009) [arXiv:0809.4903 [hep-ex]].

[21] D. Alves *et al.*, *Simplified Models for LHC New Physics Searches*, arxiv:1105.2838; this is the model of Section IV.E with "topology (B+B)".

[22] E. L. Berger, Q. -H. Cao, C. -R. Chen, C. S. Li and H. Zhang, *"Top Quark Forward-Backward Asymmetry and Same-Sign Top Quark Pairs,"* Phys. Rev. Lett. **106**, 201801 (2011) [arXiv:1101.5625 [hep-ph]].

[23] R. Contino and G. Servant, *"Discovering the top partners at the LHC using same-sign dilepton final states,"* JHEP **0806**, 026 (2008) [arXiv:0801.1679 [hep-ph]].

[24] B. Lillie, J. Shu and T. M. P. Tait, *"Top Compositeness at the Tevatron and LHC,"* JHEP **0804**, 087 (2008) [arXiv:0712.3057 [hep-ph]].

[25] A. Pomarol and J. Serra, *"Top Quark Compositeness: Feasibility and Implications,"* Phys. Rev. D **78**, 074026 (2008) [arXiv:0806.3247 [hep-ph]].

[26] K. Kumar, T. M. P. Tait and R. Vega-Morales, *"Manifestations of Top Compositeness at Colliders,"* JHEP **0905**, 022 (2009) [arXiv:0901.3808 [hep-ph]].

[27] CMS Collaboration, *"Measurement of the b-tagging efficiency using $t\bar{t}$ events"*, PAS BTV-11-003, in preparation.

[28] M. Narain for BTV POG, `https://indico.cern.ch/getFile.py/access?contribId=0&resId=1&materialId=slides&confId=163892`

[29] *"Fake Rates for Dilepton Analyses"*, CMS AN-2010/257.

[30] D0 Collaboration, "First measurement of the forward-backward charge asymmetry in top quark pair production", Phys.Rev.Lett.100:142002, (2008)

[31] CDF Collaboration, "Forward-Backward Asymmetry in Top Quark Production in $p\bar{p}$ Collisions at $sqrts = 1.96$ TeV", Phys.Rev.Lett.101:202001, (2008)

[32] CDF Collaboration, "Evidence for a Mass Dependent Forward-Backward Asymmetry in Top Quark Pair Production", arXiv:1101.0034, (2011)

[33] M.R. Buckley et. al, "Light Z' Bosons at the Tevatron", arXiv:1103.6035, (2011)

[34] Moira I. Gresham et. al, "On Models of New Physics for the Tevatron Top AFB", arXiv:1103.3501, (2011)

[35] Z.Ligeti et. al, "Explaining the t tbar forward-backward asymmetry without dijet or flavor anomalies", arXiv:1103.2757, (2011)

[36] Q.H. Cao et. al. Phys.Rev.D81, 114004 (2010)

[37] CMS AN-2011/137

[38] ATLAS Collaboration, "Search for anomalous production of prompt like-sign muon pairs and constraints on physics beyond the Standard Model with the ATLAS detector", [arXiv:1201.1091 [hep-ex]], submitted to *Phys. Rev. D*.

[39] J. A. Aguilar-Saavedra, "Effective four-fermion operators in top physics: a roadmap", Nucl. Phys. B843 (2011), arXiv:1008:3562.

[40] "Search for like-sign top quark pair production at CDF with 6.1 fb^{-1}", CDF/PHYS/EXO/PUBLIC/10466, `http://www-cdf.fnal.gov/physics/exotic/r2a/20110407.samesigndileptons/sstops.pdf`

[41] http://lhcnewphysics.org/l.006.00.r000, Simplified model by Felix Yu, UCI

[42] http://arxiv.org/abs/hep-ph/0512284,SUSY Gluinos to light stop

[43] http://arxiv.org/abs/1004.2256,more SUSY Gluinos to light stop

[44] "Computing the contamination from fakes in leptonic final statess", CMS AN2010-261.

A Further Fake Rate Discussion

Here we address some general questions about the Fake Rate (FR) method that have been asked in many different occasions. They are

1. What about the heavy flavor (HF) composition? How can you use the same method in this analysis (where the fakes are mostly not from HF) and in the untagged analysis (where the fakes are mostly from HF)?
2. What is this story of the parton P_T dependence all about?
3. Why do you take 50% as an uncertainty?
4. What about signal contamination?
5. If you have an over-prediction in the $t\bar{t}$ closure test, why don't you correct for that?
6. Can this be improved?

A.1 Heavy Flavor composition

The first thing to realize is that this question only really applies to electrons. Reasonably high P_T muons in CMS that are not from EWK sources are dominantly from HF, e.g.,

- Typically we find that 85-90% of Fakeable Objects (FO) in the QCD MC are from HF.
- Even for this analysis, where the HF lepton background in $t\bar{t}$ has been strongly suppressed by the ≥ 2 btag requirement, the remaining muon BG is mostly from HF. This can be best seen by the entries corresponding to the lines $t\bar{t} \to \ell(b \to \ell)X$ and $t\bar{t} \to \ell(\not{b} \to \ell)X$ in the $\mu\mu$ column of Table 10. This shows that in $t\bar{t}$ MC the predicted BG with muons from HF (≈ 0.14 events) is much larger than the BG with muons from other sources (≈ 0.02 events).

For electrons, the HF dependence can be controlled by carefully choosing what to use in the "extrapolation", *i.e.*, what electron requirements are loosened in going from the full electron selection to the FO selection. This is discussed in Reference [29]. Briefly, there are three general ways of defining the FO (V1, V2, V3):

- V1 = extrapolate in ID and ISO
- V2 = extrapolate in ID only
- V3 = extrapolate in ISO only

Extrapolating in ID introduces a HF dependence: electrons in HF are "real", therefore the extrapolation in ID depends on the HF composition. If one does not worry about HF, V1 and V2 are sensible choices, with some distinct advantages over V3, namely: V2 is the most stable wrt parent parton P_T and V1 gives the best statistical power. In the $H \to WW$ analysis, for example, we use V1. On the other hand, V3 is the most stable against the HF dependence, but has the worst parton P_T dependence (this dependence will be discussed in Section A.2).

For SUSY analyses we worry about HF and we use V3, *i.e.*, we extrapolate mostly in ISO. A priori we do not expect a huge dependence of V3 on HF because the FR of fake electrons from udsg and HF cannot be that different: in both cases we are talking about electrons originating from jets, and the properties of jets from udgs are not markedly different from those from b. But this needs to be tested, see below.

We have performed these tests a few times, the best record of these is Reference [29]. Here we summarize the results from that note.

We measure the electron FR in data QCD events with an away jet of 40 GeV. We then apply this FR to FO in QCD events selected in the same way but with the away jet b-tagged. We compare the yield predicted by the FR method with the number of electrons passing the cuts in the sample. We find a ratio predicted/observed = 1.17 ± 0.05. Note that this test is not 100% clean. There is an additional bias because the act of tagging most likely changes the underlying P_T of the partons in the event (for example: btagging is not flat vs jet P_T).

We also perform the same test in MC. Here we did not have enough stats, so we had to use the muon-enriched sample. This may introduce yet more bias on the away jet (now the away jet not only is b-tagged, but it is most likely a $b \to \mu$ decay). The result on MC is predicted/observed = 0.75 ± 0.06.

The bottom line is that we find that enriching the sample in HF changes the electron FR by something of order 20%. These changes are due to some combination of HF effects and kinematical changes in the sample due to the HF enrichment requirements. We did not try to separate them out. But the conclusion is that the method works well enough on both HF-rich and HF-poor event samples in both data and MC.

It is also interesting to note that the V1 and V2 FR lead to an underprediction in the HF enriched samples, just as can be argued from first principles. For data we find predicted/observed = 0.69 ± 0.07 and 0.60 ± 0.06 for V1 and V2 respectively; in MC we find predicted/observed = 0.27 ± 0.04 (V1) and 0.30 ± 0.04 (V2).

Finally, just for fun, we repeat the exercise for muons. In data we find predicted/observed = 1.03 ± 0.03, perfectly consistent with 1; in MC we find this ratio to be 0.81 ± 0.01, suggesting that indeed there must be some bias in going from the QCD to the muon enriched sample.

A.2 Parton P_T dependence

The isolation of a lepton of a given P_T depends on the P_T of the mother parton. This is easy to understand, *e.g.*, a 19 GeV muon from the decay of a 20 GeV b-quark will be quite isolated because the rest of the b-decay products can only take up 1 GeV of momentum. On the other hand a 19 GeV muon from the decay of a 60 GeV b-quark will be much less isolated.

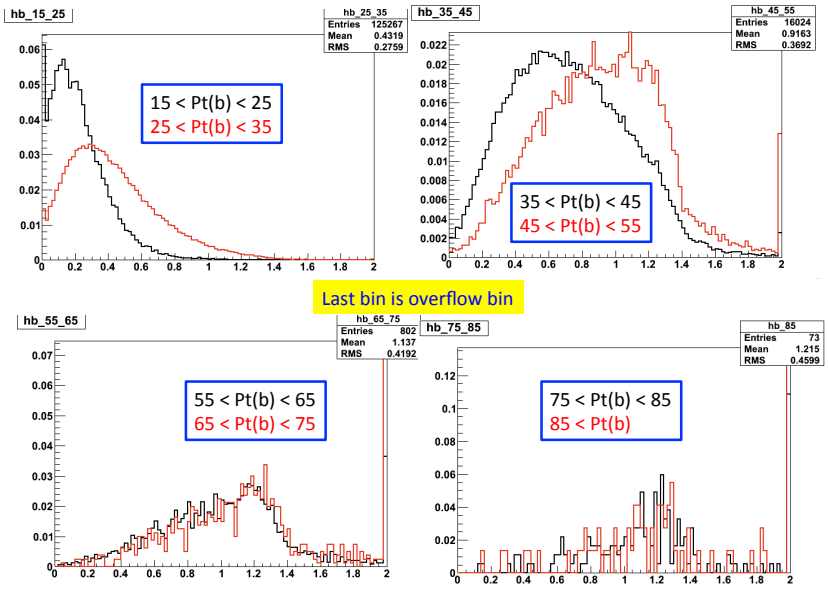

Figure 34: Isolation for a MC muon from $b \to \mu$ decays of 14 GeV $< P_T <$ 16 GeV for different intervals of the parent b-quark P_T.

This is a **huge** effect, as can be seen from Figure 34. As a result, extrapolations in isolation are very sensitive to the parent parton P_T distribution. We have found that this effect can be mitigated by reducing the range of isolation over which we extrapolate. This is why all our isolation extrapolations start from iso < 0.4 or 0.6, not iso $< \infty$.

The muon FR is essentially an extrapolation in isolation since it is almost[6)] the only handle that can be used to separate fake muons from EWK muons. Thus the muon FR, as well as the V3 electron FR, are quite sensitive to the P_T of the partons from which the lepton originates.

[6)] The other handle is impact parameter, which is used and which is insensitive to the parton P_T; however, by itself it does not provide enough of a lever arm.

Figures 5 and 6 show the muon and electron FR measured in data QCD events with different minimum requirements on the away jet P_T. To the extent that these events are mostly di-jets, the away jet P_T is a measure of the P_T of the parton from which the lepton originates. We see that as we reduce the away jet P_T the FR goes up. This is what is expected from Figure 34.

We think that it would be a mistake to take the variations of Figures 5 and 6 too literally. The away jet P_T is only an approximation to the parent parton P_T. Things are not that simple. For example, there are 3-jet events, there is gluon splitting inside a jet, and last but not least the P_T distributions of jets in QCD events is steeply falling, while the P_T distribution of jets in the backgrounds to dileptonic SUSY sources is not.

A.3 Where does the 50% uncertainty come from?

Most (all?) systematic uncertainties are judgement calls. The choice of 50% (over)covers the variations of Figures 5 and 6. It (over)covers the variations seen in the HF tests (Section A.1). It just-about covers the closure tests in the $t\bar{t}$ sample (Table 9 in this note, but also results from References [4] and [29]). After playing around with various options, and after having looked under the hood as we were developing this methodology as far back as 2008, we have developed a sense of how much we can trust the method. It is not perfect: 50% is perhaps conservative but we feel is a realistic estimate. Finally, 50% is a nice round number.

A.4 What about signal contamination?

The signal can have fake leptons. These are subtracted off by the fake rate procedure. To be consistent, in signal MC we only count leptons that are truth matched to EWK sources, *i.e.*, decays of W, Z, chargino, etc.

The second effect is that in a SUSY event a lepton from EWK sources can fail the full lepton ID selection but pass the looser fakeable object (FO) selection. These events would then increase the count of FO failing the full selection and therefore increase the background prediction. To account for this effect in signal MC, we count the number of such events, we weight them by their corresonding fake rate factors, and we then subtract them off from the acceptance.

Here is a back of the envelope estimate of the size of the effect. The probability for a lepton to fail the isolation cuts is of the order 20%, see Figure 2. For events with two such leptons, the probability that a signal event contaminates the FO sideband is then $\approx 40\%$. These events are then weighted by a FR, which is of order 10%, see Figures 5 and 6. Therefore the size of the effect that we correct for is of order 4%.

This last effect can in principle be taken into account "ab-initio" in the formulation of the FR method, see for example the discussion of the parameter p in Reference [44]. However this causes significant mathematical complications. To minimize these complications, in applying this method to the generic SS analysis the authors of Reference [44] took a constant FR, independent of P_T and η. In addition, there is the question of what exactly to take for p, which is the probability for a signal lepton to pass the loose cuts but fail the tight cuts. This probability is in general a function of the signal itself, *e.g.*, leptons in signals with more hadronic activity will have higher probabilities of failing the isolation cut. To avoid these complications we have decided to leave this p factor out, and then apply a correction at the end.

A.5 Why not correct for the over prediction in $t\bar{t}$ MC?

We are not correcting for the overprediction in $t\bar{t}$ MC (Table 9) for the following reasons.

In a search for new physics we prefer to err on the side of overestimating rather than underestimating the background. The resulting "overoptimism" of the limits is not a big effect, see Table 18.

We do not fully understand where this overprediction comes from, and so we are not comfortable correcting for it. The hypothesis is that it is due to differences in parton P_T between $t\bar{t}$ and the QCD sample where the FR is measured. We have evidence that there is an effect of this sort, see Section 11.3 and Figure 7 of Reference [29], but it was not quantified at the time. Since then we have tried to look at this in more detail. Preliminary results point in the same direction, but the studies were never completed.

Finally, in the limit that the data and MC QCD FR are the same, the correction is equivalent to counting FO in data and multiplying them by the ratio of BG leptons to FO in MC. This seems to us to be going a bit too far away from the data driven methodology.

A.6 Can the method be improved?

The method can be improved by reducing the parton P_T dependence of the FR. One would need to "sculpt" the away-jet P_T distribution to better match the expected P_T distribution of partons in the BG. This assumes that we can indeed show quantitatively that the overprediction in $t\bar{t}$ is from parton P_T.

One of these days, when we are not in a mad rush for ICHEP or Moriond, or chasing some SUSY scan, or fixing the hyphens in the paper drafts, or adding lines of NLL+NLO+PDF uncertainties to cross-sections of processes that do not exist, we might actually do it. However we don't think that we can go much below something like 30% on the systematic uncertainty, and the improvement will not be a game changer.

B Results - Exclusive Yields

The information in this appendix is not used quantitatively anywhere.

The tighter H_T and $\not\!\!E_T$ search regions used for the SUSY production scenarios and defined in Section 3 can be defined exclusively and cover the same phase space without an overlap between regions:

1. Exclusive low-H_T low-$\not\!\!E_T$ region: $200 < H_T < 320$ GeV, $50 < \not\!\!E_T < 120$ GeV.
2. Exclusive low-H_T high-$\not\!\!E_T$ region: $200 < H_T < 320$ GeV, $\not\!\!E_T > 120$ GeV.
3. Exclusive high-H_T low-$\not\!\!E_T$ region: $H_T > 320$ GeV, $50 < \not\!\!E_T < 120$ GeV.
4. Exclusive high-H_T high-$\not\!\!E_T$ region: $H_T > 320$ GeV, $\not\!\!E_T > 120$ GeV.

The exclusive high-H_T high-$\not\!\!E_T$ region is the same as its inclusive version.

In the following we report exclusive breakdown of the expected and observed events in the H_T-$\not\!\!E_T$ SUSY search regions. These are reported in Tables 20 to 22. The formatting of these tables is the same as in Section 7. Results for the exclusive high-H_T high-$\not\!\!E_T$ region are not repeated and can be found in Table 15.

Source	ee	$\mu\mu$	eμ	all
$t\bar{t} \to \ell\ell X$	0.017 ± 0.013	0.000 ± 0.013	0.000 ± 0.013	0.017 ± 0.013
$t\bar{t}$ other	0.000 ± 0.013	0.000 ± 0.013	0.000 ± 0.013	0.000 ± 0.013
$t\bar{t} \to \ell(b \to \ell)X$	0.000 ± 0.013	0.000 ± 0.013	0.000 ± 0.013	0.000 ± 0.013
$t\bar{t} \to \ell(\not{b} \to \ell)X$	0.026 ± 0.019	0.000 ± 0.013	0.049 ± 0.028	0.075 ± 0.034
t, s-channel	0.000 ± 0.057	0.000 ± 0.057	0.000 ± 0.057	0.000 ± 0.057
t, t-channel	0.000 ± 0.055	0.000 ± 0.055	0.000 ± 0.055	0.000 ± 0.055
tW	0.000 ± 0.045	0.000 ± 0.045	0.000 ± 0.045	0.000 ± 0.045
$Z \to ee$	0.000 ± 0.429	0.000 ± 0.429	0.000 ± 0.429	0.000 ± 0.429
$Z \to \mu\mu$	0.000 ± 0.429	0.000 ± 0.429	0.000 ± 0.429	0.000 ± 0.429
$Z \to \tau\tau$	0.000 ± 0.429	0.000 ± 0.429	0.000 ± 0.429	0.000 ± 0.429
W+jets	0.000 ± 1.808	0.000 ± 1.808	0.000 ± 1.808	0.000 ± 1.808
WW	0.000 ± 0.019	0.000 ± 0.019	0.000 ± 0.019	0.000 ± 0.019
Vγ	0.000 ± 0.248	0.000 ± 0.248	0.000 ± 0.248	0.000 ± 0.248
$W\gamma^* \to \ell\nu ee$	0.000 ± 0.097	0.000 ± 0.097	0.000 ± 0.097	0.000 ± 0.097
$W\gamma^* \to \ell\nu\mu\mu$	0.000 ± 0.075	0.000 ± 0.075	0.000 ± 0.075	0.000 ± 0.075
$W\gamma^* \to \ell\nu\tau\tau$	0.000 ± 0.028	0.000 ± 0.028	0.000 ± 0.028	0.000 ± 0.028
WZ	0.005 ± 0.005	0.000 ± 0.003	0.000 ± 0.003	0.005 ± 0.005
ZZ	0.000 ± 0.000	0.000 ± 0.000	0.000 ± 0.000	0.000 ± 0.000
dp$W^{\pm}W^{\pm}$	0.000 ± 0.004	0.000 ± 0.004	0.000 ± 0.004	0.000 ± 0.004
spW^-W^-	0.000 ± 0.001	0.000 ± 0.001	0.000 ± 0.001	0.000 ± 0.001
spW^+W^+	0.000 ± 0.006	0.000 ± 0.006	0.000 ± 0.006	0.000 ± 0.006
$t\bar{t}\gamma$	0.000 ± 0.059	0.000 ± 0.059	0.000 ± 0.059	0.000 ± 0.059
$t\bar{t}W$	0.028 ± 0.006	0.041 ± 0.006	0.077 ± 0.009	0.146 ± 0.012
$t\bar{t}Z$	0.003 ± 0.001	0.009 ± 0.003	0.009 ± 0.002	0.020 ± 0.004
$WW\gamma$	0.000 ± 0.015	0.000 ± 0.015	0.000 ± 0.015	0.000 ± 0.015
WWW	0.000 ± 0.000	0.000 ± 0.000	0.000 ± 0.000	0.000 ± 0.000
WWZ	0.000 ± 0.000	0.000 ± 0.000	0.000 ± 0.000	0.000 ± 0.000
WZZ	0.000 ± 0.000	0.000 ± 0.000	0.000 ± 0.000	0.000 ± 0.000
ZZZ	0.000 ± 0.000	0.000 ± 0.000	0.000 ± 0.000	0.000 ± 0.000
Total MC	0.079 ± 0.025	0.049 ± 0.007	0.135 ± 0.030	0.263 ± 0.039
LM6	0.000 ± 0.000	0.000 ± 0.000	0.000 ± 0.000	0.000 ± 0.000
SF	0.00 ± 0.58	0.00 ± 0.37	0.18 ± 0.55	0.18 ± 0.55
DF	0.00 ± 0.14	0.00 ± 0.10	0.00 ± 0.16	0.00 ± 0.16
SF + DF	$0.00 \pm 0.50 \pm 0.00$	$0.00 \pm 0.31 \pm 0.00$	$0.18 \pm 0.45 \pm 0.09$	$0.18 \pm 0.45 \pm 0.09$
Charge Flips	$0.009 \pm 0.004 \pm 0.002$	- $\pm$ -	$0.010 \pm 0.004 \pm 0.002$	$0.019 \pm 0.006 \pm 0.004$
MC Pred	$0.036 \pm 0.008 \pm 0.018$	$0.049 \pm 0.007 \pm 0.025$	$0.086 \pm 0.009 \pm 0.043$	$0.171 \pm 0.014 \pm 0.086$
Total Pred	$0.045 \pm 0.501 \pm 0.018$	$0.049 \pm 0.315 \pm 0.025$	$0.272 \pm 0.447 \pm 0.098$	$0.366 \pm 0.447 \pm 0.123$
data	1	0	1	2

Table 20: Observed event yields in the exclusive low-H_T high-$\not{E}_T$ region ($200 < H_T < 320$ GeV, $\not{E}_T > 120$ GeV) compared to expectations from simulation alone, and from the data-driven methods. The upper part of the table is based on simulation only and is used only as a reference. The lower part is the main result of the analysis. The SF (DF) contributions are for events with one (two) fake leptons. The *MC Pred* contribution includes contributions from genuine same-sign lepton pairs (a sum of the rows from $V\gamma$ down to ZZZ). Entries with zero contributing events are reported with an uncertainty corresponding to one event. This uncertainty is not added to the total MC contribution. Systematic uncertainties (the second uncertainty if present) are displayed only for the final combined type of background, no systematic uncertainty is added for estimates with zero entries. Systematic uncertainties are 100% correlated among the channels.

Source	ee	$\mu\mu$	eμ	all
$t\bar{t} \to \ell\ell X$	0.151 ± 0.056	0.000 ± 0.013	0.081 ± 0.036	0.232 ± 0.066
$t\bar{t}$ other	0.000 ± 0.013	0.000 ± 0.013	0.000 ± 0.013	0.000 ± 0.013
$t\bar{t} \to \ell(b \to \ell)X$	0.016 ± 0.016	0.014 ± 0.014	0.025 ± 0.025	0.055 ± 0.033
$t\bar{t} \to \ell(\not{b} \to \ell)X$	0.135 ± 0.047	0.000 ± 0.013	0.149 ± 0.054	0.284 ± 0.072
t, s-channel	0.000 ± 0.057	0.000 ± 0.057	0.000 ± 0.057	0.000 ± 0.057
t, t-channel	0.000 ± 0.055	0.000 ± 0.055	0.000 ± 0.055	0.000 ± 0.055
tW	0.000 ± 0.045	0.000 ± 0.045	0.016 ± 0.045	0.016 ± 0.045
$Z \to ee$	0.000 ± 0.429	0.000 ± 0.429	0.000 ± 0.429	0.000 ± 0.429
$Z \to \mu\mu$	0.000 ± 0.429	0.000 ± 0.429	0.000 ± 0.429	0.000 ± 0.429
$Z \to \tau\tau$	0.000 ± 0.429	0.000 ± 0.429	0.000 ± 0.429	0.000 ± 0.429
W+jets	0.000 ± 1.808	0.000 ± 1.808	0.000 ± 1.808	0.000 ± 1.808
WW	0.000 ± 0.019	0.000 ± 0.019	0.000 ± 0.019	0.000 ± 0.019
Vγ	0.000 ± 0.248	0.000 ± 0.248	0.000 ± 0.248	0.000 ± 0.248
$W\gamma^* \to \ell\nu ee$	0.000 ± 0.097	0.000 ± 0.097	0.000 ± 0.097	0.000 ± 0.097
$W\gamma^* \to \ell\nu\mu\mu$	0.000 ± 0.075	0.000 ± 0.075	0.000 ± 0.075	0.000 ± 0.075
$W\gamma^* \to \ell\nu\tau\tau$	0.000 ± 0.028	0.000 ± 0.028	0.000 ± 0.028	0.000 ± 0.028
WZ	0.005 ± 0.005	0.012 ± 0.007	0.004 ± 0.004	0.020 ± 0.009
ZZ	0.000 ± 0.000	0.000 ± 0.000	0.000 ± 0.000	0.000 ± 0.000
dp$W^{\pm}W^{\pm}$	0.000 ± 0.004	0.000 ± 0.004	0.000 ± 0.004	0.000 ± 0.004
sp$W^{-}W^{-}$	0.000 ± 0.001	0.000 ± 0.001	0.001 ± 0.001	0.001 ± 0.001
sp$W^{+}W^{+}$	0.000 ± 0.006	0.000 ± 0.006	0.000 ± 0.006	0.000 ± 0.006
$t\bar{t}\gamma$	0.000 ± 0.059	0.000 ± 0.059	0.000 ± 0.059	0.000 ± 0.059
$t\bar{t}W$	0.147 ± 0.013	0.175 ± 0.014	0.277 ± 0.017	0.599 ± 0.026
$t\bar{t}Z$	0.027 ± 0.004	0.035 ± 0.005	0.059 ± 0.006	0.120 ± 0.009
$WW\gamma$	0.000 ± 0.015	0.000 ± 0.015	0.000 ± 0.015	0.000 ± 0.015
WWW	0.000 ± 0.000	0.000 ± 0.000	0.000 ± 0.000	0.000 ± 0.000
WWZ	0.000 ± 0.000	0.000 ± 0.000	0.001 ± 0.001	0.001 ± 0.001
WZZ	0.000 ± 0.000	0.000 ± 0.000	0.000 ± 0.000	0.000 ± 0.000
ZZZ	0.000 ± 0.000	0.000 ± 0.000	0.000 ± 0.000	0.000 ± 0.000
Total MC	0.480 ± 0.076	0.236 ± 0.021	0.614 ± 0.074	1.329 ± 0.108
LM6	0.000 ± 0.000	0.000 ± 0.000	0.000 ± 0.000	0.000 ± 0.000
SF	0.24 ± 0.55	0.00 ± 0.37	0.27 ± 0.59	0.51 ± 0.75
DF	0.00 ± 0.14	0.00 ± 0.10	0.00 ± 0.16	0.00 ± 0.16
SF + DF	$0.24 \pm 0.47 \pm 0.12$	$0.00 \pm 0.31 \pm 0.00$	$0.27 \pm 0.49 \pm 0.14$	$0.51 \pm 0.68 \pm 0.25$
Charge Flips	$0.065 \pm 0.012 \pm 0.013$	- $\pm$ -	$0.079 \pm 0.011 \pm 0.016$	$0.144 \pm 0.017 \pm 0.029$
MC Pred	$0.178 \pm 0.014 \pm 0.089$	$0.222 \pm 0.016 \pm 0.111$	$0.344 \pm 0.019 \pm 0.172$	$0.744 \pm 0.029 \pm 0.372$
Total Pred	$0.479 \pm 0.473 \pm 0.148$	$0.222 \pm 0.315 \pm 0.111$	$0.694 \pm 0.495 \pm 0.219$	$1.394 \pm 0.685 \pm 0.451$
data	0	0	1	1

Table 21: Observed event yields in the exclusive low-H_T low-$\not\!\!E_T$ region ($200 < H_T < 320$ GeV, $50 < \not\!\!E_T < 120$ GeV) compared to expectations from simulation alone, and from the data-driven methods. The upper part of the table is based on simulation only and is used only as a reference. The lower part is the main result of the analysis. The SF (DF) contributions are for events with one (two) fake leptons. The *MC Pred* contribution includes contributions from genuine same-sign lepton pairs (a sum of the rows from $V\gamma$ down to ZZZ). Entries with zero contributing events are reported with an uncertainty corresponding to one event. This uncertainty is not added to the total MC contribution. Systematic uncertainties (the second uncertainty if present) are displayed only for the final combined type of background, no systematic uncertainty is added for estimates with zero entries. Systematic uncertainties are 100% correlated among the channels.

C Results - Additional Breakdown of Yields

The information in this appendix is not used quantitatively anywhere.

The search regions used in this analysis and defined in Section 3 can be defined exclusively in either H_T or $\not\!\!E_T$ as seen in the projection plots in Figure 9, where the search region breakdown in $\not\!\!E_T$ was done as:

1. $H_T > 80$ GeV, $30 < \not\!\!E_T < 50$ GeV.
2. $H_T > 80$ GeV, $50 < \not\!\!E_T < 120$ GeV.
3. $H_T > 80$ GeV, $\not\!\!E_T > 120$ GeV.

and in H_T as

1. $80 < H_T < 200$ GeV, $\not\!\!E_T > 30$ GeV.
2. $200 < H_T < 320$ GeV, $\not\!\!E_T > 30$ GeV.
3. $H_T > 320$ GeV, $\not\!\!E_T > 30$ GeV.

In the following we report the breakdown of the expected and observed events in the H_T-$\not\!\!E_T$ SUSY search regions. These are reported in Tables 23 to 28. The formatting of these tables is the same as in Section 7.

Source	ee	$\mu\mu$	eμ	all
$t\bar{t} \to \ell\ell X$	0.067 ± 0.031	0.000 ± 0.013	0.061 ± 0.036	0.129 ± 0.047
$t\bar{t}$ other	0.000 ± 0.013	0.000 ± 0.013	0.000 ± 0.013	0.000 ± 0.013
$t\bar{t} \to \ell(b \to \ell)X$	0.025 ± 0.025	0.020 ± 0.017	0.019 ± 0.019	0.065 ± 0.035
$t\bar{t} \to \ell(\not{b} \to \ell)X$	0.076 ± 0.036	0.016 ± 0.016	0.138 ± 0.053	0.230 ± 0.066
t, s-channel	0.000 ± 0.057	0.000 ± 0.057	0.000 ± 0.057	0.000 ± 0.057
t, t-channel	0.000 ± 0.055	0.000 ± 0.055	0.000 ± 0.055	0.000 ± 0.055
tW	0.000 ± 0.045	0.000 ± 0.045	0.000 ± 0.045	0.000 ± 0.045
$Z \to ee$	0.000 ± 0.429	0.000 ± 0.429	0.000 ± 0.429	0.000 ± 0.429
$Z \to \mu\mu$	0.000 ± 0.429	0.000 ± 0.429	0.000 ± 0.429	0.000 ± 0.429
$Z \to \tau\tau$	0.000 ± 0.429	0.000 ± 0.429	0.000 ± 0.429	0.000 ± 0.429
W+jets	0.000 ± 1.808	0.000 ± 1.808	0.000 ± 1.808	0.000 ± 1.808
WW	0.000 ± 0.019	0.000 ± 0.019	0.000 ± 0.019	0.000 ± 0.019
Vγ	0.000 ± 0.248	0.000 ± 0.248	0.000 ± 0.248	0.000 ± 0.248
$W\gamma^* \to \ell\nu ee$	0.000 ± 0.097	0.000 ± 0.097	0.000 ± 0.097	0.000 ± 0.097
$W\gamma^* \to \ell\nu\mu\mu$	0.000 ± 0.075	0.000 ± 0.075	0.000 ± 0.075	0.000 ± 0.075
$W\gamma^* \to \ell\nu\tau\tau$	0.000 ± 0.028	0.000 ± 0.028	0.000 ± 0.028	0.000 ± 0.028
WZ	0.005 ± 0.005	0.000 ± 0.003	0.006 ± 0.004	0.011 ± 0.006
ZZ	0.000 ± 0.000	0.000 ± 0.000	0.000 ± 0.000	0.000 ± 0.000
dp$W^{\pm}W^{\pm}$	0.000 ± 0.004	0.000 ± 0.004	0.000 ± 0.004	0.000 ± 0.004
spW^-W^-	0.000 ± 0.001	0.000 ± 0.001	0.000 ± 0.001	0.000 ± 0.001
spW^+W^+	0.000 ± 0.006	0.000 ± 0.006	0.000 ± 0.006	0.000 ± 0.006
$t\bar{t}\gamma$	0.000 ± 0.059	0.000 ± 0.059	0.000 ± 0.059	0.000 ± 0.059
$t\bar{t}W$	0.131 ± 0.012	0.134 ± 0.012	0.247 ± 0.016	0.512 ± 0.024
$t\bar{t}Z$	0.024 ± 0.004	0.041 ± 0.005	0.062 ± 0.006	0.127 ± 0.009
$WW\gamma$	0.000 ± 0.015	0.000 ± 0.015	0.000 ± 0.015	0.000 ± 0.015
WWW	0.000 ± 0.000	0.000 ± 0.000	0.001 ± 0.000	0.001 ± 0.001
WWZ	0.000 ± 0.000	0.000 ± 0.000	0.000 ± 0.000	0.000 ± 0.000
WZZ	0.000 ± 0.000	0.000 ± 0.000	0.000 ± 0.000	0.000 ± 0.000
ZZZ	0.000 ± 0.000	0.000 ± 0.000	0.000 ± 0.000	0.000 ± 0.000
Total MC	0.329 ± 0.055	0.211 ± 0.026	0.535 ± 0.069	1.075 ± 0.092
LM6	0.000 ± 0.000	0.000 ± 0.000	0.000 ± 0.000	0.000 ± 0.000
SF	0.27 ± 0.54	0.00 ± 0.37	0.39 ± 0.57	0.66 ± 0.72
DF	0.00 ± 0.14	0.00 ± 0.10	0.00 ± 0.16	0.00 ± 0.16
SF + DF	$0.27 \pm 0.45 \pm 0.14$	$0.00 \pm 0.31 \pm 0.00$	$0.39 \pm 0.47 \pm 0.19$	$0.66 \pm 0.65 \pm 0.33$
Charge Flips	$0.035 \pm 0.009 \pm 0.007$	- $\pm$ -	$0.057 \pm 0.011 \pm 0.011$	$0.092 \pm 0.014 \pm 0.018$
MC Pred	$0.160 \pm 0.014 \pm 0.080$	$0.175 \pm 0.013 \pm 0.088$	$0.316 \pm 0.018 \pm 0.158$	$0.651 \pm 0.026 \pm 0.326$
Total Pred	$0.468 \pm 0.453 \pm 0.159$	$0.175 \pm 0.315 \pm 0.088$	$0.759 \pm 0.470 \pm 0.250$	$1.402 \pm 0.653 \pm 0.464$
data	1	1	0	2

Table 22: Observed event yields in the exclusive high-H_T low-$\not{E}_T$ region ($H_T > 320$ GeV, $50 < \not{E}_T < 120$ GeV) compared to expectations from simulation alone, and from the data-driven methods. The upper part of the table is based on simulation only and is used only as a reference. The lower part is the main result of the analysis. The SF (DF) contributions are for events with one (two) fake leptons. The *MC Pred* contribution includes contributions from genuine same-sign lepton pairs (a sum of the rows from $V\gamma$ down to ZZZ). Entries with zero contributing events are reported with an uncertainty corresponding to one event. This uncertainty is not added to the total MC contribution. Systematic uncertainties (the second uncertainty if present) are displayed only for the final combined type of background, no systematic uncertainty is added for estimates with zero entries. Systematic uncertainties are 100% correlated among the channels.

Source	ee	$\mu\mu$	eμ	all
$t\bar{t} \to \ell\ell X$	0.342 ± 0.077	0.000 ± 0.199	0.440 ± 0.084	0.782 ± 0.114
$t\bar{t}$ other	0.000 ± 0.199	0.000 ± 0.199	0.000 ± 0.199	0.000 ± 0.199
$t\bar{t} \to \ell(b \to \ell)X$	0.015 ± 0.199	0.037 ± 0.199	0.038 ± 0.199	0.089 ± 0.199
$t\bar{t} \to \ell(\not{b} \to \ell)X$	0.175 ± 0.054	0.000 ± 0.199	0.129 ± 0.046	0.304 ± 0.071
t, s-channel	0.000 ± 0.057	0.000 ± 0.057	0.000 ± 0.057	0.000 ± 0.057
t, t-channel	0.000 ± 0.055	0.000 ± 0.055	0.000 ± 0.055	0.000 ± 0.055
tW	0.000 ± 0.045	0.000 ± 0.045	0.000 ± 0.045	0.000 ± 0.045
$Z \to ee$	0.000 ± 0.429	0.000 ± 0.429	0.000 ± 0.429	0.000 ± 0.429
$Z \to \mu\mu$	0.000 ± 0.429	0.000 ± 0.429	0.000 ± 0.429	0.000 ± 0.429
$Z \to \tau\tau$	0.000 ± 0.429	0.000 ± 0.429	0.000 ± 0.429	0.000 ± 0.429
W+jets	0.000 ± 1.808	0.000 ± 1.808	0.000 ± 1.808	0.000 ± 1.808
WW	0.000 ± 0.019	0.000 ± 0.019	0.000 ± 0.019	0.000 ± 0.019
Vγ	0.000 ± 0.248	0.000 ± 0.248	0.000 ± 0.248	0.000 ± 0.248
$W\gamma^* \to \ell\nu ee$	0.000 ± 0.097	0.000 ± 0.097	0.000 ± 0.097	0.000 ± 0.097
$W\gamma^* \to \ell\nu\mu\mu$	0.000 ± 0.075	0.000 ± 0.075	0.000 ± 0.075	0.000 ± 0.075
$W\gamma^* \to \ell\nu\tau\tau$	0.000 ± 0.028	0.000 ± 0.028	0.000 ± 0.028	0.000 ± 0.028
WZ	0.012 ± 0.007	0.004 ± 0.004	0.006 ± 0.006	0.022 ± 0.010
ZZ	0.000 ± 0.000	0.001 ± 0.001	0.000 ± 0.000	0.001 ± 0.001
dp$W^{\pm}W^{\pm}$	0.000 ± 0.004	0.000 ± 0.004	0.000 ± 0.004	0.000 ± 0.004
spW^-W^-	0.000 ± 0.001	0.000 ± 0.001	0.000 ± 0.001	0.000 ± 0.001
spW^+W^+	0.000 ± 0.006	0.000 ± 0.006	0.000 ± 0.006	0.000 ± 0.006
$t\bar{t}\gamma$	0.000 ± 0.059	0.000 ± 0.059	0.000 ± 0.059	0.000 ± 0.059
$t\bar{t}W$	0.121 ± 0.011	0.202 ± 0.014	0.312 ± 0.018	0.635 ± 0.026
$t\bar{t}Z$	0.023 ± 0.004	0.035 ± 0.005	0.046 ± 0.006	0.104 ± 0.009
$WW\gamma$	0.000 ± 0.015	0.000 ± 0.015	0.000 ± 0.015	0.000 ± 0.015
WWW	0.000 ± 0.000	0.000 ± 0.000	0.000 ± 0.000	0.000 ± 0.000
WWZ	0.000 ± 0.000	0.000 ± 0.000	0.000 ± 0.000	0.000 ± 0.000
WZZ	0.000 ± 0.000	0.000 ± 0.000	0.001 ± 0.000	0.001 ± 0.000
ZZZ	0.000 ± 0.000	0.000 ± 0.000	0.000 ± 0.000	0.000 ± 0.000
Total MC	0.688 ± 0.096	0.279 ± 0.030	0.971 ± 0.102	1.938 ± 0.143
LM6	0.000 ± 0.000	0.000 ± 0.000	0.000 ± 0.000	0.000 ± 0.000
SF	0.12 ± 0.52	0.09 ± 0.13	0.57 ± 0.57	0.79 ± 0.73
DF	0.00 ± 0.14	0.02 ± 0.02	0.01 ± 0.13	0.03 ± 0.13
SF + DF	$0.12 \pm 0.43 \pm 0.06$	$0.11 \pm 0.13 \pm 0.06$	$0.58 \pm 0.53 \pm 0.29$	$0.82 \pm 0.69 \pm 0.41$
Charge Flips	$0.320 \pm 0.029 \pm 0.064$	- $\pm$ -	$0.323 \pm 0.024 \pm 0.065$	$0.643 \pm 0.038 \pm 0.129$
MC Pred	$0.156 \pm 0.014 \pm 0.078$	$0.243 \pm 0.016 \pm 0.121$	$0.365 \pm 0.020 \pm 0.183$	$0.764 \pm 0.029 \pm 0.382$
Total Pred	$0.599 \pm 0.428 \pm 0.118$	$0.354 \pm 0.131 \pm 0.134$	$1.271 \pm 0.528 \pm 0.350$	$2.224 \pm 0.692 \pm 0.574$
data	0	0	1	1

Table 23: Observed event yields for $80 < H_T < 200$ GeV and $\not{E}_T > 30$ GeV compared to expectations from simulation alone, and from the data-driven methods. The *simulated backgrounds* contribution includes contributions from genuine same-sign lepton pairs (WZ, ZZ, leptons from same-sign W from single-parton, double-parton, and $t\bar{t}W$ production, etc.), as well as electrons from converted photons in $V\gamma$ production. Entries with zero contributing events are reported with an uncertainty corresponding to one event. This uncertainty is not added to the total MC contribution. Systematic uncertainties (the second uncertainty if present) are displayed only for the final combined type of background, no systematic uncertainty is added for estimates with zero entries. Systematic uncertainties are 100% correlated among the channels.

Source	ee	$\mu\mu$	eμ	all
$t\bar{t} \to \ell\ell X$	0.194 ± 0.060	0.000 ± 0.199	0.105 ± 0.044	0.298 ± 0.074
$t\bar{t}$ other	0.000 ± 0.199	0.000 ± 0.199	0.000 ± 0.199	0.000 ± 0.199
$t\bar{t} \to \ell(b \to \ell)X$	0.029 ± 0.199	0.052 ± 0.199	0.025 ± 0.199	0.105 ± 0.044
$t\bar{t} \to \ell(\not{b} \to \ell)X$	0.196 ± 0.057	0.004 ± 0.199	0.287 ± 0.074	0.487 ± 0.094
t, s-channel	0.000 ± 0.057	0.000 ± 0.057	0.000 ± 0.057	0.000 ± 0.057
t, t-channel	0.077 ± 0.077	0.000 ± 0.055	0.000 ± 0.055	0.077 ± 0.077
tW	0.000 ± 0.045	0.000 ± 0.045	0.016 ± 0.045	0.016 ± 0.045
$Z \to ee$	0.000 ± 0.429	0.000 ± 0.429	0.000 ± 0.429	0.000 ± 0.429
$Z \to \mu\mu$	0.000 ± 0.429	0.000 ± 0.429	0.000 ± 0.429	0.000 ± 0.429
$Z \to \tau\tau$	0.000 ± 0.429	0.000 ± 0.429	0.000 ± 0.429	0.000 ± 0.429
W+jets	0.000 ± 1.808	0.000 ± 1.808	0.000 ± 1.808	0.000 ± 1.808
WW	0.000 ± 0.019	0.000 ± 0.019	0.000 ± 0.019	0.000 ± 0.019
Vγ	0.000 ± 0.248	0.000 ± 0.248	0.000 ± 0.248	0.000 ± 0.248
$W\gamma^* \to \ell\nu ee$	0.000 ± 0.097	0.000 ± 0.097	0.000 ± 0.097	0.000 ± 0.097
$W\gamma^* \to \ell\nu\mu\mu$	0.000 ± 0.075	0.000 ± 0.075	0.000 ± 0.075	0.000 ± 0.075
$W\gamma^* \to \ell\nu\tau\tau$	0.000 ± 0.028	0.000 ± 0.028	0.000 ± 0.028	0.000 ± 0.028
WZ	0.010 ± 0.007	0.012 ± 0.007	0.014 ± 0.008	0.036 ± 0.013
ZZ	0.000 ± 0.000	0.000 ± 0.000	0.001 ± 0.001	0.001 ± 0.001
dp$W^{\pm}W^{\pm}$	0.000 ± 0.004	0.000 ± 0.004	0.000 ± 0.004	0.000 ± 0.004
spW^-W^-	0.000 ± 0.001	0.000 ± 0.001	0.001 ± 0.001	0.001 ± 0.001
spW^+W^+	0.000 ± 0.006	0.000 ± 0.006	0.000 ± 0.006	0.000 ± 0.006
$t\bar{t}\gamma$	0.000 ± 0.059	0.000 ± 0.059	0.000 ± 0.059	0.000 ± 0.059
$t\bar{t}W$	0.218 ± 0.016	0.272 ± 0.017	0.473 ± 0.023	0.963 ± 0.032
$t\bar{t}Z$	0.043 ± 0.005	0.055 ± 0.006	0.101 ± 0.008	0.199 ± 0.012
$WW\gamma$	0.000 ± 0.015	0.000 ± 0.015	0.000 ± 0.015	0.000 ± 0.015
WWW	0.000 ± 0.000	0.000 ± 0.000	0.000 ± 0.000	0.000 ± 0.000
WWZ	0.000 ± 0.000	0.000 ± 0.000	0.001 ± 0.001	0.001 ± 0.001
WZZ	0.000 ± 0.000	0.000 ± 0.000	0.000 ± 0.000	0.000 ± 0.000
ZZZ	0.000 ± 0.000	0.000 ± 0.000	0.000 ± 0.000	0.000 ± 0.000
Total MC	0.767 ± 0.116	0.395 ± 0.036	1.025 ± 0.094	2.187 ± 0.154
LM6	0.000 ± 0.000	0.000 ± 0.000	0.000 ± 0.000	0.000 ± 0.000
SF	0.73 ± 0.63	0.10 ± 0.22	0.52 ± 0.60	1.36 ± 0.87
DF	0.04 ± 0.12	0.00 ± 0.10	0.02 ± 0.13	0.05 ± 0.18
SF + DF	$0.77 \pm 0.59 \pm 0.39$	$0.10 \pm 0.10 \pm 0.05$	$0.53 \pm 0.55 \pm 0.27$	$1.41 \pm 0.81 \pm 0.70$
Charge Flips	$0.058 \pm 0.008 \pm 0.012$	- $\pm$ -	$0.070 \pm 0.008 \pm 0.014$	$0.128 \pm 0.011 \pm 0.026$
MC Pred	$0.272 \pm 0.018 \pm 0.136$	$0.340 \pm 0.019 \pm 0.170$	$0.593 \pm 0.026 \pm 0.296$	$1.205 \pm 0.037 \pm 0.602$
Total Pred	$1.101 \pm 0.588 \pm 0.409$	$0.444 \pm 0.106 \pm 0.178$	$1.197 \pm 0.553 \pm 0.399$	$2.742 \pm 0.814 \pm 0.928$
data	1	1	2	4

Table 24: Observed event yields for $200 < H_T < 320$ GeV and $\not{E}_T > 30$ GeV compared to expectations from simulation alone, and from the data-driven methods. The *simulated backgrounds* contribution includes contributions from genuine same-sign lepton pairs (WZ, ZZ, leptons from same-sign W from single-parton, double-parton, and $t\bar{t}W$ production, etc.), as well as electrons from converted photons in $V\gamma$ production. Entries with zero contributing events are reported with an uncertainty corresponding to one event. This uncertainty is not added to the total MC contribution. Systematic uncertainties (the second uncertainty if present) are displayed only for the final combined type of background, no systematic uncertainty is added for estimates with zero entries. Systematic uncertainties are 100% correlated among the channels.

Source	ee	$\mu\mu$	eμ	all
$t\bar{t} \to \ell\ell X$	0.068 ± 0.199	0.000 ± 0.199	0.108 ± 0.046	0.176 ± 0.056
$t\bar{t}$ other	0.000 ± 0.199	0.000 ± 0.199	0.000 ± 0.199	0.000 ± 0.199
$t\bar{t} \to \ell(b \to \ell)X$	0.025 ± 0.199	0.052 ± 0.199	0.031 ± 0.199	0.108 ± 0.044
$t\bar{t} \to \ell(\not{b} \to \ell)X$	0.175 ± 0.054	0.016 ± 0.199	0.212 ± 0.063	0.403 ± 0.084
t, s-channel	0.000 ± 0.057	0.000 ± 0.057	0.000 ± 0.057	0.000 ± 0.057
t, t-channel	0.000 ± 0.055	0.000 ± 0.055	0.000 ± 0.055	0.000 ± 0.055
tW	0.000 ± 0.045	0.000 ± 0.045	0.000 ± 0.045	0.000 ± 0.045
$Z \to ee$	0.000 ± 0.429	0.000 ± 0.429	0.000 ± 0.429	0.000 ± 0.429
$Z \to \mu\mu$	0.000 ± 0.429	0.000 ± 0.429	0.000 ± 0.429	0.000 ± 0.429
$Z \to \tau\tau$	0.000 ± 0.429	0.000 ± 0.429	0.000 ± 0.429	0.000 ± 0.429
W+jets	0.000 ± 1.808	0.000 ± 1.808	0.000 ± 1.808	0.000 ± 1.808
WW	0.000 ± 0.019	0.000 ± 0.019	0.000 ± 0.019	0.000 ± 0.019
Vγ	0.000 ± 0.248	0.000 ± 0.248	0.000 ± 0.248	0.000 ± 0.248
$W\gamma^* \to \ell\nu ee$	0.000 ± 0.097	0.000 ± 0.097	0.000 ± 0.097	0.000 ± 0.097
$W\gamma^* \to \ell\nu\mu\mu$	0.000 ± 0.075	0.000 ± 0.075	0.000 ± 0.075	0.000 ± 0.075
$W\gamma^* \to \ell\nu\tau\tau$	0.000 ± 0.028	0.000 ± 0.028	0.000 ± 0.028	0.000 ± 0.028
WZ	0.012 ± 0.007	0.001 ± 0.003	0.011 ± 0.006	0.024 ± 0.009
ZZ	0.000 ± 0.000	0.000 ± 0.000	0.000 ± 0.000	0.000 ± 0.000
dp$W^{\pm}W^{\pm}$	0.000 ± 0.004	0.000 ± 0.004	0.000 ± 0.004	0.000 ± 0.004
spW^-W^-	0.000 ± 0.001	0.000 ± 0.001	0.001 ± 0.001	0.001 ± 0.001
spW^+W^+	0.000 ± 0.006	0.000 ± 0.006	0.000 ± 0.006	0.000 ± 0.006
$t\bar{t}\gamma$	0.000 ± 0.059	0.000 ± 0.059	0.000 ± 0.059	0.000 ± 0.059
$t\bar{t}W$	0.232 ± 0.016	0.260 ± 0.016	0.499 ± 0.023	0.991 ± 0.033
$t\bar{t}Z$	0.054 ± 0.006	0.069 ± 0.007	0.124 ± 0.009	0.247 ± 0.013
$WW\gamma$	0.000 ± 0.015	0.000 ± 0.015	0.000 ± 0.015	0.000 ± 0.015
WWW	0.000 ± 0.000	0.000 ± 0.000	0.001 ± 0.001	0.002 ± 0.001
WWZ	0.000 ± 0.000	0.000 ± 0.000	0.000 ± 0.000	0.000 ± 0.000
WZZ	0.000 ± 0.000	0.000 ± 0.000	0.000 ± 0.000	0.000 ± 0.000
ZZZ	0.000 ± 0.000	0.000 ± 0.000	0.000 ± 0.000	0.000 ± 0.000
Total MC	0.568 ± 0.070	0.398 ± 0.037	0.989 ± 0.085	1.954 ± 0.116
LM6	0.000 ± 0.000	0.186 ± 0.186	0.383 ± 0.275	0.569 ± 0.332
SF	0.27 ± 0.54	0.10 ± 0.22	0.83 ± 0.63	1.21 ± 0.78
DF	0.00 ± 0.14	0.00 ± 0.10	0.00 ± 0.16	0.00 ± 0.16
SF + DF	$0.27 \pm 0.45 \pm 0.14$	$0.10 \pm 0.10 \pm 0.05$	$0.83 \pm 0.54 \pm 0.42$	$1.21 \pm 0.72 \pm 0.60$
Charge Flips	$0.074 \pm 0.014 \pm 0.015$	- $\pm$ -	$0.082 \pm 0.013 \pm 0.016$	$0.155 \pm 0.019 \pm 0.031$
MC Pred	$0.299 \pm 0.019 \pm 0.149$	$0.330 \pm 0.018 \pm 0.165$	$0.637 \pm 0.026 \pm 0.319$	$1.266 \pm 0.036 \pm 0.633$
Total Pred	$0.646 \pm 0.453 \pm 0.203$	$0.435 \pm 0.106 \pm 0.173$	$1.550 \pm 0.545 \pm 0.524$	$2.630 \pm 0.717 \pm 0.876$
data	1	1	0	2

Table 25: Observed event yields for $H_T > 320$ GeV and $\not{E}_T > 30$ GeV compared to expectations from simulation alone, and from the data-driven methods. The *simulated backgrounds* contribution includes contributions from genuine same-sign lepton pairs (WZ, ZZ, leptons from same-sign W from single-parton, double-parton, and $t\bar{t}W$ production, etc.), as well as electrons from converted photons in $V\gamma$ production. Entries with zero contributing events are reported with an uncertainty corresponding to one event. This uncertainty is not added to the total MC contribution. Systematic uncertainties (the second uncertainty if present) are displayed only for the final combined type of background, no systematic uncertainty is added for estimates with zero entries. Systematic uncertainties are 100% correlated among the channels.

Source	ee	$\mu\mu$	eμ	all
$t\bar{t} \to \ell\ell X$	0.141 ± 0.046	0.000 ± 0.199	0.201 ± 0.060	0.343 ± 0.076
$t\bar{t}$ other	0.000 ± 0.199	0.000 ± 0.199	0.000 ± 0.199	0.000 ± 0.199
$t\bar{t} \to \ell(b \to \ell)X$	0.027 ± 0.199	0.066 ± 0.199	0.032 ± 0.199	0.126 ± 0.045
$t\bar{t} \to \ell(\not{b} \to \ell)X$	0.184 ± 0.057	0.004 ± 0.199	0.166 ± 0.054	0.354 ± 0.079
t, s-channel	0.000 ± 0.057	0.000 ± 0.057	0.000 ± 0.057	0.000 ± 0.057
t, t-channel	0.077 ± 0.077	0.000 ± 0.055	0.000 ± 0.055	0.077 ± 0.077
tW	0.000 ± 0.045	0.000 ± 0.045	0.000 ± 0.045	0.000 ± 0.045
$Z \to ee$	0.000 ± 0.429	0.000 ± 0.429	0.000 ± 0.429	0.000 ± 0.429
$Z \to \mu\mu$	0.000 ± 0.429	0.000 ± 0.429	0.000 ± 0.429	0.000 ± 0.429
$Z \to \tau\tau$	0.000 ± 0.429	0.000 ± 0.429	0.000 ± 0.429	0.000 ± 0.429
W+jets	0.000 ± 1.808	0.000 ± 1.808	0.000 ± 1.808	0.000 ± 1.808
WW	0.000 ± 0.019	0.000 ± 0.019	0.000 ± 0.019	0.000 ± 0.019
Vγ	0.000 ± 0.248	0.000 ± 0.248	0.000 ± 0.248	0.000 ± 0.248
$W\gamma^* \to \ell\nu ee$	0.000 ± 0.097	0.000 ± 0.097	0.000 ± 0.097	0.000 ± 0.097
$W\gamma^* \to \ell\nu\mu\mu$	0.000 ± 0.075	0.000 ± 0.075	0.000 ± 0.075	0.000 ± 0.075
$W\gamma^* \to \ell\nu\tau\tau$	0.000 ± 0.028	0.000 ± 0.028	0.000 ± 0.028	0.000 ± 0.028
WZ	0.003 ± 0.003	0.000 ± 0.003	0.020 ± 0.010	0.023 ± 0.011
ZZ	0.000 ± 0.000	0.000 ± 0.000	0.000 ± 0.000	0.001 ± 0.000
dp$W^{\pm}W^{\pm}$	0.000 ± 0.004	0.000 ± 0.004	0.000 ± 0.004	0.000 ± 0.004
spW^-W^-	0.000 ± 0.001	0.000 ± 0.001	0.000 ± 0.001	0.000 ± 0.001
spW^+W^+	0.000 ± 0.006	0.000 ± 0.006	0.000 ± 0.006	0.000 ± 0.006
$t\bar{t}\gamma$	0.000 ± 0.059	0.000 ± 0.059	0.000 ± 0.059	0.000 ± 0.059
$t\bar{t}W$	0.107 ± 0.011	0.148 ± 0.012	0.274 ± 0.018	0.529 ± 0.024
$t\bar{t}Z$	0.039 ± 0.005	0.032 ± 0.004	0.081 ± 0.007	0.152 ± 0.010
$WW\gamma$	0.000 ± 0.015	0.000 ± 0.015	0.000 ± 0.015	0.000 ± 0.015
WWW	0.000 ± 0.000	0.000 ± 0.000	0.000 ± 0.000	0.000 ± 0.000
WWZ	0.000 ± 0.000	0.000 ± 0.000	0.000 ± 0.000	0.000 ± 0.000
WZZ	0.000 ± 0.000	0.000 ± 0.000	0.000 ± 0.000	0.001 ± 0.000
ZZZ	0.000 ± 0.000	0.000 ± 0.000	0.000 ± 0.000	0.000 ± 0.000
Total MC	0.578 ± 0.109	0.251 ± 0.037	0.776 ± 0.086	1.605 ± 0.144
LM6	0.000 ± 0.000	0.000 ± 0.000	0.000 ± 0.000	0.000 ± 0.000
SF	0.50 ± 0.65	0.30 ± 0.20	0.70 ± 0.59	1.50 ± 0.90
DF	0.04 ± 0.12	0.02 ± 0.02	0.02 ± 0.13	0.07 ± 0.18
SF + DF	$0.53 \pm 0.61 \pm 0.27$	$0.32 \pm 0.20 \pm 0.16$	$0.71 \pm 0.55 \pm 0.36$	$1.57 \pm 0.85 \pm 0.78$
Charge Flips	$0.166 \pm 0.020 \pm 0.033$	- $\pm$ -	$0.148 \pm 0.017 \pm 0.030$	$0.313 \pm 0.026 \pm 0.063$
MC Pred	$0.149 \pm 0.012 \pm 0.075$	$0.181 \pm 0.013 \pm 0.091$	$0.376 \pm 0.022 \pm 0.188$	$0.706 \pm 0.028 \pm 0.353$
Total Pred	$0.850 \pm 0.611 \pm 0.279$	$0.502 \pm 0.197 \pm 0.184$	$1.238 \pm 0.551 \pm 0.405$	$2.589 \pm 0.846 \pm 0.863$
data	0	1	1	2

Table 26: Observed event yields for $H_T > 80$ GeV and $30 < \not{E}_T < 50$ GeV compared to expectations from simulation alone, and from the data-driven methods. The *simulated backgrounds* contribution includes contributions from genuine same-sign lepton pairs (WZ, ZZ, leptons from same-sign W from single-parton, double-parton, and $t\bar{t}W$ production, etc.), as well as electrons from converted photons in $V\gamma$ production. Entries with zero contributing events are reported with an uncertainty corresponding to one event. This uncertainty is not added to the total MC contribution. Systematic uncertainties (the second uncertainty if present) are displayed only for the final combined type of background, no systematic uncertainty is added for estimates with zero entries. Systematic uncertainties are 100% correlated among the channels.

Source	ee	$\mu\mu$	eμ	all
$t\bar{t} \to \ell\ell X$	0.446 ± 0.090	0.000 ± 0.199	0.434 ± 0.085	0.880 ± 0.124
$t\bar{t}$ other	0.000 ± 0.199	0.000 ± 0.199	0.000 ± 0.199	0.000 ± 0.199
$t\bar{t} \to \ell(b \to \ell)X$	0.042 ± 0.199	0.054 ± 0.199	0.062 ± 0.199	0.157 ± 0.055
$t\bar{t} \to \ell(\not{b} \to \ell)X$	0.287 ± 0.068	0.016 ± 0.199	0.323 ± 0.080	0.626 ± 0.106
t, s-channel	0.000 ± 0.057	0.000 ± 0.057	0.000 ± 0.057	0.000 ± 0.057
t, t-channel	0.000 ± 0.055	0.000 ± 0.055	0.000 ± 0.055	0.000 ± 0.055
tW	0.000 ± 0.045	0.000 ± 0.045	0.016 ± 0.045	0.016 ± 0.045
$Z \to ee$	0.000 ± 0.429	0.000 ± 0.429	0.000 ± 0.429	0.000 ± 0.429
$Z \to \mu\mu$	0.000 ± 0.429	0.000 ± 0.429	0.000 ± 0.429	0.000 ± 0.429
$Z \to \tau\tau$	0.000 ± 0.429	0.000 ± 0.429	0.000 ± 0.429	0.000 ± 0.429
W+jets	0.000 ± 1.808	0.000 ± 1.808	0.000 ± 1.808	0.000 ± 1.808
WW	0.000 ± 0.019	0.000 ± 0.019	0.000 ± 0.019	0.000 ± 0.019
Vγ	0.000 ± 0.248	0.000 ± 0.248	0.000 ± 0.248	0.000 ± 0.248
$W\gamma^* \to \ell\nu ee$	0.000 ± 0.097	0.000 ± 0.097	0.000 ± 0.097	0.000 ± 0.097
$W\gamma^* \to \ell\nu\mu\mu$	0.000 ± 0.075	0.000 ± 0.075	0.000 ± 0.075	0.000 ± 0.075
$W\gamma^* \to \ell\nu\tau\tau$	0.000 ± 0.028	0.000 ± 0.028	0.000 ± 0.028	0.000 ± 0.028
WZ	0.021 ± 0.009	0.016 ± 0.008	0.010 ± 0.006	0.047 ± 0.014
ZZ	0.000 ± 0.000	0.001 ± 0.001	0.001 ± 0.001	0.001 ± 0.001
dp$W^{\pm}W^{\pm}$	0.000 ± 0.004	0.000 ± 0.004	0.000 ± 0.004	0.000 ± 0.004
spW^-W^-	0.000 ± 0.001	0.000 ± 0.001	0.001 ± 0.001	0.001 ± 0.001
spW^+W^+	0.000 ± 0.006	0.000 ± 0.006	0.000 ± 0.006	0.000 ± 0.006
$t\bar{t}\gamma$	0.000 ± 0.059	0.000 ± 0.059	0.000 ± 0.059	0.000 ± 0.059
$t\bar{t}W$	0.354 ± 0.020	0.446 ± 0.022	0.737 ± 0.028	1.538 ± 0.041
$t\bar{t}Z$	0.063 ± 0.007	0.095 ± 0.008	0.148 ± 0.010	0.305 ± 0.014
$WW\gamma$	0.000 ± 0.015	0.000 ± 0.015	0.000 ± 0.015	0.000 ± 0.015
WWW	0.000 ± 0.000	0.000 ± 0.000	0.001 ± 0.000	0.002 ± 0.001
WWZ	0.000 ± 0.000	0.000 ± 0.000	0.001 ± 0.001	0.001 ± 0.001
WZZ	0.000 ± 0.000	0.001 ± 0.000	0.000 ± 0.000	0.001 ± 0.000
ZZZ	0.000 ± 0.000	0.000 ± 0.000	0.000 ± 0.000	0.000 ± 0.000
Total MC	1.213 ± 0.119	0.629 ± 0.041	1.734 ± 0.127	3.576 ± 0.179
LM6	0.000 ± 0.000	0.000 ± 0.000	0.000 ± 0.000	0.000 ± 0.000
SF	0.63 ± 0.60	0.00 ± 0.37	0.90 ± 0.63	1.53 ± 0.82
DF	0.00 ± 0.14	0.00 ± 0.10	0.01 ± 0.13	0.01 ± 0.13
SF + DF	$0.63 \pm 0.53 \pm 0.32$	$0.00 \pm 0.31 \pm 0.00$	$0.91 \pm 0.59 \pm 0.45$	$1.54 \pm 0.79 \pm 0.77$
Charge Flips	$0.301 \pm 0.028 \pm 0.060$	- $\pm$ -	$0.361 \pm 0.026 \pm 0.072$	$0.662 \pm 0.038 \pm 0.132$
MC Pred	$0.439 \pm 0.023 \pm 0.220$	$0.559 \pm 0.024 \pm 0.280$	$0.901 \pm 0.031 \pm 0.450$	$1.899 \pm 0.045 \pm 0.949$
Total Pred	$1.372 \pm 0.527 \pm 0.390$	$0.559 \pm 0.315 \pm 0.280$	$2.170 \pm 0.595 \pm 0.644$	$4.102 \pm 0.795 \pm 1.230$
data	1	1	1	3

Table 27: Observed event yields for $H_T > 80$ GeV and $50 < \not{E}_T < 120$ GeV compared to expectations from simulation alone, and from the data-driven methods. The *simulated backgrounds* contribution includes contributions from genuine same-sign lepton pairs (WZ, ZZ, leptons from same-sign W from single-parton, double-parton, and $t\bar{t}W$ production, etc.), as well as electrons from converted photons in $V\gamma$ production. Entries with zero contributing events are reported with an uncertainty corresponding to one event. This uncertainty is not added to the total MC contribution. Systematic uncertainties (the second uncertainty if present) are displayed only for the final combined type of background, no systematic uncertainty is added for estimates with zero entries. Systematic uncertainties are 100% correlated among the channels.

Source	ee	$\mu\mu$	eμ	all
$t\bar{t} \to \ell\ell X$	0.017 ± 0.199	0.000 ± 0.199	0.017 ± 0.199	0.034 ± 0.199
$t\bar{t}$ other	0.000 ± 0.199	0.000 ± 0.199	0.000 ± 0.199	0.000 ± 0.199
$t\bar{t} \to \ell(b \to \ell)X$	0.000 ± 0.199	0.020 ± 0.199	0.000 ± 0.199	0.020 ± 0.199
$t\bar{t} \to \ell(\not{b} \to \ell)X$	0.076 ± 0.199	0.000 ± 0.199	0.139 ± 0.049	0.215 ± 0.060
t, s-channel	0.000 ± 0.057	0.000 ± 0.057	0.000 ± 0.057	0.000 ± 0.057
t, t-channel	0.000 ± 0.055	0.000 ± 0.055	0.000 ± 0.055	0.000 ± 0.055
tW	0.000 ± 0.045	0.000 ± 0.045	0.000 ± 0.045	0.000 ± 0.045
$Z \to ee$	0.000 ± 0.429	0.000 ± 0.429	0.000 ± 0.429	0.000 ± 0.429
$Z \to \mu\mu$	0.000 ± 0.429	0.000 ± 0.429	0.000 ± 0.429	0.000 ± 0.429
$Z \to \tau\tau$	0.000 ± 0.429	0.000 ± 0.429	0.000 ± 0.429	0.000 ± 0.429
W+jets	0.000 ± 1.808	0.000 ± 1.808	0.000 ± 1.808	0.000 ± 1.808
WW	0.000 ± 0.019	0.000 ± 0.019	0.000 ± 0.019	0.000 ± 0.019
Vγ	0.000 ± 0.248	0.000 ± 0.248	0.000 ± 0.248	0.000 ± 0.248
$W\gamma^* \to \ell\nu ee$	0.000 ± 0.097	0.000 ± 0.097	0.000 ± 0.097	0.000 ± 0.097
$W\gamma^* \to \ell\nu\mu\mu$	0.000 ± 0.075	0.000 ± 0.075	0.000 ± 0.075	0.000 ± 0.075
$W\gamma^* \to \ell\nu\tau\tau$	0.000 ± 0.028	0.000 ± 0.028	0.000 ± 0.028	0.000 ± 0.028
WZ	0.010 ± 0.007	0.001 ± 0.003	0.000 ± 0.003	0.011 ± 0.007
ZZ	0.000 ± 0.000	0.000 ± 0.000	0.001 ± 0.001	0.001 ± 0.001
dp$W^{\pm}W^{\pm}$	0.000 ± 0.004	0.000 ± 0.004	0.000 ± 0.004	0.000 ± 0.004
sp$W^{-}W^{-}$	0.000 ± 0.001	0.000 ± 0.001	0.001 ± 0.001	0.001 ± 0.001
sp$W^{+}W^{+}$	0.000 ± 0.006	0.000 ± 0.006	0.000 ± 0.006	0.000 ± 0.006
$t\bar{t}\gamma$	0.000 ± 0.059	0.000 ± 0.059	0.000 ± 0.059	0.000 ± 0.059
$t\bar{t}W$	0.111 ± 0.011	0.139 ± 0.012	0.273 ± 0.017	0.523 ± 0.024
$t\bar{t}Z$	0.018 ± 0.004	0.032 ± 0.005	0.042 ± 0.005	0.092 ± 0.008
$WW\gamma$	0.000 ± 0.015	0.000 ± 0.015	0.000 ± 0.015	0.000 ± 0.015
WWW	0.000 ± 0.000	0.000 ± 0.000	0.000 ± 0.000	0.001 ± 0.000
WWZ	0.000 ± 0.000	0.000 ± 0.000	0.000 ± 0.000	0.000 ± 0.000
WZZ	0.000 ± 0.000	0.000 ± 0.000	0.000 ± 0.000	0.000 ± 0.000
ZZZ	0.000 ± 0.000	0.000 ± 0.000	0.000 ± 0.000	0.000 ± 0.000
Total MC	0.231 ± 0.039	0.192 ± 0.024	0.475 ± 0.055	0.898 ± 0.071
LM6	0.000 ± 0.000	0.186 ± 0.186	0.383 ± 0.275	0.569 ± 0.332
SF	0.00 ± 0.58	0.00 ± 0.37	0.32 ± 0.57	0.32 ± 0.57
DF	0.00 ± 0.14	0.00 ± 0.10	0.00 ± 0.16	0.00 ± 0.16
SF + DF	$0.00 \pm 0.50 \pm 0.00$	$0.00 \pm 0.31 \pm 0.00$	$0.32 \pm 0.47 \pm 0.16$	$0.32 \pm 0.47 \pm 0.16$
Charge Flips	$0.043 \pm 0.010 \pm 0.009$	- $\pm$ -	$0.035 \pm 0.008 \pm 0.007$	$0.078 \pm 0.013 \pm 0.016$
MC Pred	$0.139 \pm 0.013 \pm 0.069$	$0.172 \pm 0.013 \pm 0.086$	$0.319 \pm 0.018 \pm 0.160$	$0.630 \pm 0.026 \pm 0.315$
Total Pred	$0.181 \pm 0.501 \pm 0.070$	$0.172 \pm 0.315 \pm 0.086$	$0.679 \pm 0.474 \pm 0.228$	$1.033 \pm 0.474 \pm 0.355$
data	1	0	1	2

Table 28: Observed event yields for $H_T > 80$ GeV and $\not{E}_T > 120$ GeV compared to expectations from simulation alone, and from the data-driven methods. The *simulated backgrounds* contribution includes contributions from genuine same-sign lepton pairs (WZ, ZZ, leptons from same-sign W from single-parton, double-parton, and $t\bar{t}W$ production, etc.), as well as electrons from converted photons in $V\gamma$ production. Entries with zero contributing events are reported with an uncertainty corresponding to one event. This uncertainty is not added to the total MC contribution. Systematic uncertainties (the second uncertainty if present) are displayed only for the final combined type of background, no systematic uncertainty is added for estimates with zero entries. Systematic uncertainties are 100% correlated among the channels.